INVESTIGATIONS INTO IMPROVING THE PERFORMANCE OF DISCHARGE-PUMPED RARE-GAS-HALIDE EXCIMER LASERS

S.A. Fairlie

A Thesis Submitted for the Degree of PhD
at the
University of St Andrews

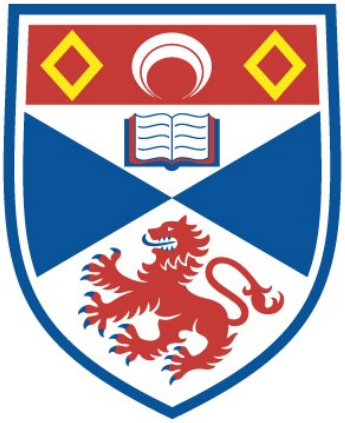

1993

Investigations Into Improving The Performance Of Discharge-Pumped Rare-Gas-Halide Excimer Lasers

A thesis presented by S A Fairlie

to the University of St Andrews

in application for the degree of PhD

August 1992

ProQuest LLC.
789 East Eisenhower Parkway
P.O. Box 1346
Ann Arbor, MI 48106 – 1346

Declaration

I hereby certify that this thesis has been composed by me as a true record of my work and has not previously been presented for consideration in relation to any other degree or professional qualification.

I was admitted to the science faculty of the University of St. Andrews under Ordinance General no.12 on the 1st of September 1988 and as a candidate for the degree of PhD on the 1st of September 1989.

S A Fairlie

Certificate

I certify that S A Fairlie has spent the equivalent of twelve terms engaged in research in the Department of Physics and Astronomy of the University of St. Andrews and that he has fulfilled the regulations appropriate to the degree of PhD.

Dr. P W Smith

(Research Supervisor)

Copyright

Acknowledgements

I would like to thank Dr. Paul Smith whose guidance, encouragement and enthusiasm for this work was much appreciated and to my colleagues in the Department of Physics and Astronomy for many interesting and enlightening discussions. Special thanks must also go to AEA Technology Culham who funded this research and in particular to my industrial supervisor, Dr. Mike Osborne for his helpful comments and advice. Lastly, I would like to thank the people of St. Andrews and North East Fife for making life more enjoyable throughout the period of my study.

Abstract

The construction and operation of a small active volume, discharge pumped, rare gas halide excimer laser is described. The values of laser output parameters such as pulse duration, pulse energy and overall efficiency presently achieved with such systems are much less that theoretical studies predict. The performance of this laser when pumped using a novel pulsed power modulator design containing nonlinear capacitors to produce a very fast risetime voltage pulse is contrasted with the performance obtained from a conventional driver circuit. The purpose of this was to determine if such circuits could lead to improvements in glow discharge stability and also laser pumping efficiency by quickly achieving the optimum pumping rates predicted by theory. It was concluded that while the rapid establishment of optimum pumping conditions may be beneficial, too fast a rate of rise of discharge current appears to be detrimental to discharge stability, probably due to skin effects. Having established that premature glow discharge collapse is a serious limiting factor in producing long duration excimer laser pulses, a study is carried out of the factors believed to influence discharge stability. While the effects of halogen donors on discharge stability have received most attention in the past the part played by the other constituents of the laser gas mix tends to have been neglected. A theoretical and experimental study of the role of the rare gas partners, xenon, krypton and argon is presented. It is well known that gas mixes using helium as the buffer gas perform less well than with a neon buffer and this is attributed to the driving of discharge instabilities rather than kinetic factors. A comparison of the relative influences of the buffer gases helium, neon and argon on discharge stability is carried out and claims by other workers for improved laser performance using a mixed helium / argon buffer are tested. Finally, in an attempt to inhibit the mechanisms driving glow discharge collapse, the effects of externally applied magnetic fields on discharge stability and laser performance are investigated.

Contents

Introduction

This thesis deals with the identification and understanding of the processes that currently limit the performance of discharge pumped rare gas halide excimer lasers. The values of laser output parameters presently achieved, such as optical pulse duration and output pulse energy as well as overall pumping efficiency, are considerably less than theoretical studies predict. It is hoped that by characterising these performance limiting processes advances can be made in excimer laser design and operation.

Chapter 1 deals with the current state of excimer laser knowledge. A brief history of the development of these lasers is given as well as some of the more important theory of excimer laser operation, discharge physics and pulsed power technology. The information gained from this review of the subjects used to design and build a discharge pumped excimer laser system which is utilised in all the subsequent experiments. Chapter 2 describes the design, construction and commissioning of this system.

In the quest for improved pumping efficiency and laser pulse durations, chapter 3 concerns the adaptation of the laser to pumping by an advanced pulse power architecture using nonlinear ferroelectric capacitors. This work was not particularly successful in achieving its stated aims but it did help to confirm glow discharge instability as the major performance limiting factor in discharge pumped excimer lasers.

Chapter 4 gives a detailed analysis of the current state of knowledge on the nature of excimer glow discharge stability. The various theories proposed to explain discharge evolution and the premature termination of lasing are described. Most explanations for discharge collapse are centred on the role played by halogen donor molecules but evidence is presented to indicate that the rare gas partner may also play an important part in these mechanisms. The influences of various buffer gasses on discharge instability are treated in chapter 5.

Chapter 6 describes the use of two, more advanced techniques for studying the nature of glow discharge evolution. These are used to help determine any differences in the

discharge collapse processes that occur when using different buffer gas compositions and halogen donor concentrations.

Finally, in chapter 7, the effects of an externally applied magnetic field on excimer laser performance are investigated. The influence of both constant and spatially variant magnetic field distributions on the nature of excimer glow discharge behaviour are evaluated. The construction of an all solid state thyratron trigger unit and a description of the methods of high voltage and current measurement used are presented as appendices.

Chapter 1

Historical and Theoretical Background

1.1 Historical Perspective

In order to put the research presented in this thesis in its proper context it is necessary to present a brief history of the development of excimer lasers. This is not intended to be a comprehensive account but merely an overview of the chronology to help appreciate where the present research fits in the overall development of this type of laser.

Excimers are molecules which can only exist with one or more of the constituent atoms in an electronically excited state. These molecules are metastable in that their lowest energy state does not correspond to a stably bound system, following radiative decay to the ground state they dissociate.

$$A + B \text{ ----> } (AB)^* \qquad 1.1$$

$$(AB)^* \text{ ----> } A + B + h\nu \qquad 1.2$$

In general the ground states of such systems are repulsive or very weakly bound so that dissociation takes place rapidly at ordinary temperatures. By considering the spontaneous emission lifetimes of typical excimer systems of a few ns and the very short dissociation times for the ground state, ~10^{-13} s, their potential as laser media can be appreciated. Provided that gas temperatures are not high enough to thermally populate the lower state it is possible to form a population inversion between the bound and dissociative states to produce laser action.

The potential of excimers to act as laser media was first suggested by Houtermans, (1), in 1960 but it was not until 1970 that lasing was first demonstrated in an excimer system by Basov, (2),using liquid Xe.

Lasing in rare gas halide molecules was first observed in 1974 by Searles and Hart, (3), in $XeBr^*$ at 282 nm by electron beam pumping. This was quickly followed by the achievement of laser action in KrF^* (249 nm) and $XeCl^*$ (308 nm) by Ewing and Brau, (4). The XeF^* laser (351 nm) was demonstrated in 1975 by Ault, Bradford and Bhaumik,

(5) and ArF^* (193 nm) by Hoffman, Hays and Tisone, (6). Again electron beam pumping was used in each case.

The pumping of rare gas halide excimers by self sustained discharges followed rapidly on from their initial discovery. Self sustained discharge pumping of XeF^* was first demonstrated in 1975 by Burnham, Harris and Djeu. This method of excitation has become almost universal and was chosen for the laser system described in this thesis.

More recent work has been concerned with the scaling up of laser systems to larger active volumes to produce larger pulse energies and durations. Many workers have chosen to work with $XeCl^*$ as a number of factors combine to make this the best performing excimer for both high energy and long pulse duration experiments. An example of a large output energy $XeCl^*$ was described in 1982 by Watanabe and Endoh, (8), by scaling up the active volume and laser gain length. Using this technique $XeCl^*$ pulses of up to 13.8 J were obtained by discharge pumping a 4 litre active volume. This approach was continued in 1984 by Champagne, Dudas and Wexler, (9), who achieved 60 J $XeCl^*$ pulses, although at a reduced efficiency, by applying more sophisticated pulsed power and preionisation techniques to a large active volume machine.

From the beginnings of rare-gas halide excimer lasers the high quantum efficiency was noted and it was realised that the overall efficiency would be limited by the excimer molecule formation and quenching rates. Typical overall efficiencies for the early discharge pumped machines were in the region of 1 or 2% with even the first ever example of a self sustained discharge pumped $XeCl^*$ laser yielding an impressive 0.8% efficiency, (10). More recently, kinetic studies have been carried out to theoretically determine the maximum possible overall efficiency of $XeCl^*$ lasers. The comprehensive treatment by Ohwa and Obara, (11), predicted that pumping a gas mixture rich in HCl at the high pump power density of 3.5 $MWcm^{-3}$ should lead to efficiencies of up to 12.5%. These predictions were tested experimentally in 1991 by D Lo and J Xie, (12), by high density pumping a small active volume. Although the specific laser output power was high and an impressive 21 Joules per litre was extracted from the active medium, both overall efficiency and laser

pulse duration were poor. Typical overall efficiencies of current $XeCl^*$ systems are in the region of 4%.

Some of the most important applications for rare gas halide excimer lasers are concerned with the etching and surface treatment of industrial materials. The high spatial resolution resultant from their short wavelength makes them particularly suitable for tasks such as submicrometer lithography of silicon wafers. Excimer lasers have also been used to precision etch diffraction gratings where their ability to deliver a relatively large amount of energy to the target on a timescale of around 20 ns removes the need for the highly stable optics required by other alternatives such as CO_2 lasers. It was identified early in the development of excimer lasers that extending the optical pulse duration from a few tens of ns upwards could prove useful for certain applications. $XeCl^*$ lasers have been used in surgery by employing fibre optic catheters, problems however have been encountered with optical damage due to the high peak power levels in the fibre. By using laser pulses with durations in excess of 100 ns the same energy can be delivered in each shot but at a smaller peak power level, below the optical damage threshold.

An important scientific application of excimer lasers is the pumping of broadband dye lasers to generate laser light at wavelengths that are otherwise difficult to obtain with a high degree of tunability. In this case the duration of the dye laser output will be limited by the duration of the excimer pump pulse and so the advantage of long duration excimer laser pulses can be seen. It has also been noted that the increased number of cavity round trips associated with long pulse operation could allow increased control of beam divergence where unstable resonator optics are used. This could be especially useful for applications where beam quality is important such as the driving of optical parametric oscillators.

Much of the effort expended on increasing pulse duration has centred on understanding the mechanisms of glow discharge stability and in matching the pulsed power engineering to the laser requirements. Discharge stability is a large subject in itself and will be dealt with in more detail in chapter 4. To date the longest pulse duration obtained from a rare-gas halide discharge pumped laser is 1.5 μs by Taylor and Leopold in 1985, (13), although the pulse energy was very small. Combining past achievements into

one system to produce a long pulse duration, high efficiency, high pulse energy excimer laser remains an elusive goal.

1.2 Physics of Rare Gas Halide Excimer Lasers

In this section the physics behind the operation of rare-gas halide excimer lasers will be briefly described. A more detailed account of the underlying theory behind these systems is given by Brau, (14).

Fig. 1.1

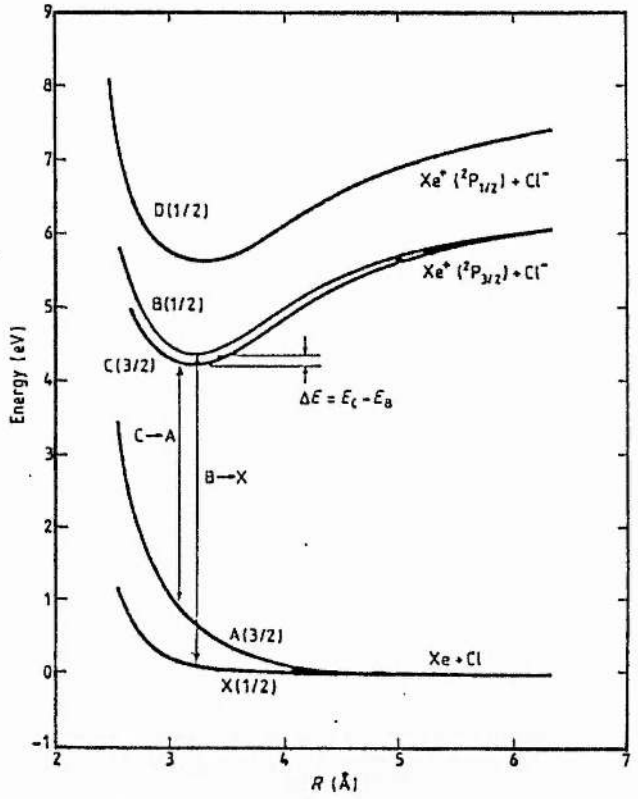

Electronic states of the XeCl molecule (reproduced from D Lo and C E Zheng; "The role of the $C(^3/_2)$ state in a XeCl Discharge laser;" J. Phys. D, Appl. Phys, vol 20, p 714-7, 1987)

A diagram of energy level against inter-nuclear separation for a typical excimer, in this case $XeCl^*$, is given in fig. 1.1. The rare-gas halides have three bound excited states which are ionic in nature. These are conventionally known as the B,C and D states in

ascending order of energy although in $XeCl^*$ and XeF^* the B and C states are inverted with the C state lying slightly lower than the B state. There are also three covalent ground states. The lowest state is generally mildly repulsive and is known as the X state although again $XeCl^*$ and XeF^* prove to be exceptions with a weakly attractive X state. The remaining states are nearly degenerate and mildly repulsive and are known together as the A state. In most rare-gas halide lasers the radiative transition is from the B to the X state although lasing in XeF^* has been obtained between the C and A states in a broad band centred on 483 nm. (15)

The rare-gas halide excimers are all pumped by the excitation of a plasma containing a halogen donating molecule and one or more rare gases. The major excitation techniques employed are high pressure self sustained glow discharges within the laser gas and pumping by high energy electron beams generated by an external source. Some experimenters have used electron beam sustained discharges, first demonstrated by Mangano and Jacob in 1975 (16), but this method has proved to be disadvantageous and has fallen out of favour.

The main pumping reaction is generally by three body recombination of rare-gas and halogen ions:

$$Xe^+ + F^- + Ne \longrightarrow XeF^* + Ne \qquad 1.3$$

with the halogen ions being ionised by dissociative attachment of low energy electrons to a halogen donor molecule.

$$F_2 + e^- \longrightarrow F^- + F^+ \qquad 1.4$$

The rare-gas ions may be formed by many different processes but a common route in discharges is by multiple stage photoionisation:

$$Xe^* + h\nu \longrightarrow Xe^+ + e \qquad 1.5$$

this route to excimer formation is particularly efficient and is known as the ionic channel.

A second method of excimer production that is also important is by direct reaction between rare-gas excited states and halogen molecules.

$$Kr^* + F_2 \longrightarrow KrF^* + F \qquad 1.6$$

The mechanism for this reaction is analogous to the 'harpooning' reactions between alkali metals and halogens in which the valence electron of the alkali metal can transfer to the halogen molecule from distances as large as 0.5 to 1.0 nm forming an ionic bond. The reaction rate constant for this reaction is rapid and has been measured at around $7x10^{10}$ cm^3s^{-1}, (17).

There are many other routes to excimer formation involving ions and excited states of the buffer gas as well as the halogen donor and the rare gas partner in the lasing excimer. The buffer gas performs an important kinetic function, as opposed to just influencing electrical parameters, in that it provides a means of relaxing vibrationally excited species. On formation most excimer molecules are in highly vibrationally excited states yet the upper laser levels occur near the bottom of the vibrational manifold, $v=0,1,2$. Relaxation of these vibrationally excited states by collision with buffer gas atoms is therefore essential for efficient laser operation. The buffer gas is also responsible for mixing the B and C states in cases where they lie close together in energy, for example in XeCl*.

With such a complex kinetic scheme and many competing reactions it is inevitable that unfavourable reactions will take place and in certain cases unwanted absorption of laser photons by constituents of the discharge plasma may be significant. This is the case with $XeBr^*$ and $KrCl^*$ where excimer formation turns out by chance to be inefficient due to unfavourable kinetics. Although these excimers have been made to lase their inherent inefficiency has hindered their development as practical laser sources.

As well as the efficient formation of excimer molecules, it is an essential requirement that quenching of the upper laser states by other species should be small in relation to depopulation by stimulated emission. A comprehensive explanation of excited state quenching has been made by Rokni et al. (19) and certain important points are worth noting. Taking the KrF^* laser as an example, measurements of performance at various gas proportions have concluded that if excess Kr is present three body quenching of the KrF^* by Kr atoms to produce K_2F^* may be significant, (20), (21).

$$KrF^* + 2Kr \text{ ----> } Kr_2F^* + Kr \qquad 1.7$$

The resultant trimer loses energy by spontaneous emission in a broadband centred on 415 nm. Similarly if Ar or Ne buffer gases are present significant quenching by the following reactions can take place:

$$KrF^* + Kr + Ar \text{ ----> } Kr_2F^* + Ar \qquad 1.8$$

$$KrF^* + Kr + Ne \text{ ----> } Kr_2F^* + Ne \qquad 1.9$$

In XeF^* the analogous quenching reactions are also significant. It was once thought that quenching of XeF^* by Xe proceeded at a faster rate than the equivalent quenching of KrF^* by Kr, (19) but the consensus is that this not the case, (22). It is generally accepted however that three body quenching of XeF^* by Ar proceeds at a faster rate than the equivalent reaction with Ne. This helps to explain why Ne has been found to be a better buffer gas than Ar in XeF^* lasers.

1.3 Characteristics of Excimer Laser Discharges

1.3.1 Discharge Physics

As all the work described in this thesis is concerned with self sustained discharge pumped excimer lasers it is felt worthwhile to introduce some background discharge physics. This section is not intended to be a comprehensive account of gas discharges but is included to explain some of the relevant basic theory and to emphasise some of the aspects of electrical discharges that are essential for the understanding of discharge pumped excimer lasers that will be treated more fully in subsequent chapters.

All self sustained discharge pumped excimer lasers operate with the active medium in a region of high electric field between the electrodes. Pumping of the active medium occurs through collisions by high energy electrons and to a lesser extent ions created by the electrical discharge conditions. Gas kinetic considerations described in the previous section dictate that the total gas pressure in an excimer mix should be of the order of a few atmospheres. This is necessary so that the excimer forming reactions and other favourable processes can progress at a sufficiently fast rate to produce optical gain. This requirement to operate at high pressures introduces electrical problems as electrical breakdown in such gases is usually by means of one or more high current density arcs. The localised nature of

arcs makes them unsuitable for pumping purposes as the resultant energy deposition in the active medium is similarly localised leading to conditions of non-uniform optical gain.

A fuller description of the mechanisms of high pressure discharges applicable to lasers such as CO_2 TEA and rare gas halide excimers are given in the paper by Palmer, (23) but essentially arc formation occurs where the local electric field associated with the space charge of the head of a single avalanche event becomes comparable to the applied electric field between the electrodes. In this case the motion of any neighbouring avalanches that may be forming will be more strongly influenced by the space charge field than by the applied field so that these smaller avalanches will be deviated towards the main avalanche, augmenting it and hence fuelling the runaway process that generates an arc. Arc formation can be suppressed by limiting the discharge current using a resistively ballasted pin array electrode or other similar means and although this has been tried, (24), it is generally not practical for the discharge current values generally required for excimer pumping.

In cases where many streamer events occur in close proximity so that the resultant space charge retains a high degree of homogeneity with no one avalanche growing to an extent where it can greatly influence its neighbours a high pressure glow discharge can form. The formation of a uniform high pressure glow is an essential criterion for the efficient discharge pumping of excimer lasers. The high pressure glow mode is only metastable however and tends to degrade into the more stable arc state. The formation and maintenance of the high pressure glow against its inherent instability is the subject of much current research and conflict of opinion and is dealt with in detail from chapter 4 onwards.

An essential requirement for the production of a glow discharge is some form of preionisation, that is seeding of the discharge volume with electron-ion pairs immediately before the application of the electric field between the electrodes so that a large number of small streamers can quickly form in close proximity. The methods currently used for preionisation are discussed in section 1.3.2.

To fully quantify laser performance it is necessary to be able to measure discharge parameters such as the self sustaining glow voltage, V_{ss}, and hence the electrical power deposition in the discharge. In general the electrical characteristics of the discharge do not

obey Ohm's law in that the voltage current curve is not linear, the discharge current is largely independent of the discharge self sustaining voltage and tends to be determined by the external circuit parameters. A schematic diagram of the general form of the voltage/ current characteristic is given in fig. 1.2.

Fig 1.2

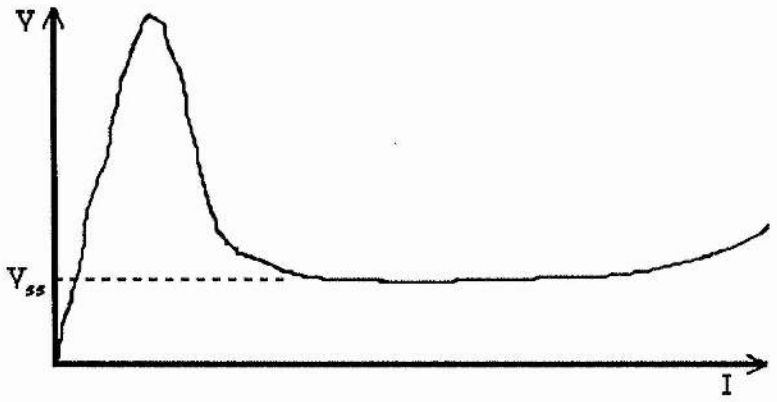

Current Voltage Characteristic For A Typical Excimer Discharge

The pump power deposited in the laser medium is given by the product of the head current and the self sustaining voltage. The head current is straightforward to measure but the self sustaining voltage is more difficult because of the series head inductance. The voltage measured across the laser head must be treated as the sum of the true self sustaining voltage and the voltage generated across the inductance associated with the discharge by changes in the head current. Only if the head current is constant and $dI/dt = 0$, will the measured head voltage be equal to the self sustaining voltage.

It is advantageous that the inductance associated with the discharge is known as accurately as possible. The inductance can be estimated from simple geometry by the application of the loop inductance formula for two parallel current carrying sheets, as seen in Fig. 1.3.

Fig. 1.3

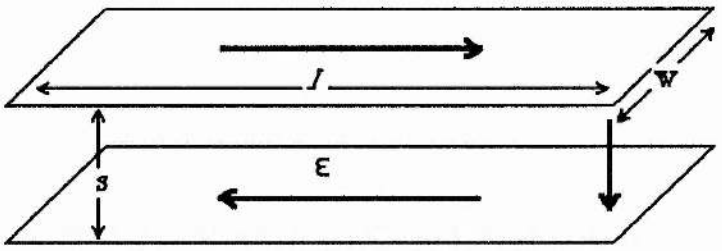

Diagram showing the method for calculating loop self inductances

From, (25),the self inductance of a generalised current volume distribution as given by eqn 1.10 is:

$$L = \frac{1}{\mu_0 I^2} \int_{\infty} B^2 d\tau \qquad 1.10$$

where I is the total loop current and B is the magnetic induction at each elemental volume $d\tau$ throughout the total volume enclosing the current loop. For the purposes of the geometry considered here, with w >> s and no magnetic materials present this expression reduces to simple geometric factors to give:

$$L = \frac{\mu_0 l\ s}{w} \qquad 1.11$$

This method can give a rough value for the head inductance, its main inaccuracy arising from the geometric approximations usually necessary and the ignoring of edge effects due to the finite width of the current feeds, (and the discharge electrodes).

Another method of estimating the inductance associated with the discharge and its feeds arises if the pulse modulator circuit is tested by firing into a resistive dummy load in place of the discharge. If the load is chosen so that it occupies the same geometry as the discharge and hence forms the same loop inductance as the discharge, then the leading edge of the voltage pulse across the load will be determined by the associated RL time constant. This can be approximated thus:

$$V(t) = A[1-\exp(-Lt/R)] \qquad 1.12$$

where A is the maximum amplitude of the voltage pulse, R is the load resistance and L is the inductance of the load and current feeds. If t is chosen such that $t = t_1$ when $A/V(t) = e$ then the expression becomes:

$$t_1 = -\frac{L}{R} \qquad 1.13$$

By substituting the known experimental values of t_1 and R a value for L can be determined. This method however assumes that the current (and hence voltage) rise-time at the load is determined by the load itself and its inductance and not by the limitations of the switching element.

1.3.2 Preionisation

Many different methods of preionisation have been employed in excimer lasers. It has been shown that for effective preionisation the discharge needs to be seeded with a minimum of between 10^5 and 10^7 electrons cm^{-3} and also that high spatial uniformity is essential, (26),(27). Any means of meeting these criteria should in theory be sufficient to produce an acceptable glow discharge, the multiplicity of preionisation methods currently used however indicates that producing such a glow discharge is not as straightforward as might seem. Different preionisation methods have their advantages and disadvantages making them attractive for laser systems built on different scales for different applications.

A simple and widely used preionisation method, popular in early machines and still used in some commercial systems is the spark gap array. The laser head contains a line or array of sharp points or blades arranged adjacent to the main active volume and connected so that a discharge consisting of a series of arcs is struck between the array and a nearby grounded electrode. The spark array can be built into one of the electrodes or displaced to one side of the active volume. In all cases preionisation takes place by photoionisation of the discharge medium by the UV light from the spark array.

Spark arrays although simple and reliable have serious disadvantages. The spark array must be carefully designed to illuminate the discharge volume with a uniform UV flux to avoid inhomogeneities which may manifest themselves later in the main discharge. The

time delay between the spark arrays firing and the the onset of the main discharge may be incapable of being adjusted, especially if the spark array is powered by current from the main discharge in a 'double discharge' configuration, and problems with damage to the spark array points can reduce performance after prolonged use.

Radioactive sources have been proposed and used to a limited extent for the preionisation of excimer lasers, (28). The most promising schemes for radioactive preionisation involve the use of α sources and have the advantage of compactness and extreme simplicity. No electrical connections are required and timing synchronisataion is dispensed with as the preionisation source is 'on' all the time. The main disadvantage appears to be that with most schemes initial ion densities may only marginally exceed the minimum threshold for the production of a stable discharge due to physical limitations on the size of the source, the isotopes available and the electron attaching nature of excimer laser gas mixes. The limited penetration of α particles of only a few cm in a typical gas mix restricts radioactive preionisation to relatively small discharge volume lasers. It is disappointing that more work has not been done to overcome these difficulties; this may be partially due to the lack of research workers adequately qualified in the fields of both gas lasers and handling radioactive materials and to the radiological implications of such work.

X-rays are a popular choice for providing preionisation especially in larger active volume systems. The use of X-rays can simplify the construction of the main laser electrodes generally allowing them to be solid rather than the meshes required by other systems although the electrode design must be thin enough not to attenuate the x-rays excessively.This advantage comes at the expense of having to provide an external X-ray source and in many cases the X-ray source is as large and as complex as the main discharge drive circuitry. The construction of such an X-ray source is described by F Davanloo *et al* (29).

Most X-ray sources involve vacuum diodes in which electrons from a field emission cathode are accelerated before colliding with a target of high atomic number such as tungsten or tantalum. Recent work has been done on improving such X-ray sources by the use of high efficiency cathodes (30) but fundamental engineering restrictions remain.

The most efficient preionisation has been shown to take place with fairly soft X-rays in the energy range 35 to 50 keV (30), as more energetic X-rays interact less readily with the laser gases. A major engineering problem is therefore constructing the main laser pressure vessel strongly enough to contain the laser gases at several atmospheres pressure while incorporating a window to allow penetration of the X-rays with an acceptably small attenuation. Such constraints can be overcome but without careful design X-ray preionised lasers can suffer from the same restrictions of maximum working buffer gas pressure as electron beam pumped machines.

The preionisation system chosen for the laser used in the experiments presented here was UV preionisation from a corona discharge. The construction of this preioniser, fully described in chapter 2, consists of a pair of ceramic tubes set into the anode body. Wires down the centre of these tubes are pulsed with a voltage pulse from a separate pulse discharge unit and capacitive coupling allows a corona like discharge to be struck between the tubes and the electrode body. UV light from this discharge preionises the active volume by photoionisation through the fine mesh surface of the electrode.

The advantage of this corona preioniser is its simplicity and its compactness. No windows are required in the laser pressure vessel, as with X-ray preionisation, simplifying the engineering and making high pressure operation easier to achieve. The delay time between the onset of preionisation and the main discharge is also simple to adjust for optimum performance and the preionisation uniformity is generally much better than with spark arrays.

The main disadvantages that have been identified with the corona preioniser are concerned with the lifetime of the device. After prolonged use voltage punch through may be a problem due dielectric breakdown in the ceramic. Furthermore, some discharge stability theories suggest that the mesh electrode surface, necessary to let the UV light from the corona discharge preionise the active volume, may be detrimental because of the local electric field enhancement produced.

1.4 Pulse Power Theory

An understanding of pulsed power electronics is fundamental for the effective design of discharge pumped excimer lasers. As much of the work in this thesis is concerned with the effective matching of the electrical pulsed power input to the electrical characteristics of the high power discharge it is considered worthwhile to provide an overview of some of the concepts of pulsed power generation. Although relatively simple, a lack of specialist literature makes pulsed power less widely understood than may be expected, however a basic knowledge is presupposed and only a brief account of the concepts relevant to the work presented here will be given. More detail on transmission lines theory is given in the book by D K Cheng, (31), while techniques for fast pulse generation are covered by Glasoe and Lebacqz, (32).

For a transmission line, whether distributed such as coaxial cable or a ladder network composed of discrete components, the effective impedance, Z_0, is given by:

$$Z_0 = (L/C)^{1/2} \qquad 1.14$$

where L and C are the inductance and capacitance per unit length, or in the case of a ladder network, per stage (capacitor inductor pairs). This makes the assumption that loss terms, due to the resistance associated with the inductors and the capacitor current leakage may be neglected.

By considering electrical signals propagating along transmission lines as waves, the phase velocity is found to be:

$$v_s = \frac{c}{\sqrt{(\varepsilon\mu)}} \qquad 1.15$$

with c the velocity of light and ε the dielectric constant and μ the relative permeability of the transmission line insulating medium. More usefully, for a loss-less ladder network the one-way transit time for a signal is:

$$t = n\sqrt{(LC)} \qquad 1.16$$

where n is the number of stages. By varying the values of the ladder inductors and capacitors, a transmission line of any chosen impedance and transit time can be built subject to the availability of components.

At the interfaces between transmission lines of differing characteristic impedances partial reflection and transmission of voltage steps will occur. The voltage reflection and transmission coefficients at the junction between two media of characteristic impedances Z_0 and Z_1, for a wave originating in medium Z_0 are:

$$\rho_R = \frac{Z_0 - Z_1}{Z_0 + Z_1} \qquad 1.17$$

$$\rho_T = \frac{2Z_0}{Z_0 + Z_1} \qquad 1.18$$

Pulse generation is usually effected by the rapid short circuiting of one end of a charged transmission line using a fast acting switch as seen in fig. 1.4. For this to work properly the closing time of the switch should be short in comparison to the transmission line transit time; in this sense the *closing time* is not simply the time taken for the mechanical or electrical continuity to complete but must also take account of the inductance associated with the switch and more correctly should be taken as the current rise-time of the circuit configuration. If the switch closing time is not short compared with the transit time then the transmission line will tend to behave as a lumped capacitance equal to the total capacitance of the line. Provided that the switch closing time is short and the inductance associated with the switch and the load is small then the pulse duration will be twice the transit time of the line.

For maximum power transfer and to eliminate voltage reflections then R_L should equal Z_0. In this case the voltage pulse across R_L will be of an amplitude of half the charging voltage, V_0, and last for a duration of twice the transmission line transit time.

Fig. 1.4

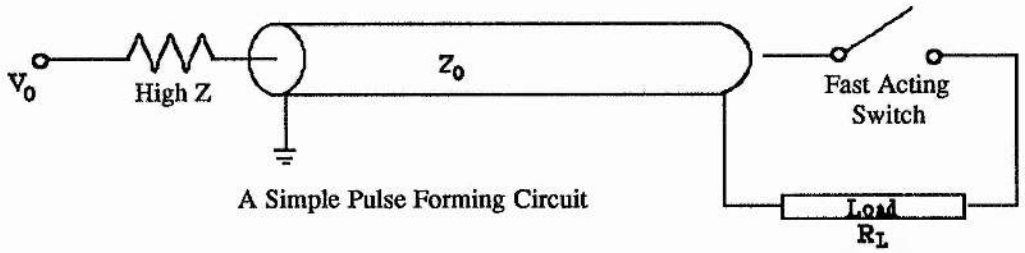

A Simple Pulse Forming Circuit

More complex structures can be built from transmission lines of different characteristic impedances to make use of voltage reflection and transmission at interfaces. It will be noted from the form of the voltage transmission coefficient that voltage gain is possible allowing the construction of transmission line transformers; also, by using two equal lengths of transmission line in a Blumlein configuration a pulse of amplitude equal to the full charging voltage, V_0, can be produced with a duration of twice the transit time of one of the lines. As none of these advanced pulse power architectures were used in the subsequent experiments they will not be discussed further.

The transfer of energy between a pulse forming circuit and a laser discharge is difficult to achieve with high efficiency. In practice, laser discharges do not present a constant impedance load, but one whose current / voltage characteristic is time variant; perfect matching can only be achieved if the driving circuit is similarly time variant, which in reality is almost impossible to achieve. Many workers have tried to match pulse forming circuitry to laser discharges by analysing the nature of the discharge impedance, with limited success, (33),(34),(35) .

Some recent work, (36), has found fairly good experimental agreement if the discharge is represented by the equivalent circuit in Fig.1.5 with L_0 the inductance of the current feeds, L_1 the inductance of the discharge, R_0 a constant resistive term and R_1 a time variant resistance with time constant T_R. A dependence of these circuit parameters on the type of preionisation was noted.

Fig. 1.5

Equivalent circuit for an excimer laser discharge from, (36)

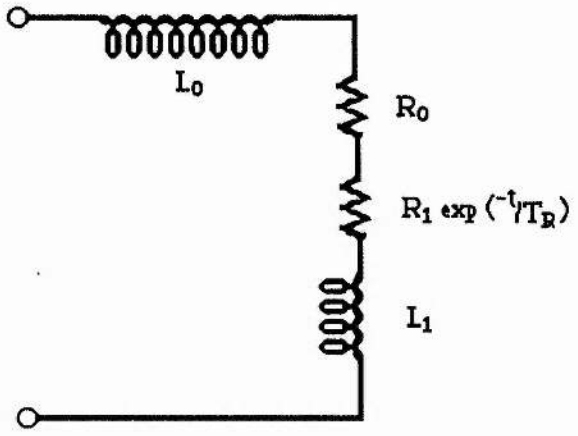

An alternative strategy is to consider the discharge as a constant voltage load, similar to the behaviour of a reverse biassed zener diode. By using this approach it has been shown by M R Osborne *et al* , (37), that impedance matching can be achieved if the discharge is driven by a pulse forming network charged to a voltage that is twice that of the discharge self sustaining glow voltage. Although this ensures the transfer of energy from the pulse forming circuit to the discharge with maximum efficiency a problem arises in that a voltage typically several times larger than the glow voltage is needed to cause the initial breakdown in the gas and establish the glow voltage, (see fig. 1.2). In this case the discharge current may be considered as being determined entirely by the impedance of the pulse forming circuit and its charging voltage.

Attempts have been made to match the output waveform of a pulse generator to the impedance of the discharge by the use of a spiker sustainer circuit, (38,39). The circuit consists of two separate, synchronised, pulse generators, the first producing a short duration pulse of high impedance to break down the gas followed by a much longer duration pulse of low impedance designed to sustain the discharge at the desired pump power level. In many cases this type of circuit has proved successful, especially where

high electrical efficiency is important and it is a circuit of this type that is responsible for the longest duration rare gas halide laser pulse yet achieved, (13).

Further theoretical background studies on the specific subject of excimer glow discharge stability are presented in chapter 4.

References

1 F G Houtermans; Helv. Phys. Acta, vol 33, p933, 1960 (in German)
2 N G Basov *et al* ; JETP Lett, vol 12, p329, 1970
3 S K Searles, G A Hart; "Stimulated Emission at 281.8 nm from XeBr;" Appl. Phys Lett, vol 27, p243, 1975
4 J J Ewing, C A Brau; "Laser action on the $^2\Sigma^+_{1/2}$ --> $^2\Sigma^+_{1/2}$ Bands of KrF and XeCl;" Appl. Phys Lett, vol 27, p350, 1975
5 E R Ault, R S Bradford, M L Bhaumik; "High Power Xenon Fluoride Laser;" Appl. Phys Lett, vol 27, p413, 1975
6 J M Hoffman, A K Hays, C G Tisone; "High Power UV Noble-Gas-Halide Lasers;" Appl. Phys Lett, vol 28, p538, 1976
7 R Burnham, N W Harris, N Djeu; "Xenon Fluoride Laser Excitation by Transverse Discharge;" Appl. Phys Lett, vol 28, p86, 1976
8 S Wanatabe, A Endoh; "Wide Aperture Self-Sustained Discharge KrF and XeCl Lasers;" Appl. Phys. Lett, vol 41, p799-801, 1982
9 L F Champagne, A J Dudas, B L Wexler; Presented at CLEO'84, Anaheim CA, June 19-22, 1984
10 R Burnham; "Improved Performance of the Discharge Pumped $XeCl^*$ Laser;" Opt. Comm, vol 24, p161, 1978
11 M Ohwa, M Obara; "Theoretical Analysis of Efficiency Scaling Laws for a Self Sustained Discharge Pumped Laser;" J Appl. Phys, vol 59, p32-41, 1986
12 D Lo, J Xie; "High Pressure Scaling of a High Current Density XeCl Laser;" J Phys D, vol 24, p1023-4, 1991
13 R S Taylor, K E Leopold; "Microsecond Duration Optical Pulses From a UV Preionised XeCl Laser;" Appl. Phys. Lett, vol 47, p81-3, 1985
14 C A Brau; "The Rare Gas Halogen Excimers;" from C K Rhodes (editor); "Excimer Lasers;" Topic in appl. phys. vol 30, 2nd edition, Ch 4, Springe Verlag, New York 1983
15 W K Bischel *et al*; "A New Blue-Green Excimer Laser in XeF;" Appl. Phys Lett, vol 34, p565, 1979
16 J A Mangano, J H Jacob; "Electron Beam Controlled Discharge Pumping of the KrF Laser;" Appl. Phys Lett, vol 27, p495, 1975
17 J E Velazco *et al*; "Quenching Rate Constants for Metastable Argon, Krypton and Xenon Atoms by Fluorine Containing Molecules and Branching Ratios for XeF^* and KrF^* Formation;" J Chem. Phys. vol 65, p3468, 1976
18 J H Jacob, J C Hsia, J A Mangano, M Rokni; "Pulse Shape and Laser Energy Extraction From e-Beam-Pumped KrF^*;" J Appl. Phys. vol. 50, p5130,1979
19 M Rokni *et al*; "Rare Gas Fluoride Lasers" IEEE J Quantum Elect. vol QE14, p464, 1978
20 Gu Zhiya *et al*; "Measuring Formation Rate Constant For Trimer Kr_2F^* in F_2/Ne/Kr Mixtures;" Chinese Phys. Lasers, vol 14(3), p175, 1987
21 F Kannari, M Obara, T Fujioka; "An Advanced Kinetic Model of Electron Beam Excited KrF Lasers Including the Vibrational Relaxation in KrF^*(B) and Collisional Mixing of KrF^*(B,C)" J Appl. Phys, vol 57(9), p4309, 1985
22 R Sauerbrey, W Walter, F K Tittel, W L Wilson; "Kinetic Processes of Electron Beam Generated XeF^* Excimers;" J Chem. Phys. 78(2), p735 1983
23 A Jay Palmer; "A Physical Model on the Limitation of Atmospheric-Pressure Glow Discharges;" Appl. Phys. Lett. vol 25, p138, 1974
24 D C Hogan, R Bruzzese, A J Kearsley, C E Webb; "Long Pulse Operation of Discharge-Excited $XeCl^*$ Lasers;" J. Phys. D, Appl. Phys, vol 14, L157-61, 1981
25 P Lorrain, D Corson; "Electromagnetic Fields and Waves;" 2nd Edition, Freeman, New York, 1970, p356
26 J I Levatter, S Lin; "Necessary Conditions for the Homogenous Formation of Pulsed Avalanche Discharges at High Gas Pressures;" J Appl. Phys, vol 51, p210,1980
27 R S Taylor; "Preionisation and Discharge Stability Study of Long Optical Pulse Duration UV-Preionised XeCl Lasers;" Appl.Phys B, vol 41, p1-24, 1986
28 I J Bigio; "Preionisation of Pulsed Gas Lasers by Radioactive Source;" IEEE Journal of Quantum Elet. vol 14, p75, 1978
29 F Davanloo, J J Coogan, T S Bowen, R K Krause, C B Collins; "Flash X-ray Source excited by Stacked Blumlein Generators;" Rev. Sci. Inst, vol 59(10) p2260-4, 1988
30 F A van Goor; "High Repetition Rate X-ray Preionisation Source;" Pulse Power for Lasers III, SPIE, Los Angeles, Jan 1991
31 D K Cheng; "Field and Wave Electromagnetics;" 2nd edition, Addison Wesley Publishing, 1989

32 G N Glasoe, J V Lebacqz; "Pulse Generators;" MIT Radiation Laboratory Series, Mc Graw Hill, New York, 1948
33 J I Levatter, R S Bradford Jr; "Water Dielectric Blumlein-Driven Fast-Electric-Discharge KrF Laser;" Appl. Phys. Lett, vol 33, p742-4, 1978
34 H Hokazono, *et al* ; "Theoretical Analysis of a Self-Sustained Discharge Pumped XeCl Laser;" J Appl. Phys, vol 56, p680-90, 1984
35 S S Anufrik, K F Znosko, A D Kurganskii; "Influence of LC-Circuit Parameters on the Output Energy of an XeCl Laser;" Sov. J. Quantum Elect, vol 19, p1433-5, 1989
36 M Leo, *et al* ; "Discharge Impedance of an Ultraviolet Preionised XeCl Laser;" J Appl. Phys, vol 70, p1168-71, 1991
37 M R Osborne, P W Smith, M H R Hutchinson; "The Effect of Pulse Forming Line Impedance on the Performance of an X-ray Preionised XeCl Discharge Laser;" Optics Comms, vol 52(6), p415-20, 1985
38 W H Long Jr, M J Plummer, E A Stapperts; "Efficient Discharge Pumping of an XeCl Laser Using a High Voltage Prepulse;' Appl. Phys. Lett, vol 43, p735-7, 1983
39 R S Taylor, KE Leopold; "Ultralong Optical Pulse Corona Preionised XeCl Laser;" J. Appl. Phys, vol 65, p22-29, 1989

Chapter 2

Design, Construction and Commissioning of the Laser System

2.1 Introduction

In this chapter the design of the laser system used for all subsequent experiments will be presented and its construction described. The design parameters of the laser system will be discussed and justified in terms of the experimental requirements and the resources available. The testing of the pulse forming network into dummy resistive loads and the commissioning of the full laser system with $XeCl^*$ is described.

2.2 Laser Modulator Circuit Design

The equivalent electrical circuit of the laser head and pulse modulator circuitry is shown in Fig. 2.1.

Fig. 2.1

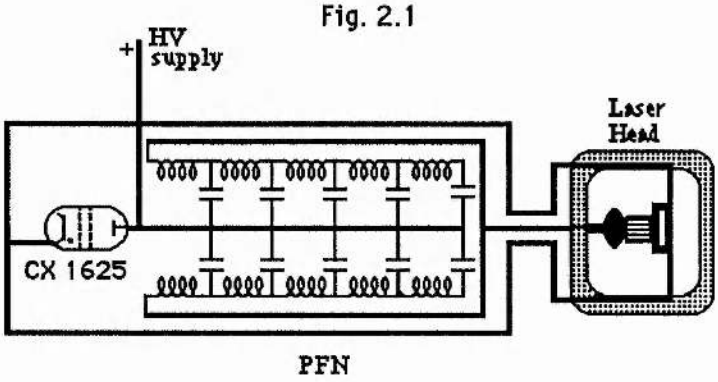

As can be seen it was decided to drive the laser by means of a simple lumped element double pulse forming network, (PFN), switched by a single ceramic thyratron. The main advantage of this approach is the flexibility to change capacitor / inductor combinations to vary PFN impedances and output pulse durations if required. Furthermore, the grounded cathode configuration and architecture adopted allowed the circuit to have a low inductance feed to the laser head which is essential for high rates of rise of current. This control over the pulsed power parameters was considered to be important for some of the intended experiments.

The PFN was switched with a ceramic thyratron of type CX 1625 supplied by EEV Ltd. This tube was specifically designed with excimer laser operation in mind and is capable of switching currents at a dI/dt of up to 300 $kA\mu s^{-1}$ with a maximum repetition rate of 1 kHz, (1). A high rate of rise of current is generally accepted as beneficial for efficient excimer operation as it allows the optimum pumping rate to be achieved quickly. The repetition rate capability of this tube is not essential as most experiments were performed at either single shot or very low frequencies, eg. below 5 Hz. Other advantages of the CX 1625 are the very low timing jitter, <3ns, and the hollow anode structure allowing the tube to withstand some current reversal without damage. This ability to handle current reversal is important as experience has shown that almost all drive configurations for discharge lasers result in some current reversal due to ringing, especially in the later stages of the pump pulse when the discharge collapses into an arc.

It has been shown theoretically, (2), that the optimum pump power density for the efficient operation of a typical excimer laser such as $XeCl^*$ lies between 300 and 500 $kWcm^{-3}$. As one of the aims of the system is to experimentally verify these predictions the PFN was designed to supply a current pulse to the laser head so as to drive it at pump power densities in the range 100 $kWcm^{-3}$ to 1 $MWcm^{-3}$ by changing the PFN impedance and the PFN charging voltage.

The pump power density in a discharge is the product of the discharge current density and the glow discharge self sustaining electric field between the electrodes. In a typical $XeCl^*$ excimer gas mix the glow voltage in the head used was found to be of the order of 1 to 2 kV for an electrode separation of 9 to 16 mm, although this depends upon many factors such as the electron attaching/detaching properties of the gas. It therefore follows that the PFN should be capable of driving the laser head with current densities of up to 1 $kAcm^{-2}$. This is a useful figure for the study of laser efficiency and discharge stability.

Since the electrode area is approximately 25 cm^2 the maximum current to be supplied by the PFN is 25 kA. The voltage rating of the high voltage ceramic capacitors that were available limited the PFN to a maximum d.c. charge of 30 kV; even if higher

rated capacitors had been available the maximum rated hold-off voltage of the CX 1625 thyratron is only 35 kV. Taking the maximum charging voltage of the PFN to be 30 kV implies that the PFN should be designed to have an impedance of about 1.2Ω.

In practice pulse forming networks with impedances as low as 1.2Ω are difficult to construct using discrete components within the constraints of physical size dictated here. The main problems arise in accurately producing suitable air cored line inductances to the required value and achieving a small enough inductance in the thyratron current return loop. The PFN was built from a $^1/_8$" thick aluminium plate on to which pairs of ceramic 'doorknob' capacitors were tightly fixed, one each side of the plate. The plate was bead blasted to remove all sharp edges that might produce corona when charged.The pairs of capacitors were mounted on a square pitch at 6 cm centres to give 5 rows each consisting of 5 capacitors on each side of the plate. In all, 50 capacitors were used. Not all the capacitors available were of the same value but they were carefully chosen so that each row totalled a capacitance as close as possible to 11 nF on each side of the plate. Rows of capacitors were joined at their outer terminals by strips of copper sheeting. Line inductors were made from straight pieces of thick (16 SWG) tinned copper wire soldered between these strips connecting the capacitors together to form a double sided pulse forming network. The loop inductance of each connecting wire was estimated as between 200 and 400 nH, with 4 wires being used in parallel on each side of the network the total inductance of each stage was taken to be 50 to 100 nH each side.

The theoretical parameters of the PFN are as follows:

Total capacitance	110 nF
Calculated impedance	1.1 to 1.5 Ω
One way transit time	110 to 160 ns

The design of the laser head and discharge electrode apparatus was adapted from a similar machine constructed at Los Alamos National Laboratory, (3). The most important features are the relatively small electrode dimensions giving a small active volume of only

25 cm long by about 1 cm high with an electrode separation of between 9 and 16 mm. The electrodes were enclosed in a cylindrical chamber with an inside diameter of 20 cm with the electrodes displaced from the centre to allow space for the possible inclusion of a gas circulation blower. In reality no such blower was fitted as gas circulation proved not to be a problem at the low repetition rates employed.

The advantages of the compact, low active volume geometry are that the laser gas fill can quickly and conveniently be changed, at a relatively low cost, to allow different experiments to be undertaken. The cost factor should not be underestimated as the high purity rare gases required by excimer lasers are expensive and have risen in price substantially in recent years. It is therefore advantageous to have a laser system with as small a gas consumption as possible so that its scientific usefulness can be maximised for a given cost. The compactness of the design also has the advantage that despite high efficiency operation output pulses are of fairly low energy making safety considerations simpler.

It is a necessary condition for the formation of a stable glow discharge in a high pressure gas that some form of preionisation is employed. Although there is some doubt over the exact preionisation requirements for a rare gas halide excimer laser it is generally accepted that glow discharge stability, and hence laser performance, improves with increasing preionisation electron density up to a threshold level, (4). The uniformity of the preionisation is also known to be of prime importance, (5,6). Preionisation requirements are discussed more fully in chapter 1. For the purposes of the intended experiments all that was required was a clean and simple method of producing the required homogeneous preionisation electron densities with maximum reliability. For this reason the corona preionisation system using a silent discharge was seen as the best solution.

Fig. 2.2

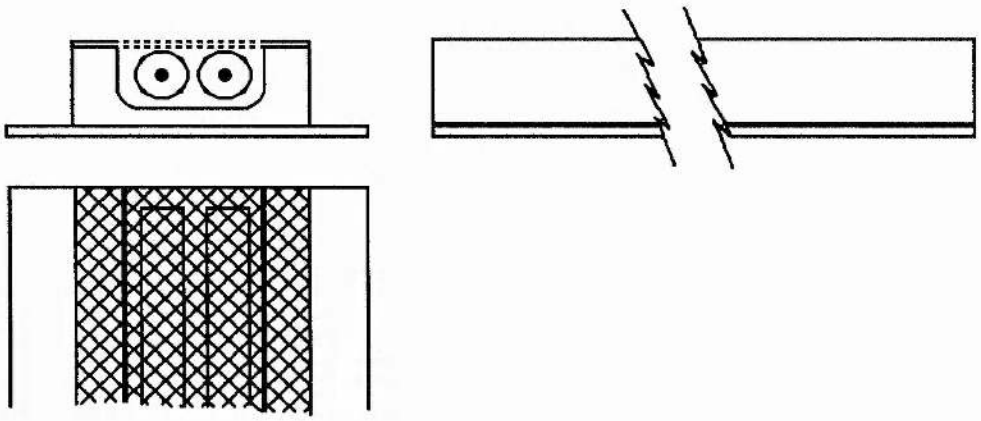

The corona preioniser shown diagramatically in Fig. 2.2 and a photograph of the anode incorporating the preioniser assembly is given in appendix 3.It was constructed from two fused alumina ceramic tubes into which were inserted copper wires to fill as fully as possible the space inside the tubes. The alumina tubes were readily available commercially and of dimensions 300 mm long by 4 mm in diameter with a 1 mm wall thickness. The tubes were carefully positioned within a slot machined into the body of the grounded electrode and the slot covered with a flat sheet of fine precision stainless steel mesh. This mesh formed the surface of the electrode and and therefore its flatness and uniformity were important. Great pains were taken to position the alumina tubes centrally within the slot with a small but uniform space around the tubes. The high relative dielectric constant of alumina, ~12, gives a fairly large capacitive coupling between the wires within the tubes and the electrode body while retaining a high dielectric breakdown strength. The capacitance between the wires and the electrode body was measured as 300 pF.

This capacitive coupling is essential for the efficient operation of the preioniser. A corona-like discharge is produced in the space within the grounded electrode surrounding the alumina tubes so that the resultant ultra-violet light preionises the gas by photoionisation through the mesh electrode surface. The amount of UV light produced, and hence the preionisation density, will increase with the corona discharge current given by:

$$J = C\frac{dV}{dt} \qquad 2.1$$

A small capacitor discharge device using a glass thyratron and capable of generating pulses in excess of 20 kV was obtained for pulsing the preioniser assembly. This unit was deliberately designed to produce a ringing waveform with high dV/dt so as to maximise the corona discharge current and hence the degree of preionisation.

The advantage of this preionisation system was its relative simplicity in relation to other alternatives such as X-rays or spark arrays. Many systems have been constructed with X-ray preionisation sources external to the laser head pressure vessel, (7,8). All such systems introduce engineering problems in that they require a relatively thin window into the pressure vessel penetrable by the X-rays without excessive attenuation. This makes the design of the pressure vessel more complicated if high buffer gas pressures are to be used, the absence of such windows when using the corona preionisation system allowed the pressure vessel to be built to withstand pressures of up to 10 bar.

The main problem encountered with the corona preioniser was the difficulty in accurately positioning the alumina tubes within the electrode body. Locating the alumina exactly centrally within the slot is essential for an even discharge and uniform preionisation as the device relies on capacitive coupling between the cores of the alumina rods and the electrode body. Preioniser lifetime was not found to be a problem provided that the preioniser voltage was kept below 20 kV so as not to stress the alumina excessively.

The main thyratron was switched by means of a specially constructed trigger generator of novel, all-solid-state design, (9). The construction of this trigger generator is described fully in appendix 1. Briefly, for maximum performance in terms of current switching rate, the CX 1625 requires a current pulse of about 50 amps total to be applied to the two priming grids for about 1 μs followed by a fast rising voltage pulse of at least 1 kV amplitude applied to the control grid, (1). This is achieved by two pulse forming circuits, one for each of the priming and control grids, each switched by a thyristor and synchronised with respect to each other by a delay section. Traditionally the trigger circuitry for large thyratrons has made use of other, smaller thyratrons with the consequent circuit complexity, bulk and lifetime limitations of gas filled devices. By using this new

design maximum thyratron performance can be obtained while gaining the cost and reliability advantages of solid state circuitry.

The laser head vessel was constructed from a rolled stainless steel flanged tube of internal diameter 20 cm by length 30 cm. The flanges were fitted with 'O' ring grooves to form a gas tight seal with the two end plates using Viton ™ 'O' rings. The end flanges of the head were fitted with adjustable pressure window mounts to allow 50 mm diameter windows of up to 10 mm thickness to be used. Excimers such as $XeCl^*$ can make do with fused quartz windows but fluorine based excimers require more expensive CaF_2 or MgF_2 windows due to their fluorine compatibility and superior transmission bandwidth. The head vessel was hydraulically tested to 120 psi.

All gas tight pipe work including the manifold to which all the gas cylinders were connected was made up from grade 316 stainless steel. This material was chosen for its high corrosion resistance and its low reactivity with fluorine and hydrogen chloride. Even so thorough passivation was required before reliable laser operation could be achieved. The manifold was built from $^1/_4$" diameter tube while the pipe from the manifold to the laser was larger $^1/_2$" diameter, this was to improve the gas evacuation rate in the manifold by the vacuum pump located close to the laser head. All pipe joints were made using 'Swagelok' stainless steel pipe unions.

The PFN and laser head assembly was securely mounted onto a cast iron surface table. Photographs showing the arrangement of the PFN and the thyratron mount are given in appendix 3. The thyratron was fixed to the table by a bracket made from $^1/_2$" aluminium plate and connected to the end of the PFN by a short length of copper braid, this allowed a small amount of relative movement between the PFN and the thyratron without placing mechanical stress on the thyratron. The thyratron was securely mounted on the bracket by the mounting flange connected to the cathode, the bracket also helped cool the thyratron by conducting unwanted heat away to the table top. Additional cooling was provided by two free mounted, mains operated fans, as the CX 1625 is fitted with cooling fins to allow forced air cooling. The cooling requirements in this case were not too demanding as only low repetition rate operation was planned. The optical resonator was made up by a pair of

external multi-layer dielectric mirrors in adjustable mounts fixed to the table surface by magnetic clamps. For safety the high voltage parts of the PFN were enclosed in a large clear perspex cover.

The CX 1625 requires both cathode heater and reservoir heater power supplies. Although it is possible to run both off the same supply, for best results it is better to have a separate reservoir supply so that the internal gas pressure can be adjusted until the tube only just holds off the required voltage until triggered. In this way the switching rate performance of the thyratron is maximised. Thyratrons work on the left half of the Paschen breakdown curve; an increase in reservoir heater voltage corresponds to an increase in tube pressure and a reduction in hold off voltage. Cathode and reservoir supplies were built using variable mains transformers and voltage step down transformers and connected using wire suitable for the large currents involved, which may be as high as 45 amps in the case of the cathode heater.

Accurate synchronization of the different elements constituting the laser system is essential for reliable, reproducible performance. The initial trigger source was from a pulse generator box producing +10 V pulses (open circuit) with a 15Ω output impedance. The pulse generation frequency was variable within the range 0.5 to 100 Hz although only the slower rates (<5 Hz) were used for triggering the laser. The pulse from this trigger source was fed to the preioniser driver and main thyratron trigger generator by 50Ω coaxial cables using BNC fittings. The delays required between these elements were provided by varying the length of the cables, as a general rule of thumb an electrical signal was taken to propagate down a coaxial cable at a rate of about 5 ns for every metre. The layout of the various elements of the system is shown in fig. 2.3.

Fig. 2.3

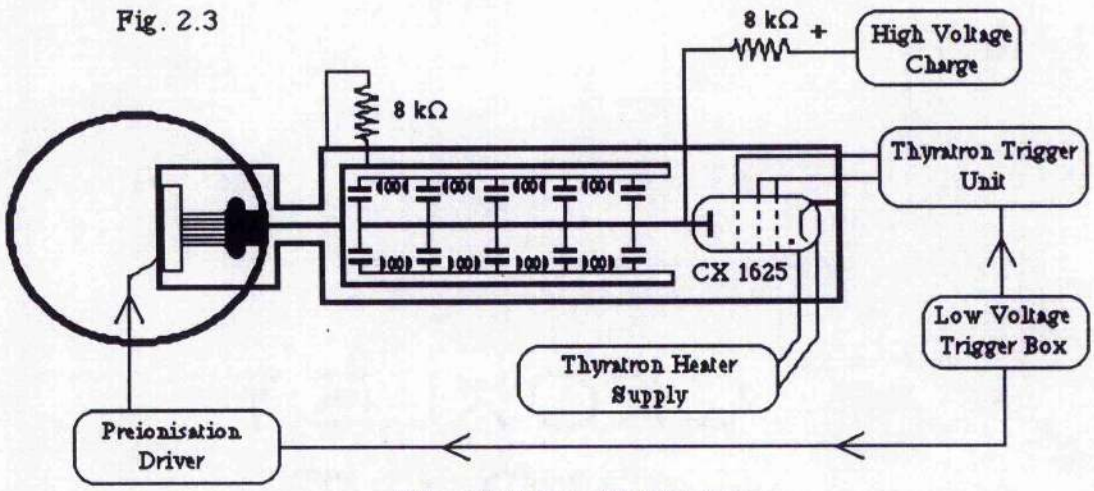

Schematic layout of the laser system

Initially problems were experienced with spurious firing of the preioniser and/or main thyratron due to the pick up of false signals. The thyratron, switching kA currents in time scales of tens of ns, produces an electrically noisy environment. This is one of the reasons for using passive delay elements rather than active delays based on low voltage electronics. Reliable firing of the laser was achieved by placing the trigger box as far away as possible from the laser, by carefully routing cables away from the thyratron and by putting delay sections into lines carrying high voltages where ever possible, i.e. between the thyratron trigger generator and the thyratron rather than on the input side of the thyratron trigger generator. Eventually after some trial and error it was possible to synchronise the firing of the main thyratron with the preioniser driver, reliably and with a sub 10 ns jitter.

2.3 Testing the PFN into a Dummy Load

Before lasing experiments could begin it was necessary to test the electrical characteristics of the pulse forming network (PFN) to check agreement with the theoretical parameters listed in the following table.

Double Pulse Forming Network	
Maximum charging voltage	30 kV
5 rows of 5 capacitors each side	
Capacitance per row	11 nF
Total capacitance	110 nF
Inductance between each row	50 - 100 nH
Estimated network impedance	1.1 - 1.5 Ω
One way transit time	110 - 160 ns

Note: the imprecision in the estimates of the network impedance and the one way transit time arises mainly from the difficulty in estimating the value of the line inductors.

Two resistive loads were built to fit into the laser head in place of the grounded anode so as to occupy the inter-electrode space. The first of these loads, shown photographically in appendix 3, consisted of a rectangular perspex block with copper plates glued to opposite faces. The larger copper plate was designed to replace the anode while the opposite, smaller plate butted hard up against the hot electrode (cathode). To ensure a good electrical connection a strip of electrically conducting rubber was placed between the cathode and the small plate, the large contact area ensuring that the rubber pad had a negligible resistance, substantially less than one ohm. Twelve moulded carbon, low inductance, resistors were soldered between the copper plates, each resistor was nominally 47Ω and the total parallel combination was measured as 4.0Ω. The advantage of this load is that it is very simple to use and the resistance is accurately known, the inductance presented by the load will be very similar to the laser discharge occupying the same space. Its main

disadvantage is that the current and voltage ratings of the carbon resistors limit the maximum voltage to which the PFN can operate.

For high voltage testing of the PFN a second load was constructed from a rectangular perspex box with copper plate electrodes built into opposite faces. This load fitted into the laser head in a similar way to the carbon resistor load, butting up to the cathode by a conductive rubber pad. By filling the load with an electrolyte such as copper sulphate solution and adjusting the electrolyte concentration the load resistance could be altered. This load was messy to use and it was difficult to accurately measure the load resistance but it could handle voltages up to the full design limits of the PFN.

Fig 2.4

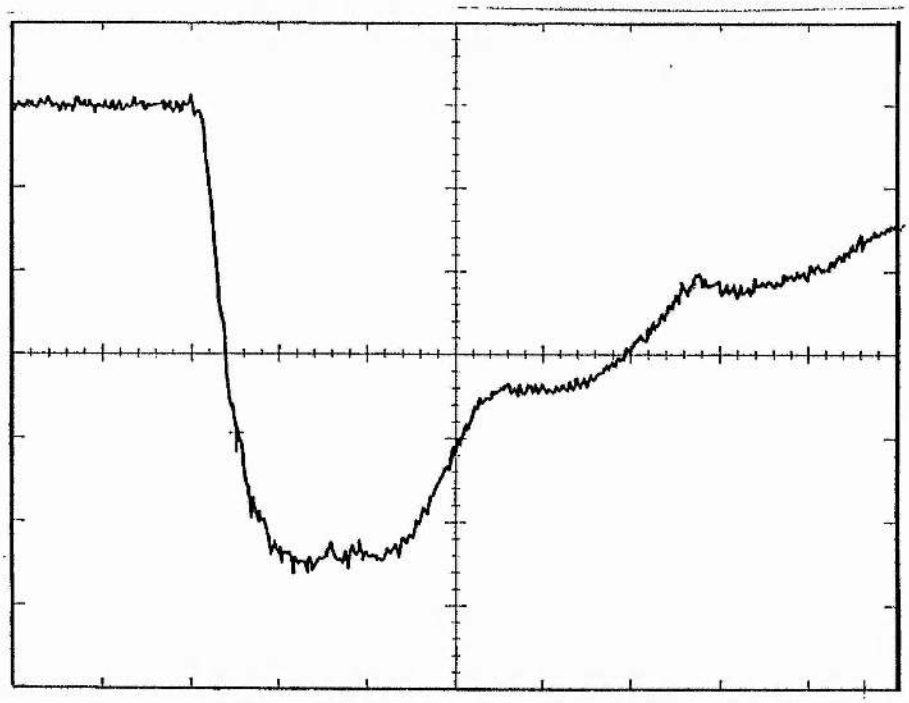

Voltage waveform across a 4Ω resistive dummy load, PFN charge 9 kV, 100 ns/div, 1400 V/div

Fig. 2.4 shows the voltage waveform across the 4Ω resistive load with the PFN charged to 9 kV. The stepped waveform was, as expected, characteristic of a PFN discharging into an over-matched load; the pulse duration is about 280 ns and the peak voltage of 7.5 kV indicates an impedance of about 0.8Ω. This value for the PFN

impedance is a little on the low side but gave a starting point for further experiments with the copper sulphate filled load.

Fig. 2.5 shows the PFN firing into the copper sulphate load set at 1.7Ω. Again a slightly stepped waveform was obtained indicating 1.7Ω to be slightly over-matched. Fig 2.6 shows the waveform from the load when set at 1.0Ω, the back swing indicating that this load is under-matched. Taking these results together it can be estimated that the effective PFN impedance is close to 1.5Ω and the two way transit time is about 300 ns ± 10 ns. The 10% to 90% voltage rise-time was measured from fig. 2.5 at 105 ns, this corresponds to a rate of rise of current of 60 $kA\mu s^{-1}$ which is within the expected operational limits of this PFN / thyratron combination considering the initial PFN charging voltage was only 15 kV.

Fig 2.5

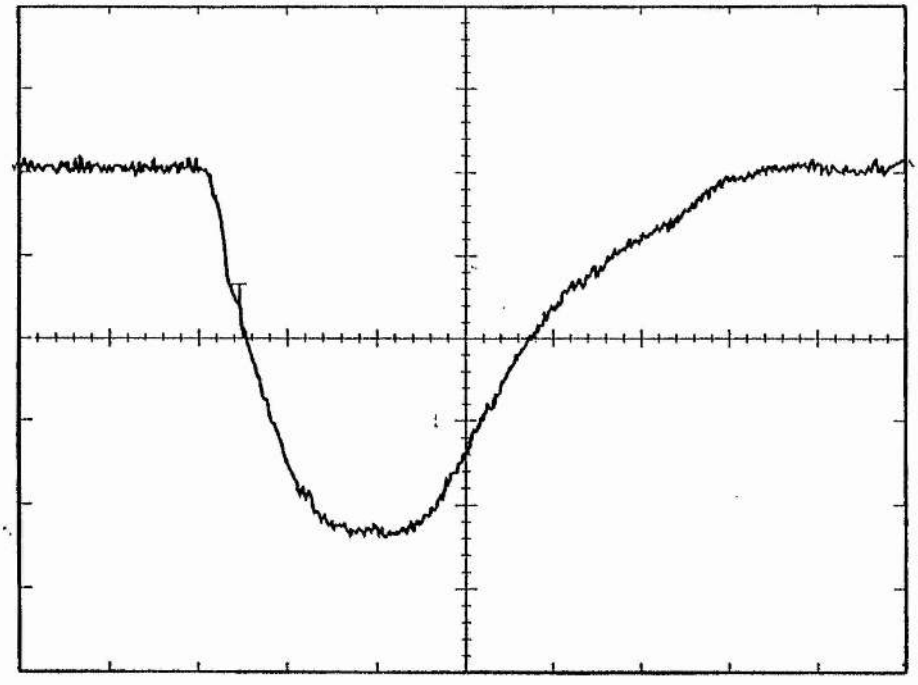

Voltage waveform across a 1.7Ω $CuSO_4$ load, PFN change 25 kV, 100 ns/div, 3.2 kV/div

Fig. 2.6

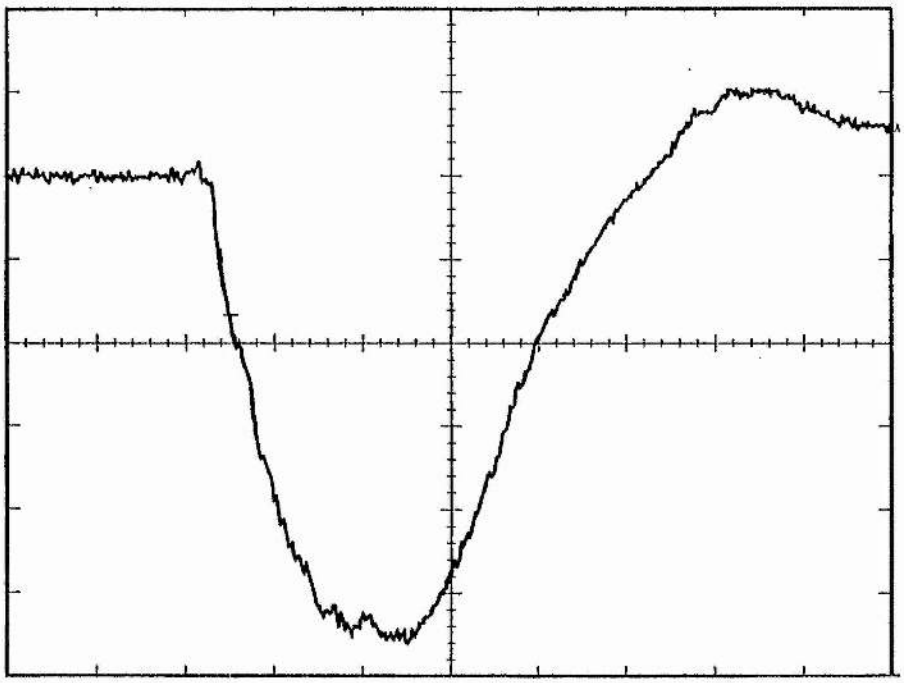

Voltage waveform across a 1.0Ω $CuSO_4$ load, PFN change 25 kV, 100 ns/div, 3.2 kV/div

2.4 Commissioning the Laser System

A series of commissioning experiments were carried out to determine the operating characteristics of the laser system and to check that the performance was comparable with that reported for similar systems elsewhere. The parameters determined during these tests serve as a bench-mark indicator of performance in subsequent experiments.

Although the the laser system was designed to operate with the whole range of rare gas halide excimers, $XeCl^*$ B→X (308 nm) was chosen for the initial trials. This is because $XeCl^*$ has been found to give the largest output energy and pulse duration of the rare gas halides and exhibits a relatively large small-signal gain. The halogen donor chosen for $XeCl^*$ was hydrogen chloride which although highly toxic and reactive is somewhat less dangerous than F_2 or NF_3 required by the fluorine excimers. Other chlorine donors such as Cl_2 or CCl_4 may be used although Cl_2 has an unfavourable absorption spectrum. Previous comparative studies have shown CCl_2F_2 to perform well, (10), but HCl was chosen because of its availability and its superiority over most other chlorine donors.

A series of parametric studies was carried out to optimise the laser output. The partial pressure of xenon was kept constant at 15 mbar, as previous experiments, (11), indicated that the laser output is only weakly dependant on xenon concentration. HCl partial pressure and the total buffer gas (Ne) pressure were varied as was the PFN charging voltage. Changing the PFN voltage not only changed the voltage rise-time but more importantly changed the head current profile and hence the pump power deposition. The electrode separation was set at 12 mm throughout the measurements.

Firstly the buffer gas pressure was kept constant and the HCl partial pressure and PFN charging voltage adjusted. The preioniser charging voltage was turned up until the laser output stabilized indicating that the threshold preionisation electron density had been reached. The results are shown in graph form in fig. 2.7.

While these results are interesting they are not particularly innovative as parametric studies of gas proportions have been carried out before with $XeCl^*$ lasers and obtained similar results. They do serve to confirm, however, that the system operated as expected. The results are less favourable than those obtained with a similar laser head but different thyratron, (12), but not sufficiently worse to cause concern. The differences in performance are difficult to explain fully but are most probably the result of the differing pulse power circuits used.

As the pulse durations in most cases were reasonably high but the pulse energies low, it was decided to repeat the experiments with a larger electrode spacing. The electrode separation was therefore increased to 16 mm so that the increased active volume would not only produce higher pulse energies but could also assist discharge stability and lead to longer pulse durations. The results are shown in fig. 2.8 and typical light output profiles and discharge current waveform is shown in fig. 2.9 for the gas mix 15 mbar Xe, 3 mbar HCl, 3 bars Ne.

Fig. 2.7

Graph of laser pulse duration against HCl partial pressure for various PFN charging voltages

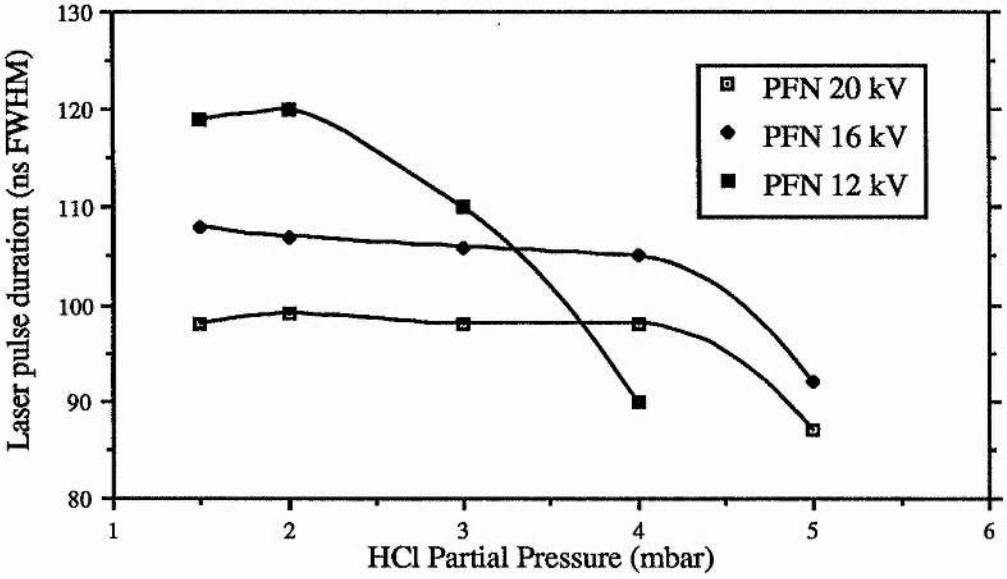

Graph of output pulse energy against HCl partial pressure for various PFN charging voltages

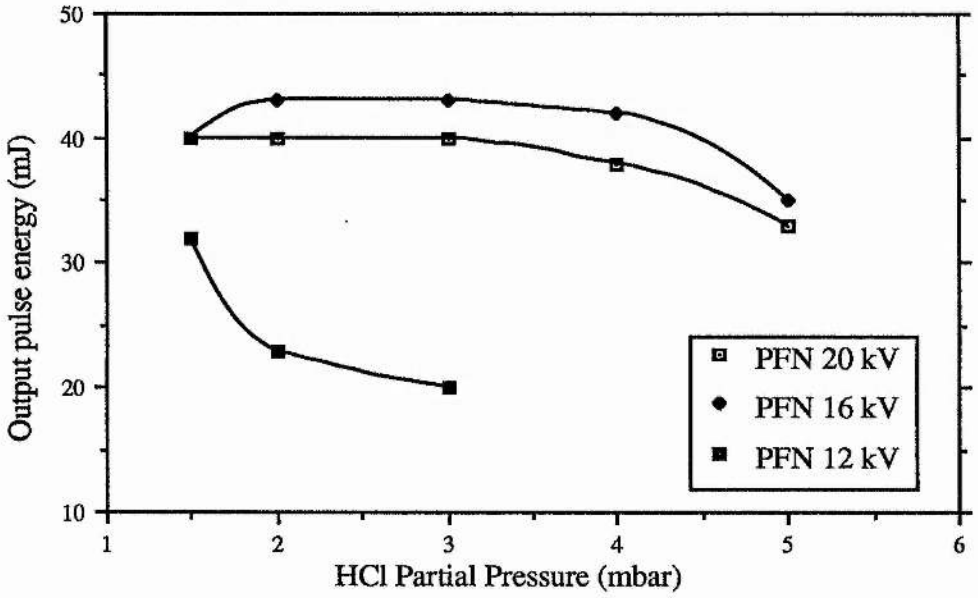

Fig. 2.8

This shows the improvement in performance with the increase in electrode separation. The longest pulse duration and the highest pulse energy were both obtained with a gas mix containing 3 mbar partial pressure HCl.

Electrode spacing 16 mm; mirrors 1 x HR, 1 x 40%R @ 308 nm; 2 x Fused silica pressure windows

Graph of laser pulse duration against HCl partial pressure for various PFN voltages

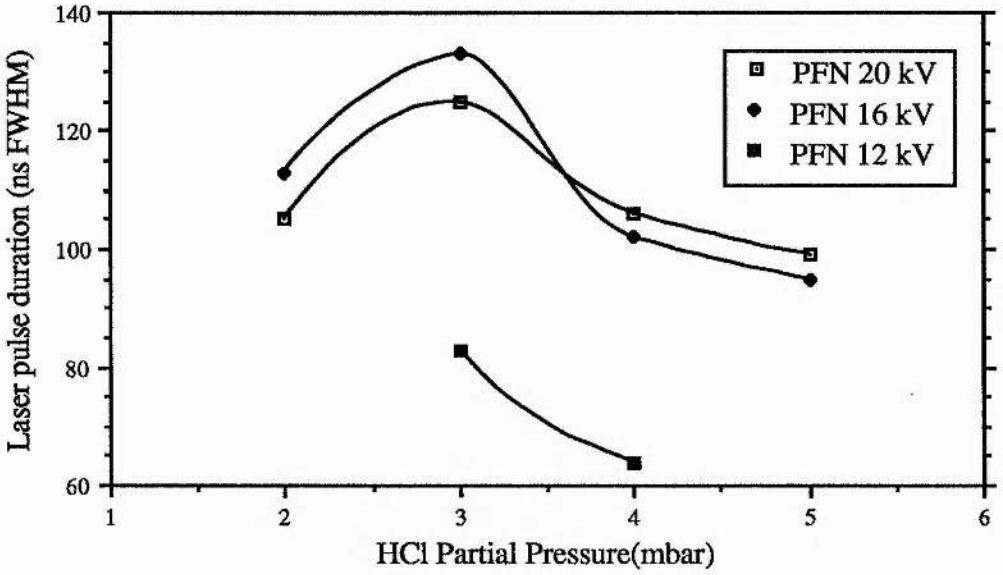

Graph of laser pulse energy against HCl partial pressure for various PFN voltages

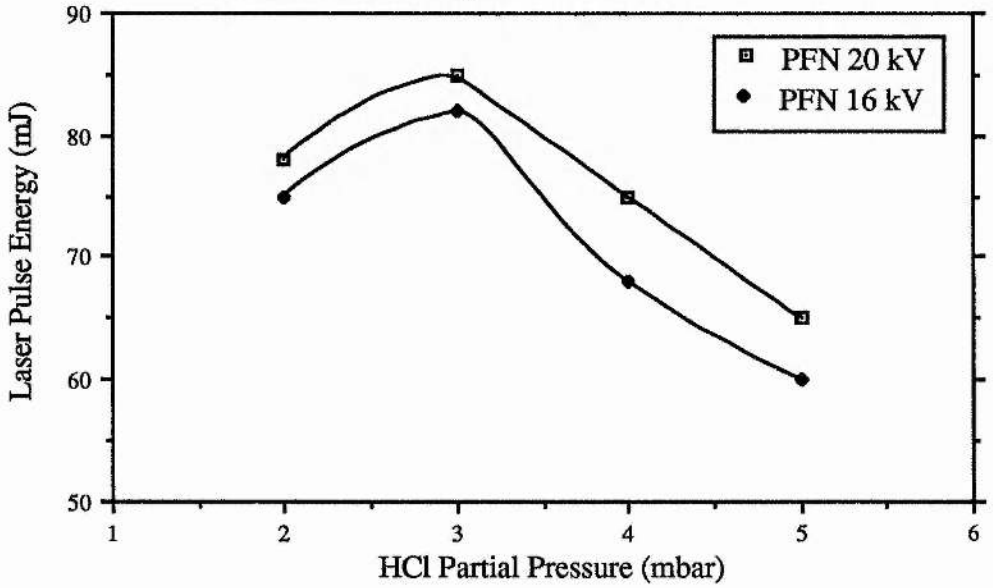

Fig. 2.9

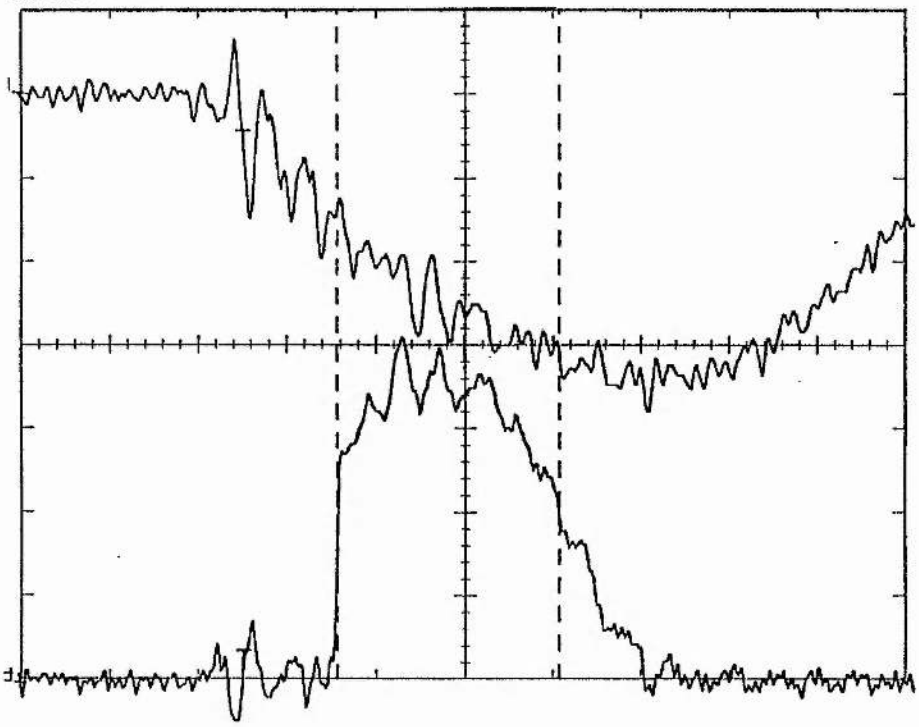

Light output profile in arbitrary units (bottom) and discharge current waveform (top) for 15 mbar Xe, 3 mbar HCl, 3 bars Ne; 16 mm electrode spacing, PFN charge 20 kV; 50 ns/div, head current 4.2 kA/div

An experiment was carried out to determine the effect of neon buffer gas pressure on laser output. The xenon and HCl partial pressures were kept constant and the PFN charging voltage was maintained at 20 kV. The results are shown in fig. 2.10

Fig. 2.10 shows that the best performance was obtained with a buffer pressure of 4 bar neon. Note that the results for 15 mbar Xe, 3 mbar HCl, 3 bar Ne do not agree exactly with fig. 2.8; although the pulse durations in fig. 2.10 are slightly shorter the pulse energies are marginally larger, this is typical of the small variations of around 5% or so in performance between similar gas fills. Note that in all cases where the pulse energies are large the accuracy quoted is approximately $\pm$ 2 mJ.

Fig 2.9
Graph of laser pulse duration against neon buffer gas pressure

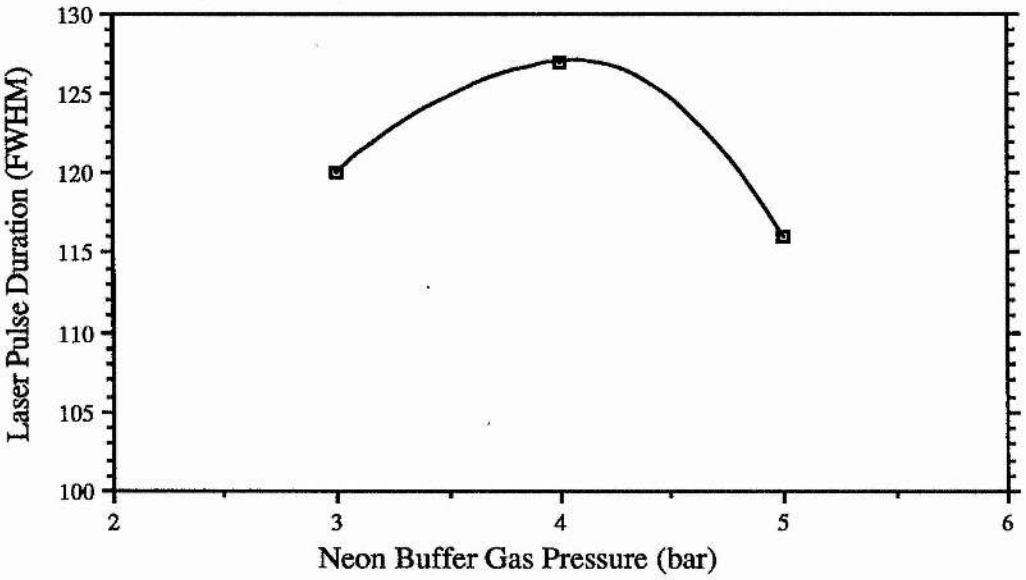

Graph of laser output pulse energy against neon buffer gas pressure

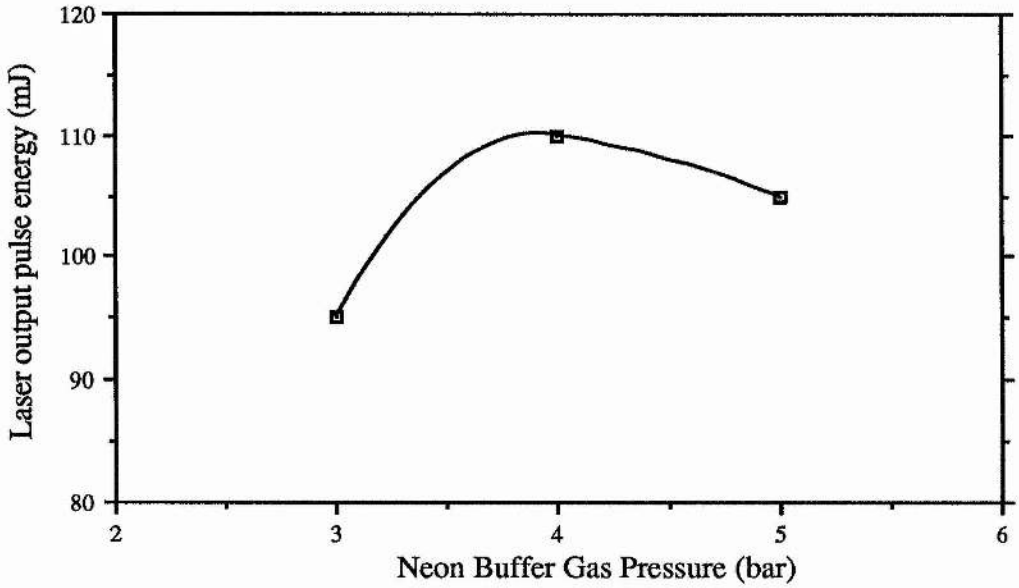

Electrode spacing 16 mm; mirrors 1 x HR, 1 x 40%R @ 308 nm; 2 x Fused silica pressure windows

Burn patterns were made onto heat sensitive paper to determine the beam profile. Taking the active volume to be 8 mm x 15 mm x 25 cm or 30 cm^3 overall and the maximum pulse energy as 110 mJ, this corresponds to 3.7 Jl^{-1} specific energy extraction. Higher specific energy extractions, in excess of 4 Jl^{-1}, have been reported in systems purpose-designed for high efficiency operation, (13), and also in a very small active volume, high density pumping device where 21 Jl^{-1} has been achieved, (14), but this is a special case. A comparison with results reported for other similar systems, (15-17), confirms that 3.7 Jl^{-1} is a respectable performance for this laser.

References

1 "Hydrogen Thyratrons," EEV Product Data
2 M M Turner, P W Smith; "Modelling of Excimer Laser Glow Discharges;" Proc. of the 9th International Conference on Gas Discharges and their Applications, p725-9,Venice, 1988
3 R C Sze; "A High Repetition Rate, Inductively Stabilized Long Pulse Excimer Laser;" Gas Flow and Chemical Lasers, 1984; Proceedings of the Fifth International Symposium, Oxford, 20-24 Aug 1984 (Bristol, Adam Hilger, 1985, p227-32)
4 J I Levatter, S-C Lin; "Necessary Conditions for the Homogeneous Formation of Pulsed Avalanche Discharges at High Gas Pressures;" J. Appl. Phys, vol 51(1), p210-22, 1980
5 V Hasson, H M von Bergman; "Spatial Control of Pulsed High-Pressure Pre-ionisation Stabilized Glow Discharges;" J. Phys. E, vol 13, p632-8, 1980
6 M Bahr, W Botticher, S Choroba; "The Time-Dependent Development of the Macroscopic Instability of a $XeCl^*$ Laser Discharge;" IEEE Transactions on Plasma Science, vol 19(2), p369-78, 1991
7 H. Shields; "Preionisation Techniques for Discharge Lasers;" Pulse Power for Lasers II, p15-23, SPIE, Los Angeles, 1989
8 F A van Goor, W J Witteman; "X-ray Preionisation for High Repetition Rate Discharge Pumped Lasers;' Gas and Metal Vapour Lasers and Applications, p91-102, SPIE, Los Angeles, 1991
9 A Dick; MSc. Report, University of St. Andrews, 1991
10 M R Osborne, "Rare-Gas-Halide Discharge Stability;" Appl. Phys B, vol 45, p285-91, 1988
11 S A Fairlie, Experiments carried out at AEA Culham, Oct 1990, Unpublished
12 P W Smith, Experiments carried out at Los Alamos, 1987, Unpublished
13 M R Osborne P W Smith, M H R Hutchinson;"The Effect of Pulse Forming Line Impedance on the Performance of an X-ray Preionised XeCl Discharge Laser;" Optics Comms. vol 52 (6), p415-20, 1985
14 D Lo, J Xie;"High Pressure Scaling of a High Current Density XeCl Laser;" J Phys. D, vol 24, p1023-4, 1991
15 W H Long Jr, M J Plummer, E A Stappaerts; "Efficient Discharge Pumping of an XeCl Laser Using a High-Voltage Prepulse;" Appl. Phys. Lett, vol 43, p735-37, 1983
16 I V Chaltakov, I V Tomov, Ch G Christov; "An Efficient High Pressure XeCl Discharge Laser with UV Preionisation;" J Phys E: Sci, Inst, vol 19, p1034-6, 1986
17 J Meyer, A Y Elezzabi; "Experimental Study of the Electron Density and Discharge Dynamics in a XeCl Excimer Laser;" J. Appl. Phys, vol 68(8), p3838-43, 1990

Chapter 3

The Application of Nonlinear Pulsed-Power Techniques to the Pumping of an XeCl* Laser

3.1 Introduction

One of the major foci of attention in the recent development of discharge pumped excimer lasers has been the design of repetitive pulse power supplies capable of delivering electrical power into the discharge at the optimum level to ensure good laser efficiency. It is believed to be advantageous, not only for good efficiency but also for discharge stability reasons, as detailed in chapter 4, that this optimum power level be achieved as quickly as possible. The optimum pump power density for efficient laser performance can be assessed either by experiment or by computer codes that model the behaviour of discharge pumped excimer lasers. A typical graph of laser efficiency as a function of pump power density calculated by a comprehensive XeCl* discharge code (1) is shown in fig. 3.1. The curve predicts that efficiencies of greater than 4% should be achievable at pump power densities between 300 and 700 $kWcm^{-3}$. This result implies that for an efficient laser pulsed power supply, power should be switched into the discharge so as to reach this range of pump power densities as quickly as possible and maintain it there for the full duration of the laser output pulse.

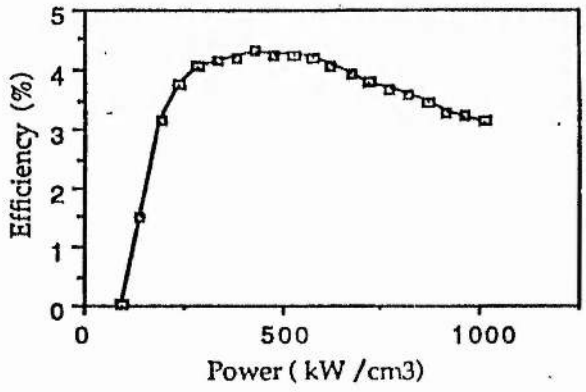

Fig. 3.1 Theoretical XeCl laser efficiency as a function of power density

None of the considerations so far have taken into account stability of the high pressure glow discharge. The glow discharge must exist with a high degree of homogeneity throughout the entire pulse duration. It is generally accepted that good discharge stability requires the voltage across the discharge electrodes, prior to breakdown, to rise on a time scale of 100 ns or less. The work presented here however indicates that too fast a voltage risetime may also have a detrimental effect on discharge stability. A fuller treatment of the factors believed to influence discharge stability is presented in chapter 4.

Low inductance rail-gap switched power supplies have been built which can achieve both a good rate of rise of pump power density and voltage rise-time across the the discharge electrodes, these spark-gap switched supplies can not be used however for high repetition rate systems or those required to have lifetimes in excess of 10^8 shots. Thyratrons can easily meet the shot lifetime requirements but unfortunately the current switching rates of the majority of commercially available types are too slow. This problem has been partly resolved by the development of ceramic thyratrons with very high current switching rates, (2), by the use of multiple paralleled thyratron arrays, (3), or by the use of magnetic compression circuits, (4),(5). This chapter describes a new type of pulsed power supply capable of meeting both the pump power density and voltage rise-time requirements. The electrical energy supplying the discharge is fed from a nonlinear pulse forming network built using high voltage ceramic capacitors specially selected for their strong nonlinear voltage characteristics. The network was shown to switch current into the discharge at a rate of up to 680 $kA\mu s^{-1}$ with a voltage rise-time of less than 50 ns. The network was switched with a CX1785 glass thyratron, the current switching rate of which (quoted by the manufacturers as 50 $kA\mu s^{-1}$ maximum) is not normally fast enough for use in conventional discharge excimer laser power supplies.

The laser driver circuit was constructed in a modular fashion so that direct comparison could be made between the conventional circuit containing a ceramic thyratron described in chapter 2 and the nonlinear circuit with glass thyratron. In this way the usefulness of the nonlinear capacitors can accurately be assessed.

3.2 theory of nonlinear pulse forming networks

The theory by which high voltage electrical pulses can have their leading edges sharpened by pulse forming networks containing nonlinear capacitors has largely been resolved. A fuller treatment of the theory is described elsewhere, (6),(7) as are methods for the theoretical analysis of pulse shaping by nonlinear means, (8). It is however relevant to explain in detail these concepts.

The theory of simple, linear, pulse forming networks is fully described in chapter 2. The simplest network that has been considered is a multi-section LC ladder in the form of a delay line as shown in fig. 3.2. In contrast to conventional magnetic compression circuits the ladder is uniform, that is each section of the ladder is identical and comprises an air-cored inductor and a nonlinear capacitor. If a high voltage pulse is injected into the line, the rise-time of its leading edge is progressively reduced as the pulse propagates causing the front of the pulse to be sharpened. The pulse sharpening process results from the voltage dependence of the phase velocity of the signals propagating along the ladder which is in turn a consequence of the the voltage dependency of the nonlinear capacitors. In an unbiassed line with no dc. offset, the crest of the pulse travels with the highest phase velocity and tends to 'catch up' with the low amplitude portion of its leading edge.

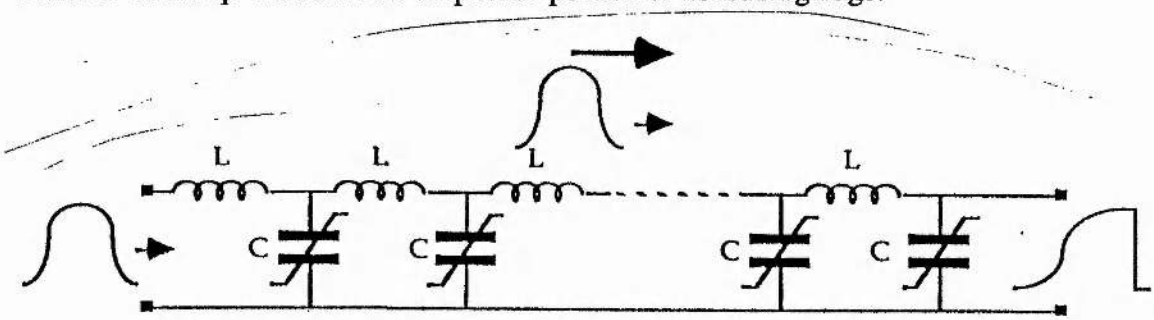

Fig. 3.2 Pulse sharpening in a nonlinear delay line

This pulse sharpening effect has previously been observed at voltages in the region of 10V using reverse biassed varactor diodes as voltage dependent capacitors. Success has also been achieved at voltages as high as 100 kV with distributed transmission lines filled with saturable ferrite material as the nonlinear medium, (9),(10). The limitation on ferrite sharpening media is the rate at which the walls of the magnetic domains within the ferrite can

move to adjust to the applied field, (12), furthermore even in their saturated state, ferrites possess a significant permeability and the resultant inductance may prove problematic for some applications. Nonlinear ferroelectric capacitors provide an alternative method of extending pulse sharpening techniques to high voltages and powers, hence their application here in powering an excimer laser.

An estimate of the total rise-time reduction of the pulse (ΔT) from the input of the ladder network to the output is given by:

$$\Delta T = n\left[\sqrt{(LC_0)} - \sqrt{(LC_s)}\right] \qquad 3.1$$

or

$$\Delta T = n\sqrt{(LC_0)}\left[1 - \sqrt{C_s/C_0}\right] \qquad 3.2$$

where n is the number of sections in the ladder, L is the value of the ladder inductors, C_0 is the value of the capacitors at zero applied voltage and C_s is the value of the capacitors at an applied voltage equal to the peak amplitude of the pulse. There is a further complication however in that the shortest risetime that can be achieved will be limited by the cut-off frequency of the ladder network at the maximum applied voltage. The minimum risetime is therefore given by the expression:

$$T_{r,min} = \frac{\pi\sqrt{LC_s}}{2} \qquad 3.3$$

An unusual feature of the sharpening process that often occurs is the appearance of a high frequency oscillation modulating the pulse waveform. The amplitude of the oscillation is generally strongest in the middle and later sections of the ladder and is thought to be caused by the tendency of the pulse to break up into a soliton array, an effect that has been observed in nonlinear ladders using varactor diodes as nonlinear capacitors, (13). The appearance of these high frequency oscillations in the nonlinear laser driving circuits caused interesting experimental results described in section 3.4 and required a redesign of the equipment to solve the problems that arose.

In practice it is very difficult to calculate accurately the degree of pulse sharpening that can be achieved on a given line; practical nonlinear capacitors are not precisely first order nonlinear in their behaviour and at high dielectric stresses their capacitance tends to saturate, (see Fig. 3.4). The most effective method of predicting behaviour is to use a computer code to carry out a numerical integration of the nonlinear coupled equations which describe the current and voltage distribution on the line, (8).

3.3 The Nonlinear Capacitors

A special batch of ceramic capacitors with a strong nonlinear characteristic were produced for this series of experiments. The capacitors contain a ferroelectric dielectric based on barium titanate but without the suppressor which is normally added during manufacture to reduce the strong capacitance / temperature characteristics of barium titanate capacitors. The inclusion of a suppressor also has the effect of minimising the fall-off in capacitance with applied voltage which for most applications is a positive benefit. As a result the capacitance of these special nonlinear capacitors at their maximum operating voltage generally drops to below 50% of the value measured at zero applied voltage; a useful property in this application as by equation 3.2 the catch-up time per stage depends upon the ratio of the stressed to unstressed capacitances. The chosen dielectric mix has a 2F4 temperature characteristic and a nominal dielectric constant of >10,000 at 25 ^{0}C. The dielectric disk contained within the capacitors was 10 mm thick and they have a design rating under pulsed conditions of 15 kV maximum, ie. a dielectric stress of 1.5 kVmm^{-1}.

The initial capacitance averaged out to approximately 3.7 nF although the range of values was large with most falling within the band 3.2 to 4.5 nF. It was discovered however that after operation in a ladder network this value tends to drop considerably due to a fairly rapid ageing process that occurs in this particular dielectric. Such ageing processes are familiar to manufacturers of ceramic capacitors and an ageing rate is often quoted as part of the capacitor specifications. The ageing effect of the capacitors used in these experiments was unfortunately found to be larger, and progress at a faster rate, than normal for commercial ceramic capacitors. While the full physical mechanisms that cause

ageing are unknown, the most likely cause is micro-cracking of the dielectric caused by the large mechanical strains resultant from the strong piezo-electric properties of this dielectric. Other experiments, (14) indicate that capacitors built with a layered dielectric structure, to relieve mechanical strain, exhibit a very much smaller ageing effect. This suggests that this type of construction could be used to build nonlinear capacitors with much better lifetime characteristics and work is progressing in this area.

Fig. 3.3

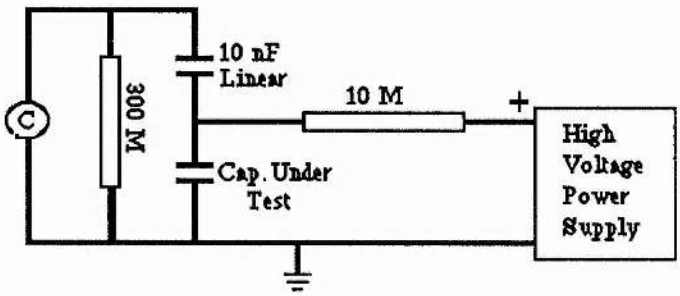

Nonlinear capacitor test circuit

To design the experiments effectively and to fully interpret the results it was necessary to measure the behaviour, and in particular the exact nonlinear characteristics of the capacitors.The differential capacitance, defined as dQ/dV, was measured at a range of d.c.bias voltages using the circuit in fig 3.3.

The purpose of the 10 nF linear capacitor was to d.c. isolate the capacitance meter from the bias supply, this results in the meter actually giving a value for the capacitance under test in series with 10 nF; the raw data therefore needed to be corrected accordingly to obtain the true differential capacitance. A representative sample of 7 of the special capacitors were tested in this manner at d.c. bias voltages from zero up to 16 kV. One of the capacitors was a 'virgin' capacitor with an initial capacitance of 4.3 nF while 5 of the others had previously been subjected to electric stresses in preliminary experiments as part of a ladder network for around 200 shots, these capacitors had initial capacitances in the range 3.1 to 4.2 nF. The final capacitor tested had also been operated as part of a ladder

network but its unstressed capacitance had dramatically fallen to only 0.8 nF. This behaviour was observed in an initially small but increasing number of capacitors as the experiments progressed.

The resultant graph is shown in fig. 3.4. The most significant feature is that regardless of initial capacitance all the capacitors fall to 0.8 ± 0.05 nF at 15 kV bias with the sole exception of the initially very low value capacitor which underwent a relatively modest fall to 0.45 nF. In general despite the unstressed capacitances covering a fairly wide range, the spread in capacitance diminishes quickly with increasing bias voltage and at biases above a few kV all the capacitors (with the one exception) exhibit remarkably similar behaviour. This is fortuitous as it allows an accurate value of the stressed capacitance, C_s, to be used in calculations and makes the construction of uniform nonlinear lines more certain despite the large range in initial capacitances.

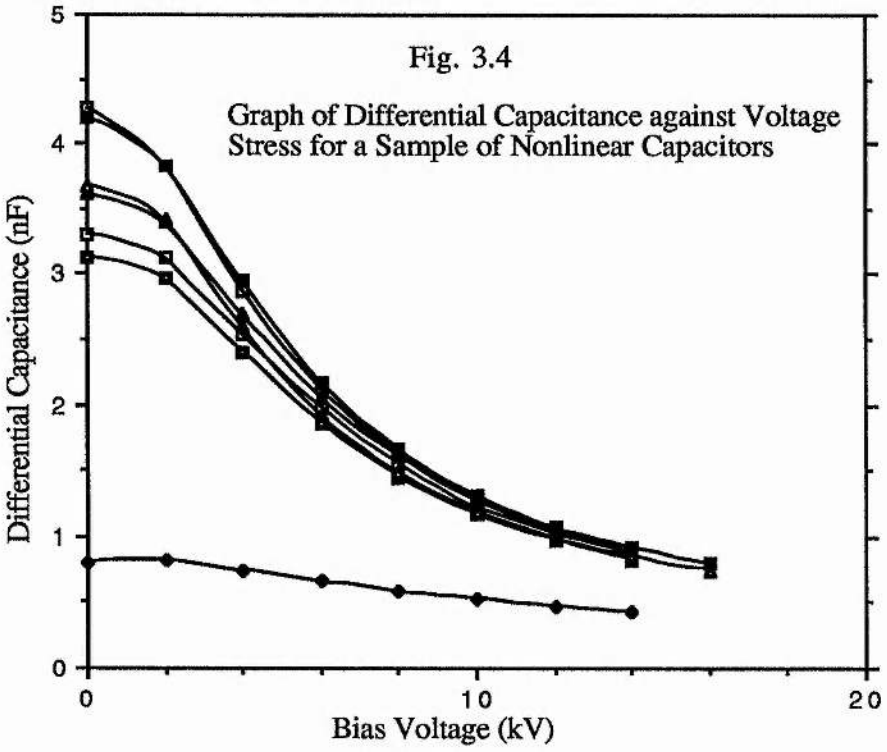

Fig. 3.4

Graph of Differential Capacitance against Voltage Stress for a Sample of Nonlinear Capacitors

A problem of more concern was the fall in unstressed capacitance with ageing. As described in section 3.2 for voltage rise-times larger than the frequency cut-off limit the

catch-up time per stage is greatest with a large initial capacitance. It was noted that as the experiments progressed the sharpening performance of the ladder networks deteriorated and it became necessary to regularly monitor the value of individual capacitors and replace those with low unstressed capacitances. The high dielectric stresses to which the capacitors were subjected also resulted in a number of total failures due to voltage flash-over damage.

3.4 Experimental Details

The method chosen for using the nonlinear capacitors to sharpen the voltage pulse used to drive the laser was to construct a ladder network from nonlinear capacitors and air-cored inductors and insert this between the existing linear pulse forming network (PFN) and the laser head. In this way the pulse generated by the PFN will propagate along the nonlinear network and the leading edge rise-time will be progressively reduced with increasing distance along the network, until the head is reached. The voltage rise-time across the head should consequentially be very fast, in comparison with conventional linear pulse power systems, resulting in rapid breakdown of the laser gas. The ceramic thyratron was substituted for a glass type CX 1785 in a low inductance housing as the very high current switching rate of the ceramic thyratron was not required. A photograph of the glass thyratron in its low inductance housing is given in appendix 3. The experimental arrangement is shown in fig. 3.5.

Fig. 3.5

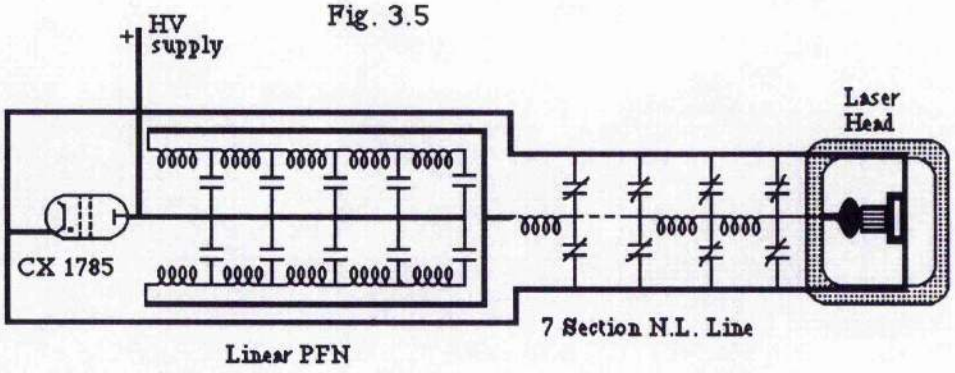

The uniform nonlinear discharge circuit

Initially it was foreseen that voltage reflections between the PFN and the nonlinear network could present problems and the nonlinear network was constructed to impedance match the PFN as closely as possible. This was a difficult task as by its very nature the impedance of the nonlinear section is voltage dependent making a perfect match impossible. The catch-up time per stage is proportional to the square root of the value of the line inductors making it advantageous to use large inductor values given the constraints of the available capacitors and the required line impedance. The stressed line impedance will determine the discharge current and therefore the laser pump power deposition rate and so the width of the nonlinear network was chosen to give a stressed impedance appropriate for the expected optimum discharge current. Given these requirements it was decided to construct the nonlinear section from 3 parallel lines each with 7 stages. Each stage consisted of 2 capacitors and a line inductance of about 150 nH. The calculated properties of the nonlinear section are summarised in the following table:-

Stressed impedance (15 kV)	3.1 Ω
Unstressed impedance	1.4 Ω
One-way transit time (stressed)	110 ns
Approximate catch-up time per stage (ΔT)	30 ns

The nonlinear section was first tested into a dummy resistive load, the results are shown in fig. 3.6.

The load used was as described in chapter 2 and consisted of moulded carbon resistors with a value of 4.9Ω. Unfortunately this load could only operate at relatively low voltages and the maximum PFN charging voltage was limited to only 5 kV, consequentially the nonlinear capacitors only operated at low voltage stresses and behaved in a linear fashion. The waveform in fig. 3.6 does however confirm that the unstressed impedance of the nonlinear section is about 1.3Ω as predicted by calculation.

Fig. 3.6

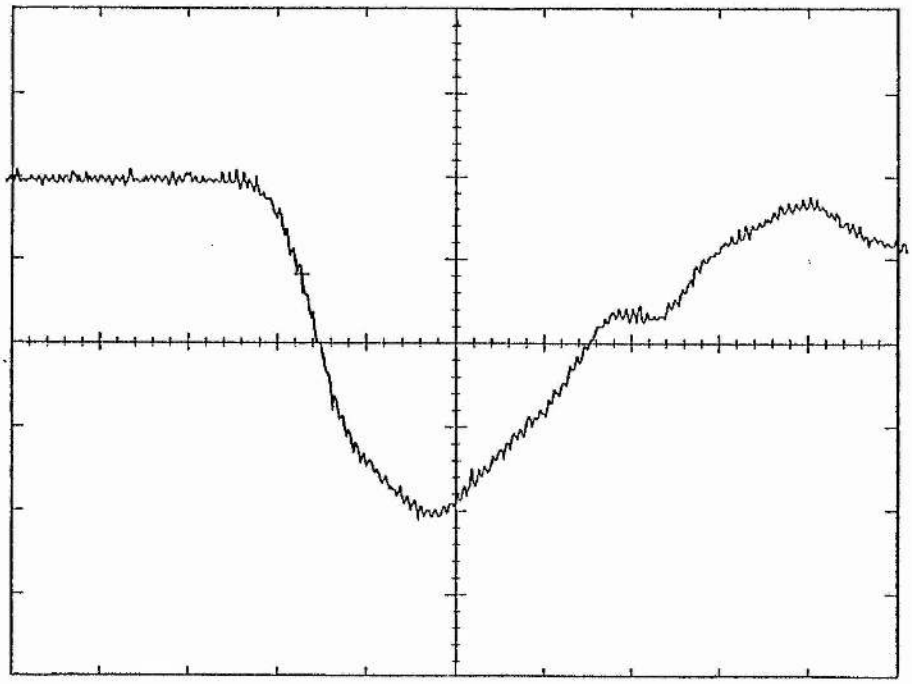

Voltage waveform across a 4.9 Ω resistive load, PFN charge 5 kV, 790 V/div. 100 ns/div

A purely resistive dummy load is a poor representation of the load the nonlinear section sees when firing into a laser head. When driving a laser the effective load is initially open circuit and therefore of infinite impedance until the laser gas breaks down, the impedance will then rapidly fall back as the glow discharge is formed. The glow discharge, once formed, does not have an impedance in the strict ohmic sense as the discharge current is dictated by the external circuit; the discharge is best approximated as a constant voltage load. It was not clear at this stage how the nonlinear section would interact with such a load and it was decided that further testing of the nonlinear section into dummy resistive loads would not be particularly useful. The decision was therefore made to proceed to pumping of $XeCl^*$ laser mixes.

The 'standard' gas mix as described in chapter 2 was used:-

15 mbar Xe

4 mbar HCl (80 mbar 5% HCl in He)

balance to 3 bar Ne

Fig. 3.7

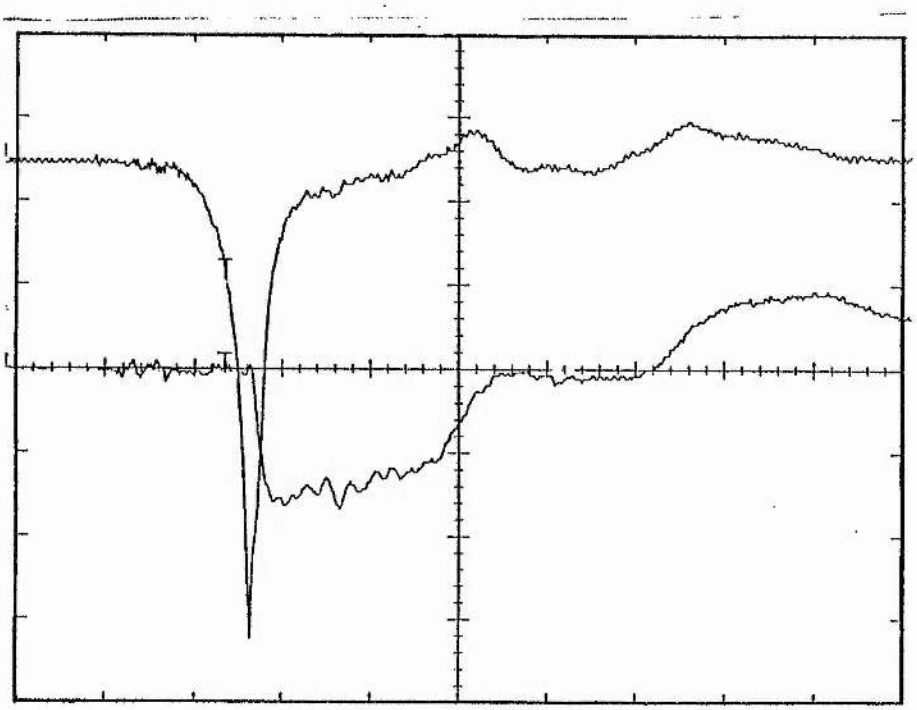

Oscilloscope traces showing laser head voltage (upper trace) and discharge current (lower trace) for a 3 line nonlinear section firing into a laser gas mix, PFN charging voltage 30 kV, head voltage 4.5 kV/div, discharge current 11.1 kA/div, 100 ns/div.

Voltage and current waveforms for the 3 line nonlinear section operating into such a gas mix with an initial PFN charging voltage of 30 kV are given in fig. 3.7. As can be seen the voltage rise-time is extremely short but the current rise-time is even more exceptional, reaching a maximum value of about 17 kA in 25 ns. This corresponds to a dI/dT of 680 $kA\mu s^{-1}$ which is remarkable considering the laser is switched by a single glass thyratron which, according to the manufacturers, is capable of a maximum direct switching rate of

only 50 $kA\mu s^{-1}$, (15). Furthermore the current waveform is close to the theoretical ideal and does not fall below 13 kA for at least 200 ns, meaning that the pump power deposition rate remains similarly constant.

Despite the encouraging features of the electrical characteristics of the pulsed power the actual laser performance was particularly poor. With mirrors of 100% and 60% nominal reflectivities output energy was at best 12 mJ per pulse with a duration of 35 ns FWHM. Returning for purposes of comparison to the commissioning experiments for the linear PFN and ceramic thyratron, with the same gas mix and optical resonator lasing commenced at a head current of about 6 kA and terminated at a head current of 11 kA (still rising). Taking the active volume to be 25 cm x 13 mm x 8 mm and the self sustaining voltage across the head to be 1500 V lasing therefore occurs at pump power densities in the range 350 to 630 $kWcm^{-3}$. These values agree with those predicted by theory for the ideal pumped power density (1) although it must be stressed that the value chosen for the self sustaining voltage was subject to an uncertainty due to the need to consider head inductance effects as the discharge current was not constant in this case. With a head current of 17 kA the pump power density is only 710 $kWcm^{-3}$ which is not unduly high. The current required to reach this pump power density was larger than in the linear system however and it was therefore concluded that the poor laser performance may be due, in part at least, to pumping the active medium at higher than the optimum current density for discharge stability. It has been observed by many workers that pumping excimer lasers at high discharge current densities leads to poor performance and premature termination of the laser pulse due to discharge instability, (16) and therefore the nonlinear section was reconstructed to deliver a smaller current into the discharge.

The nonlinear capacitors were designed to undergo their maximum fall in capacitance when biassed to 15 kV, consequentially there was a limitation on how far the discharge current can be reduced simply by lowering the initial charge on the PFN without the nonlinear benefits of the sharpening section being lost. The most effective way of tailoring the current pulse to the expected needs of the laser discharge was to reconstruct the nonlinear section to have a higher impedance by leaving only one line of 7 uniform stages.

The unstressed impedance of this single line was estimated at about 4Ω but again this was subject to a large uncertainty.

Fig. 3.8

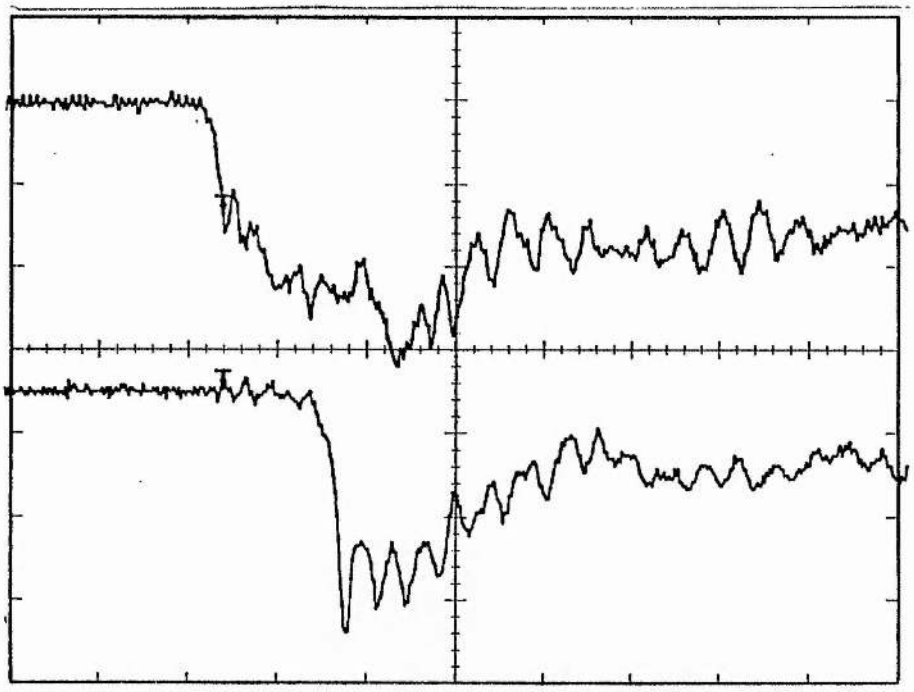

Single line nonlinear section tested into 10 Ω resistive load, PFN charged to 20 kV.
Upper trace, voltage input to N L section, 5.6 kV/div.
Lower trace, output voltage across load, 9.5 kv/div, 100 ns/div

The single line nonlinear section was fully tested into a dummy resistive load composed of low inductance, high power, carbon composition resistors. An example of the typical input and output voltage waveforms is given in fig. 3.8 for a main PFN charging voltage of 20 kV and a load resistance of 10Ω; the pulse sharpening effect can be clearly seen. Assuming the load to be purely resistive, the impedance of the nonlinear section can be calculated. Using results obtained with load resistances of 10 and 4.7Ω the effective impedance is seen to be around 2.5Ω. This is not an exact value but an equivalent based on observed behaviour. The smaller than predicted value of impedance was attributed to errors in the estimation of the line inductor values.

A necessary compromise was the abandonment of any attempt to impedance match between the PFN and the nonlinear section. This was found to be a problem as any strong reflections from the impedance mismatch would not reach the laser head for several hundred nanoseconds after which time lasing would have terminated due to one of the shut-down mechanisms. The main focus of attention was to produce a pulse close to the theoretical ideal profile for around 200 ns after which the pulse shape becomes to a large extent irrelevant.

The single nonlinear section was applied to the pumping of $XeCl^*$ using the same 'standard' gas mix as before. Traces simultaneously showing head voltage, head current and light output for an initial PFN charge of 16 kV are given in fig. 3.9. As can be seen the laser output was again somewhat disappointing with a pulse duration of only 40 ns FWHM and a pulse energy of 20 mJ. The current profile initially peaked at 8.8 kA but settled down to a fairly steady value around 7 kA which was maintained for the duration of the laser pulse and beyond. The fairly constant head current allowed an accurate estimate of the self sustaining voltage to be made and the pump power density was accordingly calculated to be 510 $kWcm^{-3}$ which is within the expected range for optimum pumping efficiency.

The reason for the poor laser performance was not forthcoming. It was speculated that with the rapid current turn-on lasing threshold is being achieved very quickly and for long pulse operation the pump power rate may have to be controlled with a higher accuracy than previously considered. In general long pulse durations have resulted from pumping at levels just above threshold to avoid halogen burn-up and the driving of associated discharge instability mechanisms, a fuller description of which are given in chapter 4. Again it was decided to further reduce the effective impedance of the nonlinear section to limit the discharge current to a value corresponding to the threshold pump power density.

Various configurations of nonlinear lines were tried involving removing some of the capacitors to leave certain stages with only one capacitor. Increasing the value of the line inductors was also tried. Non of these alterations changed the laser performance for the better.

Fig. 3.9

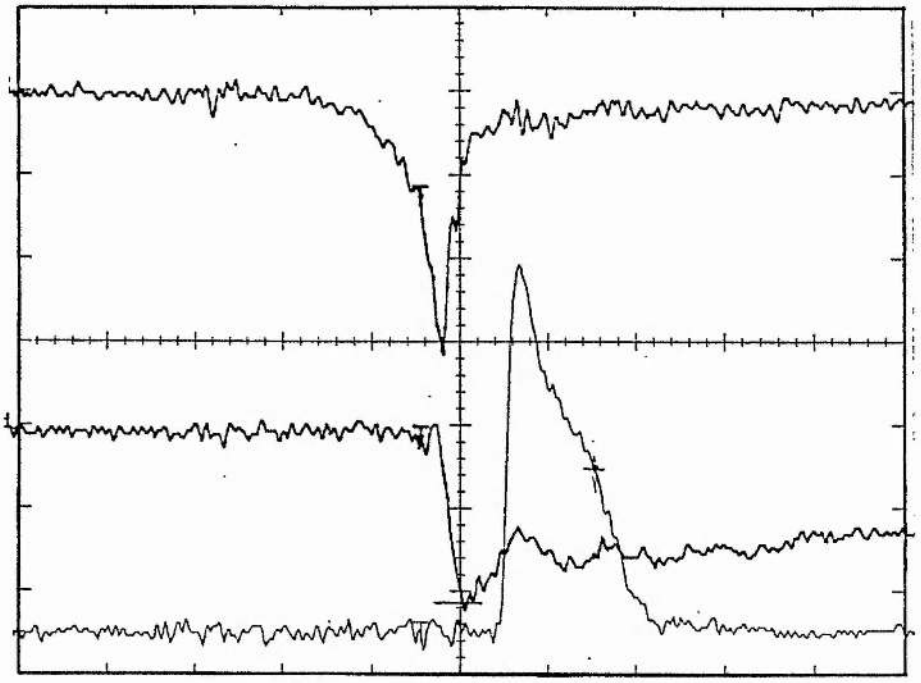

Laser head voltage (top trace), discharge current (middle trace) and light output (bottom trace) for a single 7 stage N L line, PFN charge 16 kV, head voltage 4.8 kV/div, discharge current 4.2 kA/div, 50 ns/div

It was noticed that voltage and current waveforms measured at the head were always modulated at a frequency of about 20 MHz. This effect can be seen in the trace showing the testing of the single 7 stage nonlinear line into the 10Ω dummy load, (fig. 3.8). This oscillation was seen with most of the nonlinear configurations tested but seemed to be largest in magnitude on lines with relatively large inductors; in fact it was the emergence of this large amplitude modulation in such lines which limited the extent to which the nonlinear line impedances could be increased by simply increasing the value of the line inductors.

At first the modulation was attributed to ringing between the capacitors of the final nonlinear stage and the laser head inductance. To test this theory the capacitance of the final stage was changed and extra small inductors were fitted between the end of the nonlinear line and the head, in all cases however the oscillation frequency remained close to 20 MHz

although the amplitude of oscillation did change. Simple voltage/current ringing could not therefore explain the effect.

Another possible explanation for the observed modulation is the formation of a soliton array. It is well known that solitons can form in systems where waves propagate through nonlinear media that are also frequency dispersive. The break up of a pulse into a soliton array has been observed before in nonlinear ladder networks, (6) and this effect has recently been put to use in proposals for the design of an ultra-fast burst mode pulse generator, (21).

The conditions for the formation of soliton arrays are specific in that the self phase modulation arising from the nonlinear response of the medium must exactly match the frequency dispersion of the system. For the formation of solitons on nonlinear discrete transmission lines the self phase modulation arises from the increase in phase velocity of the wave front with voltage due to the nonlinear voltage coefficient of the line capacitors. The dispersion on the other hand is partly due to the characteristics of the ladder network behaving as a low-pass passive filter with the phase velocity decreasing as the LC cut-off frequency is approached. Another mechanism that generates frequency dispersion results from the nonlinear frequency response of the capacitor dielectric due to the finite switching time of the ferroelectric domains. The formation of solitons will therefore depend on a combination of material and electrical properties of the transmission line.

By considering a real rectangular voltage pulse as a superposition of fourier frequency components it can be seen that the frequency component corresponding to the nonlinear effects and the dispersions being equal and opposite, should it exist, will grow into a soliton array. It therefore follows that *any* rectangular pulse with the necessary frequency components will develop into a soliton array provided that the transmission line is uniform ie. the nonlinear and dispersive properties stay constant along a sufficient length of line for the soliton array to form. The number of solitons and the amplitude of each one will depend on the amplitude and width of the initial pulse.

Turning to the specific example of the nonlinear line considered here it is difficult to quantify the various parameters that determine soliton formation. It can be seen however

that the strong voltage dependence of the nonlinear capacitors will result in a large nonlinear effect, previously estimated at 30 ns per stage for a 15 kV pulse. This must be balanced by a similarly large dispersion which will probably only occur as the LC cut-off frequency is approached. Using the stressed capacitance per stage of 1.6 nF in combination with a line inductance of 150 nH gives an estimate for the cut-off frequency in the region of 20 MHz, this however is subject to a large error due to the difficulty in estimating the line inductor values. It therefore seems feasible that at a frequency of 20 MHz the conditions for soliton formation could be satisfied leading to the formation of a soliton array at this repetition frequency. The formation of an electrical soliton array therefore provides a satisfactory explanation for the observed oscillations.

During the experiments to try and determine the cause of the 20 MHz modulation some unusual double pulse laser outputs were obtained. An example of such an output along with the circuit that produced it is given in fig. 3.10.

Although the current waveform is not particularly strongly modulated in this case, it appears that the pump power density is oscillating in such a manner as to give a double peaked laser output before termination. The time difference between the two peaks is close to 50 ns corresponding to an oscillation frequency of 20 MHz. It is probable that further peaks at 50 ns intervals would have been seen had lasing not terminated due to discharge instability. Although the usefulness of this effect is not apparent it is believed to be the first reported case of laser modulation by electrical solitons in the pulse power pumping scheme.

Fig. 3.10

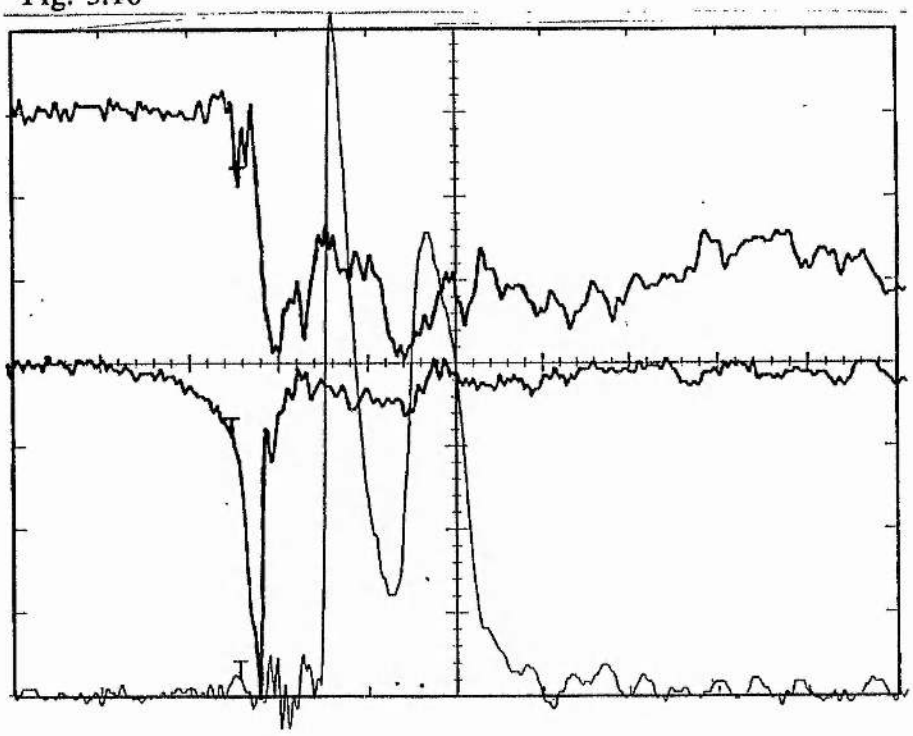

Discharge current (top trace), laser head voltage (middle trace), and laser light output (bottom trace), for an asymmetric N L line (see below), PFN charge 16 kV, head voltage 4.8 kV/div, discharge current 4.2 kA/div, 50 ns/div

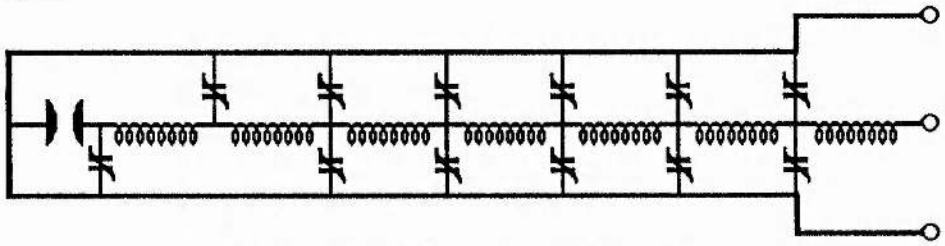

Nonlinear circuit that produced the outputs shown above

Having determined that the formation of electrical solitons in the nonlinear section were influencing the laser output it was questioned if this effect could be responsible for the premature termination and poor lase pulse energies seen so far. In many cases where poor laser performance was obtained the termination of the lasing coincided with a down turn in discharge current or a collapse in the self sustaining voltage. A particularly clear example is given in fig. 3.11 where the termination of lasing occurs in synchronization with a particularly violent fall in discharge current and the time-lag before the next upturn in current is long so that the discharge has probably collapsed making lasing impossible. It

was therefore concluded that further progress in extending laser pulse duration could only take place if soliton array formation could be suppressed.

Fig. 3.11

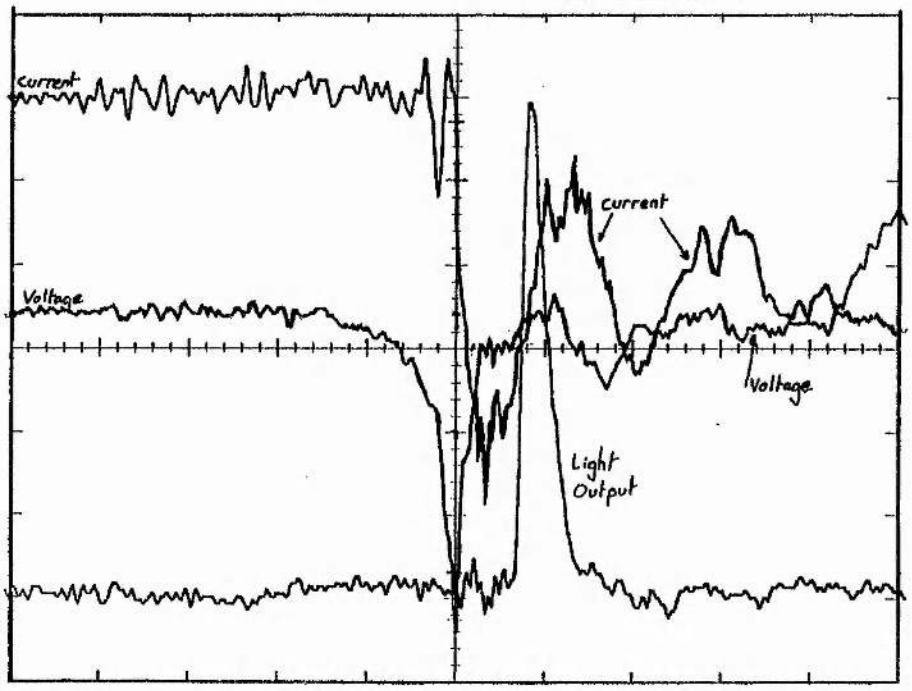

Premature termination of the laser output (bottom trace) due to soliton modulation of the discharge current. discharge current (top trace) 2.1 kA/div, head voltage (middle trace) 4.8 kV/div, 50 ns/div

To suppress the formation of solitons the uniform L C ladder network was replaced with a tapered equivalent. In the tapered line each stage consisted of a different number of capacitors and an inductance value carefully chosen so that the line impedance, $\sqrt{L/C}$, stayed constant. The first stage was built with a large capacitance/inductance combination with each subsequent stage halving the capacitance and inductance of the stage before. In this way the phase velocity of the pulse propagation increases moving along the line but by keeping the capacitace/inductance ratio constant the current pulse shape delivered into the laser head should remain close to the square ideal.

Such a tapered nonlinear network was constructed and is shown diagrammatically in fig. 3.12. Space considerations and availability of the nonlinear capacitors dictated that the nonlinear section could have only four stages, this however was felt to be adequate. It

is difficult to accurately calculate the catch-up time for this type of structure and so the network was designed from rough estimates of the catch-up time required for adequate sharpening, and from the need to maintain the impedance characteristic of each stage at the level required to ensure the desired pump power density.

Fig. 3.12

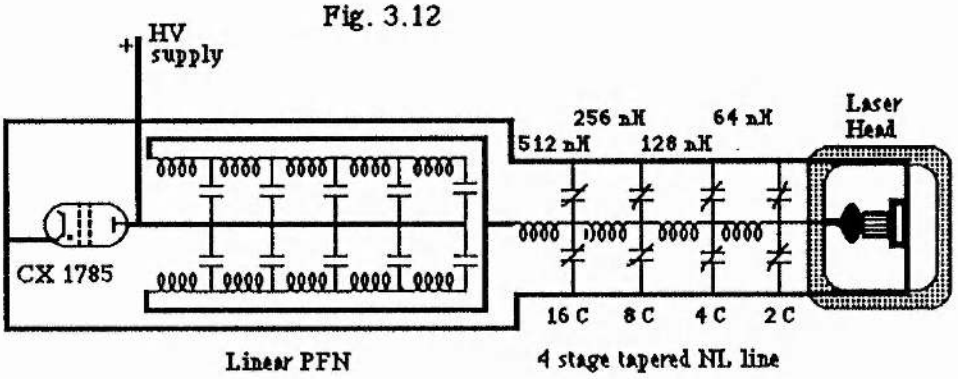

The tapered nonlinear discharge circuit

Fig. 3.13

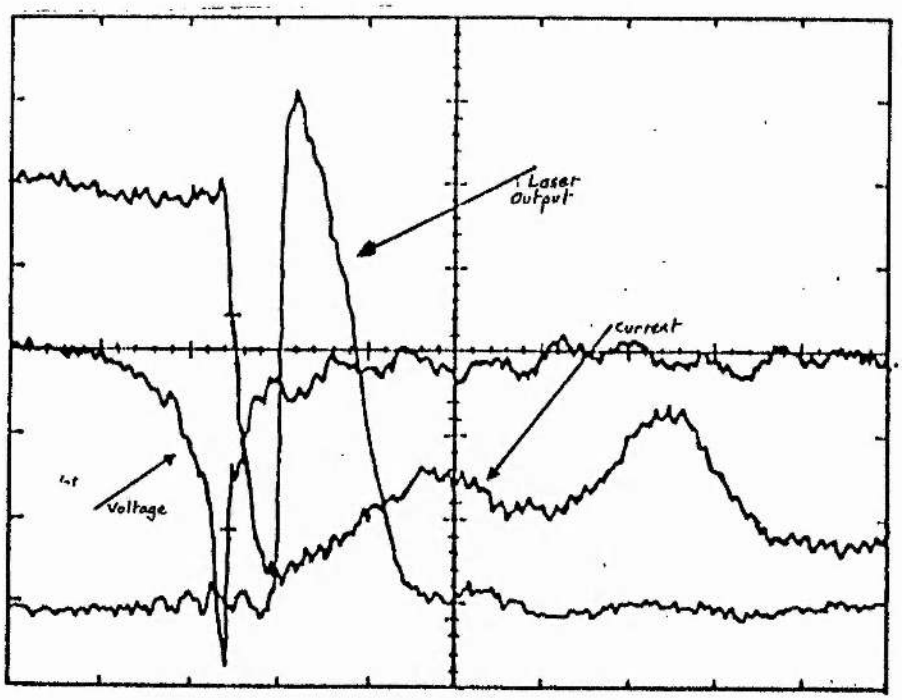

Fig. 3.13. Voltage, current and laser output waveforms for the tapered nonlinear discharge circuit shown in fig. 3.12. Voltage 4.8 kV/div. current 2.1 kA/div. 50 ns/div.

Operation with the standard gas mix under the same conditions as before gave an improved output energy of 30 mJ and a pulse duration of 45 ns FWHM. This was the best performance obtained in any of the nonlinear experiments The discharge voltage, discharge current and laser output profiles are given in fig. 3.13. It can be seen that although the laser output pulse has a smooth unmodulated profile the output pulse duration is considerably shorter than that obtained with the comparable linear discharge circuit described in chapter 2 ie. 55 mJ pulse energy and 100 ns FWHM pulse duration.

No experiments were carried out to test the repetition rate capabilities of the nonlinear capacitors because of their rapid ageing characteristics. It is thought however that if these ageing problems can be overcome there are no fundamental processes that should prevent operation at kHz repetition rates.

summary of experimental parameters

gas mix 12 mbar Xe
4 mbar HCl (80 mbar 5% HCl in He)
3 bar Ne

Pressure windows, 2 x 'Herasil' (fused quartz) plane parallel

Mirrors, 1 x HR and 1 x 40% R nominal @ 308 nm

PFN charge, 20 kV

4 stage tapered nonlinear section

Summary of best experimental results

Pulse duration 45 ns FWHM
Pulse energy 30 mJ

3.5 Conclusions and Possible Explanations

It is clear from the discharge current and voltage waveforms in the experiments with nonlinear networks that such circuits are capable of providing pumping conditions for the laser which are close to the theoretical ideal. The discharge voltage rises in a time which should be short enough for good discharge stability and the discharge current rise-time is fast enough for the optimum pump power density to be reached far more rapidly than with the linear discharge circuit. Indeed, the discharge current waveform shown in fig. 3.13 indicates that the discharge current is rising at the impressive rate of 400 $kA\mu s^{-1}$. Measurements of the discharge current and self sustaining head voltage, allowing for head inductance effects, give an estimated pump power density during lasing of 300 $kWcm^{-3}$ which is close to the theoretical ideal.

The question arises as to why the laser pulse terminates prematurely. The existence of some hidden experimental problem was discounted by estimating the intrinsic efficiency of the laser with both the linear and the nonlinear circuits. This estimate was made by dividing the laser output energy by the electrical energy deposited in the active medium up to the termination of the laser pulse. In both cases the efficiency was estimated to be around 4%, which is close to the maximum theoretical efficiency expected from fig 3.1, (1). It therefore appears that a fast turn on of current is deleterious in some way to the stability of the high pressure glow discharge that pumps the laser. The mechanism for this driving of the glow discharge into the arc state however remains unclear.

Little work has been done on the effects of current rise-time on discharge pumped excimer lasers because few previous discharge circuits have been fast enough to carry out an adequate study. One possible possible explanation that was considered was the realisation that if the current rise-time is sufficiently fast the discharge current will be confined to the outside edges of the discharge volume by skin-depth effects. Nonuniform pumping due to skin effects has been observed elsewhere in a large volume X-ray preionised discharge pumped $XeCl^*$ laser, (17), and it has been predicted to what extent skin effects will ultimately limit current rise-time while still retaining a uniform and stable glow discharge.

In order to determine if there was any evidence of inhomogeneous pumping laser burn patterns were made onto heat sensitive paper commercially available for use in facsimile machines. Due to the poor output pulse energy of the laser exposures were integrated over several shots and examples are given in fig. 3.14. These spatial profiles confirm increased laser output along the top and bottom edges of the discharge which may be attributed to increased current density in these regions.

Fig. 3.14

Laser Output Burn Patterns Made on Heat Sensitive Paper

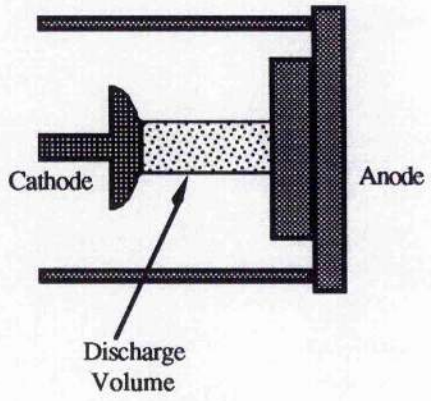

L.F.Champagne *et al* ,(17), give a comprehensive analysis of the limitations on fast current rise-times due to skin effects. The expression for the skin depth of a conductor, defined as the penetration depth at which the current falls to 1/e of its maximum value, can be written, (18):

$$\delta = \left(\frac{\rho}{\pi f \mu_0}\right)^{1/2} \qquad 3.4$$

where f is taken as the upper frequency limit of the current pulse bandwidth and ρ is the resistivity of the discharge; both of these quantities are not necessarily self explanatory and require further definition. If the leading edge of the current waveform is approximated by a sine wave an equivalent bandwidth encompassing the component frequencies of the waveform can be defined thus:-

$$BW = \frac{0.3}{\tau} \qquad 3.5$$

where τ is the 10% to 90% current rise-time. Consequently the expression for skin depth can be rewritten in the more useful form:-

$$\delta = \left(\frac{\rho\tau}{0.3\pi\mu_0}\right)^{1/2} \qquad 3.6$$

There are alternative means for obtaining the resistivity of the discharge depending on what precisely is meant by the term 'discharge resistivity.' In simple terms the discharge resistivity can be defined as the ratio of the self sustaining electric field to the discharge current density, or:

$$\rho = E_{ss}/J \qquad 3.7$$

however the applicability of this simplistic approach is uncertain as it assumes an obeyance of Ohm's law which clearly does not apply in this case. This definition of resistivity is based on the absolute resistance of the discharge at the operating point with respect to zero voltage and current and as the voltage/current characteristic in this case is nonlinear it may be more correct to use the slope or dynamic resistance at the operating point:

$$\rho = dE_{ss}/dJ \qquad 3.8$$

The slope resistance here unfortunately is not particularly useful as the operating point lies in a flat region of the voltage/current curve with a gradient close to zero because the discharge current is to a large extent governed by the external circuit rather that properties of the discharge itself, see fig. 3.15.

Fig 3.15

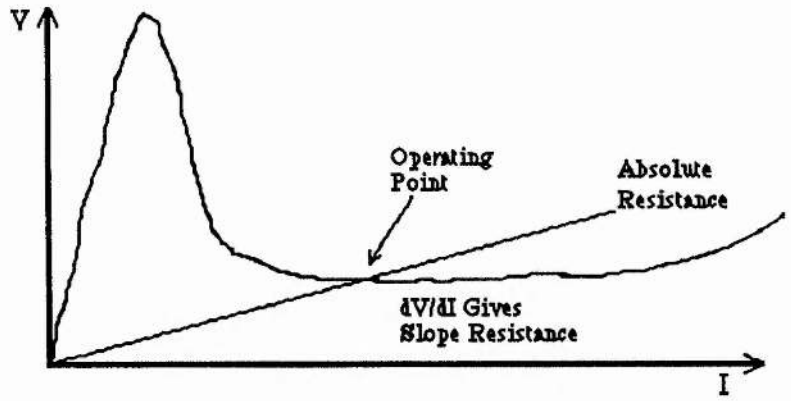

Current Voltage Characteristic For A Typical Excimer Discharge

Using the ohmic method for determining the discharge resistivity and the following typical experimental parameters:

Table 3.5.1

V_{ss}	1200V
I	7 kA
Discharge Dimensions	7 mm x 12 mm x 25 cm
t	20 ns

the skin depth is estimated to be of the order of 5 cm.

An alternative definition of the resistivity can be obtained from plasma physics. For a general plasma with free electrons and ions, which may be considered stationary because of their large relative mass, the resistivity is a function of the applied E field, (19) and is given by:

$$\rho = \frac{\omega^2 + \nu^2}{\varepsilon_0 \nu \omega_p^2} \qquad 3.9$$

where ν is the *effective collision frequency* , ω is the angular frequency of the applied field and ω_p is the *plasma frequency*.

The plasma frequency, ω_p can be written:

$$\omega_p = \left(\frac{n_e e^2}{m_e \varepsilon_0}\right)^{1/2} \qquad 3.10$$

where n_e is the electron number density, e is the electronic charge and m_e the mass of an electron. Substituting 3.10 into 3.9 gives an expression for the plasma resistivity, ρ.

$$\rho = \frac{m_e(\omega^2 + \nu^2)}{\nu n_e e^2} \qquad 3.11$$

The effective electron collision frequency is defined as the equivalent number of collisions, completely stopping the electrons, occurring in unit time that would extract the same total energy from the electrons as happens in practice. As the mass of an electron is much less than that of the species into which they are colliding the energy lost by an electron in each elastic collision will be small, the effective collision frequency will therefore be much less than the actual collision frequency.

Studies of the momentum transfer cross sections for the constituents of a typical neon buffered $XeCl^*$ gas mix indicate that most electron collisions will take place with neon atoms as although other gasses have larger cross sections, neon is by far the most plentiful constituent, (20). The electron momentum transfer cross section, σ_n, for neon is roughly constant at 2×10^{-16} cm^2 over the range of average electron energies found in an excimer discharge. The number of collisions by an electron per second will therefore be given by, $\sigma_n v_e n_n$, where v_e is the average electron velocity and n_n is the neon number density. Using values for v_e of 2×10^6 cm s^{-1} and n_n 8×10^{19} cm^{-3}, (20), based on a discharge at an E/N of about 3 Townsend at a neon pressure of 3 bar, gives a value for the total number of collisions by an individual electron of 3.2×10^{10} s^{-1}.

Classical mechanics dictates that this value for the number of collisions per second must be divided by a factor of approximately 10^4 to get the effective electron collisional frequency, ν, because of the large difference in masses between electrons and neon atoms. The value for ν therefore becomes 3.2×10^6 s^{-1}.

Returning to equation 3.11, the plasma resistivity can now be calculated using the following values summarised in table 3.5.2, derived from the measured laser parameters as used before in table 3.5.1.

Table 3.5.2

m_e	9.1×10^{-31} kg
ν	5.2×10^{7} s^{-1}
$n_e = J/ev_e$	1.3×10^{15} cm^{-3}

hence using these values $\rho = 23\ \Omega$cm.

Substituting this value of ρ into equation 3.6 using the other values from 3.5.1 gives a value for the skin depth of about 6 mm; this value is subject to a large uncertainty however, mainly due to the difficulty in estimating ν. If a larger value of ν, closer to the true collisional frequency, were used in the calculation this would have the effect of making the skin depth smaller still.

This plasma physics approach gives a value for the skin depth that could explain the concentration of the current at the outside edges of the discharge. It must be remembered however that the conventional definition of skin depth, δ, is the penetration at which the current density falls to 1/e of the value at the surface, the rate of fall in current with depth following an exponential form. As the discharge has an overall width of of only 7 mm in these experiments, in the centre of the discharge, at a penetration of 3.5 mm, the current density will still be a large fraction of the current density at the discharge surface. It is estimated that the current density in the centre of the discharge will be greater than 60% of the current density at the surface.

The question is raised as to whether the skin effect alone can explain the discharge collapse or if other factors need to be considered. It is possible that the discharge inhomogeneity resultant from the skin effect could be enhanced by other discharge instability mechanisms that involve positive feedback. In this way the skin effect could provide the initial non-uniformity of current density that could be exploited and reinforced by other mechanisms, leading to total discharge collapse. To answer this question a comprehensive analysis of up-to-date theories of excimer laser discharge instability is required and this is undertaken in chapter 4.

References:

An account of the work described in this chapter is given in the following paper:
S A Fairlie, P W Smith;"Performance Characteristics of a Discharge Pumped XeCl Laser Driven by a Pulse Forming Network Containing Nonlinear Ferroelectric Capacitors;" SPIE,"Pulsed Power For Lasers III," Los Angeles, Jan. 1991.

1 M M Turner, P W Smith; "Modelling of Excimer Laser Glow Discharges;" Proceedings of the 9th International Conference on Gas Discharges and their Applications, Venice 1988, p725-9
2 G Mc Duff, K Rust, H Menown, C Neale; "Evaluation of Bidirectionally Conducting Thyratrons for Pulsed Excimer Lasers;" Proceedings of the 16th Power Modulator Symposium, Arlington VA, 1984, p288-91
3 A J W Brown, P W Smith; "A Multi-paralleled Thyratron, Repetitively Pulsed, Power Supply for High Power Gas Lasers;" Proceedings of The 17th Power Modulator Symposium, Seattle WA, 1986, p191-95
4 I Similanski, S R Byron, T R Burkes, "Electrical Excitation of an XeCl Laser Using Magnetic Pulse Compression;" Appl. Phys. Lett, vol 40(7), p547-8, 1982
5 H Hatanaka, M Obara, "High Efficiency Operation of the High Repetition Rate Magnetic Pulse Compressor for KrF Excimer Lasers;" Proceedings of the 7th IEEE Pulsed power Conference, Monterey CA 1989, p671-7
6 C R Wilson, M M Turner, P W Smith, "Electromagnetic Shock-wave Generation in a Lumped Element Delay Line Containing Nonlinear Ferroelectric Capacitors;" Appl. Phys. Lett, vol 56, p2471-3, 1990
7 C R Wilson, M M Turner, P W Smith, "Pulse Sharpening in a Uniform LC Ladder Network Containing Nonlinear Ferroelectric Capacitors;" Proceedings of the 19th Power Modulator Symposium; San Diego CA, 1990, p204-7
8 M M Turner, G Branch, P W Smith; "Methods of Theoretical Analysis and Computer Modelling of the Shaping of Electrical Pulses by Nonlinear Transmission Lines and Lumped Element Delay Lines;"Proceedings of the 19th Power Modulator Symposium; San Diego CA, 1990
9 M Wiener; "Pulse Sharpening in Ferrite Transmission Lines;" Proceedings of 2nd IEEE Pulsed Power Conference, 1979, p91
10 Z Xinning, F Dianyuan, G Jian; "Electro-Optical Switches With Ferrite Lines;" Chinese Phys.-Lasers, vol 13, p483, July 1986
11 N Seddon, E Thornton; "A High-voltage, Short risetime, Pulse Generator Based on a Ferrite Pulse Sharpener;" Rev. Sci. Inst, vol 59(11), p2497, 1988
12 I G Katayev; "Electromagnetic Shockwaves;" Iliffe Books, London, 1966
13 H Ikezi, S S Wojtowicz, R E Waltz, J S de Grassie, D R Baker; "High Power Soliton Generation at Microwave Frequencies," J. Appl. Phys, vol 64, p3277-81, 1988
14 G Branch; Private Communication
15 EEV Hydrogen Thyratron Product Data
16 Dennis Lo, Jing-gang Xie; "High Pressure Scaling of a High Current Density XeCl Laser;" J. Phys. D, vol 24, p1023, June 1991
17 L F Champagne, A J Dudas, N W Harris; "Current Rise-time Limitations of the Large Volume X-Ray Preionised Discharge Pumped XeCl Laser," J Appl. Phys, vol 62(5), p1576-84, 1987
18 S Ramo, J R Whinnery, T van Duzer; "Fields and Waves in Communication Electronics." 2nd Edition, Wiley, New York, 1984, p149
19 A J Baden Fuller; "Microwaves;" 2nd edition, p191, Pergamon
20 M M Turner, PhD Thesis, University of St. Andrews, 1990
21 T Kuusela, J Hietarinta; "Nonlinear Electrical Transmission Line as a Burst Generator." Rev. Sci. Inst. vol 62(9), p2266-70, 1991

Chapter 4

Investigations into Optical Pulse Duration and Discharge Stability

4.1 Introduction

In theory, rare gas halide excimer lasers should be capable of long pulse or even quasi-continuous operation. The lower lasing level of excimer systems is either unbound or only weakly bound with a very short lifetime so that bottlenecking is not a problem. The upper laser level is also usually short lived with lifetimes typically less than 10 ns and consequentially energy storage in the upper laser state is small and so lasing will not occur beyond the duration of the pump power deposition.

A limiting kinetic processes in $XeCl^*$, for example, is the regeneration of the halogen donor, typically HCl. This reformation reaction typically takes place on a time scale of around 20 μs; (1), which is much longer than currently obtainable laser pulse durations. Most kinetic models assume that for typical pumping rates only a small percentage of the halogen donor molecules are involved in lasing at any time so that the halogen donor number density may be taken as constant throughout the laser pulse, (2). These facts suggest that lasing in excimer systems should occur for as long as adequate pump power deposition can be achieved. Truly continuous operation is unlikely however except in the smallest active volume systems because of the large pump energy requirements that would be encountered.

To date the longest pulse duration obtained from a discharge pumped rare gas halide excimer laser is 1.5 μs FWHM with $XeCl^*$, (3). The pulse energy of the 1.5 μs pulse was only 5 mJ, which is very low considering the active volume of 2.5 x 1.5 x 70 cm and was achieved using a very low pumping rate (~50 $kWcm^{-3}$) and a low loss optical resonator to produce photon trapping. More useful pulse energies of 100 mJ in a 750 ns pulse were obtained with the same system.

It is clear from these results that the inherent instability of the high pressure glow discharge and its tendency to collapse represents a serious limitation on discharge excimer laser performance. In almost all cases where lasing terminates before the end of the

pumping pulse, discharge instability rather than kinetic factors can be identified as the cause. The improvement of stability in high pressure glow discharges is therefore an important goal along the road to better laser performance and this can only be achieved by identifying the mechanisms that drive discharge instability.

Although pre-dating the discovery of excimer lasers R A Haas produced a comprehensive mathematical analysis of the modes of instability that occur in electrical discharges in molecular gases, (5). Of the separate instability modes identified only two occur under the physical conditions present in an excimer laser and on time-scales comparable with the duration of excimer laser outputs. Striation instability in which the output of the laser oscillates without terminating has been observed, (6), especially at high buffer gas pressures. The most important form of instability however has been identified as concerning space charge and electron interactions, the mechanisms for which are not fully understood.

In this chapter some of the mechanisms proposed to explain discharge instability will be discussed and experimental evidence considered. Most of the current explanations involve preionisation factors or properties of the halogen donor and these theories will be reviewed. Little work has been done on the part played by the rare gas component of excimer discharges and new experimental evidence is presented indicating that the rare gas partner does influence discharge stability. Possible explanations for this effect are proposed.

4.2 Theories of Discharge Stability

4.2.1 Electrical Factors Influencing Discharge Stability

It is well known that adequate preionisation is essential for the formation of a high pressure glow discharge and that to maintain the glow discharge for as long as possible certain criteria concerning electron number density and homogeneity must be met. These criteria and the methods of preionisation currently in use are covered fully in chapter 1.

Various studies have been performed on how preionisation uniformity influences discharge formation. Hasson and Bergman, (7), describe how non-uniform preionisation

from spark arrays combined with various masks results in a glow discharge forming only in the regions of high preionisation electron density. In regions of low or no preionisation either a filamentary discharge or no discharge at all forms. Similar results were obtained by S Sumida *et al* , (8), using X-ray preionisation and by Taylor, (9), using a KrF laser beam to preionise a XeCl laser by shining along the optical axis of the main laser. The advantage of this second method is that the preionisation spatial distribution can easily be precisely defined. Interestingly it shows that in the direction transverse to the current flow it is possible to produce regions of uniform and filamentary discharge. This implies that inhomogeneities in the initial preionisation influence the nature of the glow discharge and that localised preionisation deficiencies can persist throughout the duration of the discharge. It is not clear however how these discharge non-uniformities drive instabilities that result in discharge collapse. Taylor, (9), has noted that filamentary instabilities tend to emerge at the sharp boundaries of glow discharge regions corresponding to the edges of preionised and unpreionised regions. The explanation provided points to the strong preionisation electron density gradient and the resultant local electric field transverse to the applied electric field. Making the boundaries between the preionised and unpreionised regions less sharp resulted in improved performance.

Another factor that has been shown to influence glow discharge stability is the electrical pump power density. While the optimum power deposition rate for efficient lasing in XeCl* is believed to be between 300 and 700 $kWcm^{-3}$, (10), very high rates of specific energy extraction have been achieved at pump power densities in excess* of 10 $MWcm^{-3}$, (11). Although pumping efficiency in kinetic terms is reduced at high pumping rates the major drawback with this technique is the short pulse duration, ~40 ns FWHM, believed to be due to premature discharge collapse.

A detailed study of discharge stability and energy loading in the laser gas is given by Taylor, (9), and shows that filament growth leading to discharge collapse progresses at

---

* Estimated from figures given in paper

a faster rate with higher discharge current densities. For the particular system described the rate of filament growth proceeds linearly with increasing current density at current densities less than 200 Acm^{-2} and less than linearly thereafter. This saturation effect at higher current densities is explained by Taylor as possibly being due to halogen depletion effects; the role of halogen donors in stability will be discussed subsequently.

Poor discharge stability resulting in short duration laser pulses has been confirmed by other workers, (12), although direct comparisons are hard to make because of other differing factors such as different discharge geometries between machines. In general, from analysis of other workers results, long pulse durations tend to be obtained from systems with low pump power deposition rates, which is not altogether surprising.

The laser used for the experiments described in this thesis had a relatively short gain length of only 25 cm implying that for optimization in terms of output energy the small signal gain needs to be higher than in systems with longer gain lengths. The small signal gain coefficient is increased by pumping the laser at higher pump power densities, because of the increased upper state formation rate, and consequentially the laser output energy will be optimized at a relatively high pumping rate. The connection between high pumping rates and discharge instability helps to explain why short gain length systems tend to have shorter duration optical pulses. Despite the parametric survey of operating conditions carried out in chapter 2, with the laser system performance optimized for pulse energy it was difficult to obtain pulse durations much in excess of 100 ns FWHM. In terms of specific energy extraction typical outputs were in the region of 3 Joules per litre which is respectable in comparison with other systems. For comparison the long pulse duration experiments carried out by Taylor and Leopold, (13), in which the pump power rate was deliberately kept low yielded specific energy extractions of at best 1.5 Joules per litre and much lower for the longer duration pulses.

4.2.2 Halogen Donor Depletion model of Instability

It is well known that the presence of the highly electronegative halogen donor in an excimer gas mix strongly influences discharge stability. It is generally believed that the presence of some form of electron attaching species is necessary to sustain a stable discharge by balancing electron production with a loss mechanism in order to produce a steady state. Without the electron loss processes due to halogen donor dissociatve attachment it is believed that electron production mechanisms such as ionisation of rare gas excited metastables would cause the discharge current to rapidly increase, leading to the formation of high conductivity localised filaments and eventually full scale arcs.

An instability mechanism for an electron beam sustained KrF^* laser was first proposed by Daugherty *et al*, (14). The theory states that without the electron loss mechanism provided by the dissociative attachment of electrons with F_2, electron production can accelerate by ionisation of Kr^* metastables to Kr^+ ions. The ionisation potential of Kr^* is obviously much smaller than Kr atoms and the reaction rate constant is orders of magnitude larger. The electronegative halogen donor molecules therefore play an important role in preventing the electron density from increasing out of control and the consequent formation of filamentary channels leading to discharge collapse. In this way increasing halogen donor concentration should lead to more stable discharges.

It was discovered experimentally however that increasing the halogen donor concentration tends to hasten the onset of filamentary instabilities in contradiction to the theory of Daugherty. A related mechanism by which halogen donors could increase the rate of discharge collapse, known as the local halogen depletion model, was first published by C. E. Webb *et al*, (15).

It was believed that localised inhomogeneities in the electron distribution could burn-up the F_2 causing a similarly localised failure of the F_2 to limit the the electron growth rate. By this positive feedback mechanism electron production can grow unchecked in a small region leading to the formation of a filament and eventual discharge collapse. An analogous process was proposed for the other rare gas halide lasers.

A more rigourous mathematical treatment of this mechanism is given by Coutts and Webb, (16), for the $XeCl^*$ system. Starting from the electron continuity equation:

$$(d/dt)\, n_e = n_e k_{mI} [Xe^*] - k_a n_e [HCl]_t \quad 4.1$$

where k_{mI} and k_a are ionisation and dissociation attachment constants respectively and assuming all electron production to be due to ionisation of Xe^* metastables an index of the glow phase duration, τ, can be derived. If τ is defined as the time taken for the initial glow discharge electron density, $\langle n_{e0} \rangle$, to double then:

$$1/\tau^2 \sim {}^1/_2\, k_a^2 \langle n_{e0} \rangle [HCl]_0 \quad 4.2$$

The time taken for the electron density to double has been found to be a convenient measure of the discharge stability time as total discharge collapse follows rapidly on from such an increase in the electron density.

Equation 4.2 implies that the discharge lifetime increases inversely with the halogen donor concentration which is contradictory to earlier theories which proposed that stability should increase with increasing halogen donor concentration.There is considerable evidence from other workers to show that increasing halogen donor concentration leads to reduced laser pulse durations, (15, and others). The halogen donor depletion model of discharge collapse provides a plausible explanation, however it is also true that high halogen donor concentrations are unfavourable for other reasons such as absorption of laser photons and these effects must not be confused. Parametric studies of laser performance carried out during commissioning and described in chapter 2 confirm that despite increasing pulse amplitude, in many cases, increasing halogen donor concentrations lead to shorter laser pulses and this is almost certainly due to discharge collapse.

Equation 4.2 has been experimentally verified by Osborne, (17), and found to hold for neon buffered $XeCl^*$ using a wide variety of chlorine donors. Despite the chlorine donors having electron attachment rate coefficients varying by a factor of almost 20 from the lowest , CCl_2F_2, to the highest, CCl_4, the discharge stability time index, τ, was found to increase such that $\tau \propto k_a^{-1/2}$. Similarly verification has taken place over a range of initial

electron number densities, n_{e0}, and halogen partial pressures, again with neon buffered $XeCl^*$, (18). With a wide variety of chlorine donors τ has been found to be inversely proportional to the square root of the chlorine donor partial pressure. For the purposes of this experiment the initial electron number density, n_{e0}, was calculated from the following expression:

$$n_{e0} = J_0/qv_a \qquad 4.3$$

where q is the electronic charge and v_a is the electron drift velocity calculated for a particular value of E/N.

The initial discharge current density, J_0, is the current density at the point where the discharge voltage first falls to the self sustaining voltage, V_{ss}, which is not always directly apparent from head current/voltage plots due to the complication of head inductance effects, (see chapter 1). It must be assumed that the values of J_0 taken in the calculations, (18), are the result of some sort of arbitrary definition.

The dependence of τ on the halogen donor partial pressure for fluorine excimers was investigated by Osborne, (16). Surprisingly, although the data from these experiments confirmed equation 4.2 for chlorine excimers, the discharge stability time with fluorine excimers was found to be 50% of that predicted on the basis of the fluorine donor electron attachment coefficients and the chlorine data. This indicates that the halogen depletion theory of instability is incomplete in the case of excimers containing fluorine.

Possible explanations for this poorer than expected performance with fluorides have been suggested, (17). It is known that the common fluorine donors, NF_3 and F_2, are both capable of multiple halide ion donation, (19), and that this process can be significant. The effective electron attachment coefficients therefore need to be adjusted upwards to take account of the electron attaching properties of NF_2^*, NF^* and F^*. This has the effect of reducing the pulse duration predicted by theory but still not enough to agree with the chlorine excimer experiments.

It is well known that fluorine excimer performance is more sensitive to the discharge E/N value than the chlorine equivalents. It has been pointed out, (17), that this dependence on E/N not only applies to the large scale variations in E/N due to macroscopic

changes in the electrode profile but also to small scale variations resultant from electrode surface irregularities and imperfections. This will lead to localised differences in electron density which will drive the halogen donor depletion mechanism to initiate discharge collapse.

Taking the effects of multiple halide donation together with the high sensitivity to variations in E/N provides a partial explanation for the poor performance of fluoride in relation to chloride excimers. Whether these mechanisms alone can explain this discrepancy or other factors are involved remains to be seen.

4.2.3 More Recent Developments in Discharge Instability Theory

Recent work has further refined theories of discharge instability and taken into consideration other factors suspected of playing a role in driving the formation of inhomogeneities that limit discharge pumped excimer pulse duration. In particular the effects of differences in the E/N value due to localised electrode effects and the resulting changes to the electron temperature, T_e, have been analysed. These more detailed treatments have been used to extend the concepts introduced in the original local halogen donor depletion model of Coutts and Webb, (15,16) to provide a better explanation of experimental results.

The development of discharge instabilities in an $XeCl^*$ laser has been studied and described by Bahr *et al* , (20), using computer modeling verified by experiments using a machine of similar dimensions to that used in these experiments but with X-ray rather than corona preionisation. Because of the importance of this work it is considered relevant to discuss it here in some detail.

It has been identified that the dissociative electron attachment coefficient for HCl is strongly dependent on the vibrational excitation state of the HCl molecule. At higher vibrational excitations, ($\nu = 2,3,...$), the electron attachment probability increases significantly and this vibrational excitation has been found to occur more favourably at lower electron temperatures. It follows that electron attachment will consequentially be greater at lower electron temperatures. The form and stability of the discharge is therefore

strongly influenced by the electron temperature and the factors that determine the electron temperature distribution throughout the evolution of the discharge.

To describe how the history of the discharge formation influences its subsequent development, Bahr divides the evolution of a typical discharge into four stages. During the first of these stages, termed the avalanche and covering the rise in E field prior to the turn on of the current, the initial densities of Xe^* and vibrationally excited HCl will be small. With increasing E field the E/N will rise and produce excited states of xenon, (Xe^*), and HCl, (HCl $v = 2,3,...$). The rates of production of these species will depend upon the electron temperature which at this stage is a function only of the E/N. Local variations in E/N due to electrode profiles or electrode surface imperfections will result in similar regions of slightly differing T_e. Regions of high T_e will result in a slight excess of Xe^* metastables, ultimately responsible for free electron production by ionisation and regions of low T_e will have a slight excess of electron attaching vibrationally excited HCl.

With the turn-on of current and the resultant fall in voltage across the head the ignition stage begins. With this fall in E field the electron temperature will also fall, with electron cooling mainly due to the excitation of xenon and the ionisation of Xe^* metastables. The inhomogeneous distribution of Xe^* resulting from the slight differences in E/N during the avalanche stage will cause these regions to undergo the most rapid fall in T_e and consequentially the fastest growth in HCl ($v = 2,3,...$). The regions that, at the onset of the discharge, had slightly higher values of E/N will therefore, by the end of the ignition stage, be subjected to higher rates of dissociative electron attachment by HCl due to the higher concentrations of vibrationally excited HCl consequent from this lower electron temperature.

The third stage of discharge development described by Bahr has been named the burning stage and is defined as commencing when the electron attachment and production rate are nearly equal and the discharge voltage has stabilized at the self sustaining value, V_{ss}. At this stage the localised differences in E/N exert little influence on discharge evolution, the distribution of excited Xe^* and HCl ($v = 2,3,...$) states formed during the first two stages is of greater importance. In regions of lower than average T_e the higher

proportion of vibrationally excited HCl will cause a localised restraint on electron density growth. Regions of higher T_e will have an above average population of Xe^* metastables and electron density growth will proceed at a faster rate. This will result in the discharge developing into one or more constricted channels.

The final stage is the pulse decay. During this phase the voltage across the laser head will start to fall and any inhomogeneities that have developed over the first three stages will tend to be amplified as the discharge collapses. In most practical laser systems the development of inhomogeneities during the burning stage will terminate the laser output before total discharge collapse takes place.

The mechanism of Bahr's discharge instability theory is therefore somewhat contradictory to the 'classical' local halogen donor depletion model, however it is acknowledged that local depletion of the halogen donor can over-ride the mechanism in systems where the current density is high or the halogen donor concentration is small. In this way both mechanisms can be seen to operate but with one or other being dominant depending upon the individual operating conditions.

When the theory due to Bahr *et al* is applied to a real laser system it has been observed that the discharge will constrict either into a single central channel or two outer channels at the edge of the discharge volume. This will depend on the HCl concentration and the avalanche stage E field resultant from the electrode profiles. In a machine with electrode profiles that produce an enhancement of the E field at the centre of the discharge, provided that the initial halogen donor concentration is sufficiently high, the processes active during the avalanche and ignition stages will produce an excess of Xe^* at the discharge edges and an excess of HCl ($v = 2,3,...$) in the centre of the discharge. This will cause an enhancement in electron production at the discharge edges resulting in the discharge collapsing into two distinct channels.

In systems with a lower overall partial pressure of the halogen donor then local halogen donor depletion effects may dominate. This is generally characterised by the formation of an enhanced channel along the centre line of the discharge volume. This behaviour is also said to occur in high current density discharges.

The growth of discharge instabilities is also treated in another recent paper by M J Kushner, (21), in which a similar mechanism to, (20), is considered responsible. In a slightly different treatment however, emphasis is drawn to imbalances in Xe^* and HCl (v = 2,3,...) proportions on what is termed a microscopic scale of 10's to 100's of micrometres. It is pointed out that on the time-scale of a typical laser pulse of less than a few microseconds the gas particles may be considered motionless. This is a standard approximation in most discharge kinetic models. Any localised features, even on such a microscopic scale, will tend to persist through the lifetime of the discharge because of the absence of any homogenising mechanism in the direction perpendicular to the applied E field. This has been confirmed experimentally by Taylor, (9), as described earlier. Kushner calls this approximation the Stationary Kinetics Approximation, (SKA).

It is likely that during the discharge initiation phase, small perturbations in the relative proportions of Xe^* and HCl (v = 2,3,...) will be produced due to electric field non-uniformites in the vicinity of electrode surface imperfections. By considering the SKA, although these features will tend to grow in the direction of the electric field, to become regions of higher than average electron density, any growth orthogonal to the electric field will be restricted. Kushner calls these features microarcs and proposes that although each microarc is small in diameter, < 100 μm, a sufficiently large number can be initiated to grow outwards from both electrodes consuming the discharge volume. A discharge that looks like a homogeneous glow may in fact consist of a mass of microarcs and will cause termination of the laser pulse due to inhomogeneous pumping as the discharge current is channelled into the microarcs.

The theory according to Kushner implies that for a practical laser, to prevent the formation of microarcs, the electric field during the discharge avalanche and ignition stages must be maintained with a very high degree of uniformity. Inhomogeneities in the E field due to electrode surface imperfections, even on a scale as small as a few tens of micrometres, must be avoided. This is difficult to achieve in practice as even in a well designed laser the discharge will always eventually collapse into an arc; even if this occurs long after the termination of lasing it can still be problematic due to the electrode surface

oblation that will take place. Furthermore the corrosive nature of the halogen donors required in excimer gas mixes tends to produce a layer of fluorides or chlorides on the electrode surface making it difficult to retain any form of polish. The theory implies that mesh electrodes, even if particularly fine gauge, may be detrimental to good discharge stability as they will inevitably produce small scale variations in the electric field close to their surface.

4.3 Influence of Rare Gas Partners on Excimer Discharge Stability

4.3.1 Introduction

Much effort has been expended on determining the role played by halogen donors in discharge stability while less attention has been paid to the influence of the rare gas partner. In some ways the treatment of rare gases is simpler as they are monatomic and undergo only a limited range of conventional chemical reactions and then only when in an excited or ionised state. Perhaps for these reasons it has been presupposed that the relatively small partial pressure of the rare gas partner will only marginally effect discharge stability and therefore this ares has been overlooked. It must not be forgotten however that the primary electron production mechanism considered in the discharge instability theories discussed previously all involve ionisation of excited species of the rare gas partner. It may therefore be expected that the rare gas partner plays a major role in discharge stability mechanisms.

A direct comparison of different excimer laser systems such as XeF^*, KrF^* and ArF^* is difficult because of factors that can not be kept constant throughout. Although each excimer works to a similar kinetic scheme the reaction rate constants in each case are different so that differing reactions and excimer production and quenching routes take precedence. The fluorine excimers form an homologous series of laser media with a steady variation in certain properties such as wavelength and presumably discharge stability too. These variations along the series can only be due to the influence of the rare gas partner but separating kinetic and optical effects from those responsible for discharge stability is not straightforward.

4.3.2 Theoretical Comparison of the Effects of Xe, Kr and Ar on Discharge Instability Models

In the local halogen donor depletion model proposed by Coutts and Webb, (16), and the instability theories developed by Bahr *et al* , (20), and Kushner, (21), the major electron production mechanism has been identified as the ionisation of rare gas metastables. It is only the intervention of the electron loss mechanism due to dissociative attachment by halogen donor molecules that prevents the electron density from rapidly increasing in an unrestrained manner. The properties of the rare gas partner, in particular the reaction rate constants for the one, two and three step ionisation processes, are therefore central to the working of these theories. As first proposed the local halogen donor depletion mechanism concentrated on the XeCl system; the purpose of this investigation is to determine if the differences in the ionisation reaction constants between Xe, Kr and Ar can be used to predict differences in the discharge stability of XeF^*, KrF^* and ArF^* lasers.

According to Coutts and Webb, for an $XeCl^*$ laser with HCl halogen donor the electron continuity equation can be written in terms of the two stage ionisation process:

$$\left(\frac{\partial}{\partial t}\right) n_e = n_e k_{mI} [Xe^*] - k_a n_e [HCl]_t \qquad 4.4$$

where n_e is the electron number density, k_{mI} is the metastable ionisation rate constant and k_a is the HCl dissociative electron attachment rate constant. The production rate for Xe^* metastables is therefore very important and may be summed up thus:

$$\left(\frac{\partial}{\partial t}\right) [Xe^*] = n_e k_{0m} [Xe] - n_e k_{mI} [Xe^*] - n_e k_{m0} [Xe^*] - k_q [HCl] [Xe^*] \qquad 4.5$$

however, agreement with experimental results for the Xe^* metastable production rate was found to be better if allowance was made for multi-step ionisation routes via highly excited Xe metastables, Xe^{**}, hence:

$$\left(\frac{\partial}{\partial t}\right)[Xe^*] = n_e k_{0m}[Xe] - n_e(k_{mm'} + k_{m0} + k_{mI})[Xe^*] - k_q[HCl][Xe^*] \qquad 4.6$$

Experiments have shown that Xe^* quenching by HCl, as described by the last term in eqn. 4.6 is significant and that the formation of Xe^+ ions from Xe^* metastables proceeds very rapidly. The rate limiting step in the electron production equation is therefore the rate at which Xe^* metastables are produced from Xe atoms by the following reaction:

$$Xe + e^- \xrightarrow{k_{0m}} Xe^* + e^- \qquad 4.7$$

hence the electron production rate can be approximated thus:

$$\frac{\partial n_e}{\partial t} \sim n_e k_{0m}[Xe] \qquad 4.8$$

It is estimated that even if the [Xe] number density is taken to be constant, this approximation ignoring all metastable quenching is accurate to within 10%.

Taking this treatment and extending it to the XeF^* system, the only change will be in the term in equation 4.6 describing the quenching of Xe^* states by the halogen donor, F_2 being substituted for HCl. This reaction is favourable for discharge stability as it usually results in the formation of a rare gas halide molecule with a high or unity branching ratio without the production of a free electron.

$$Xe^* + HCl \xrightarrow{k_{q1}} XeCl^* + H \qquad 4.9$$

$$Xe^* + F_2 \xrightarrow{k_{q2}} XeF^* + F \qquad 4.10$$

According to Velazco *et al*, (22), the reaction rate constant k_{q1} for $XeCl^*$ production is 5.6×10^{-10} cm^3s^{-1} and k_{q2} for XeF^* production is 7.5×10^{-10} cm^3s^{-1}. Both of these are small in relation to the rate constant for ionisation of Xe^* by electron impact which is typically two orders of magnitude larger, (23), and consequentially the ionic formation route for excimer molecules is favoured. The production of free electrons in an XeF^* gas mix will therefore be described by eqn. 4.8 in the same way as with $XeCl^*$.

Extending this treatment to a comparison of XeF^*, KrF^* and ArF^*, available values for the excited state quenching rates by F_2 molecules, (23), indicate that this process can be ignored without too serious a penalty for all the rare gas fluoride excimers. The major free electron production mechanism in all cases will therefore be governed by the rate of formation of rare gas excited metastables and their subsequent ionisation by electron impact.

Available values for the reaction rates for the the production of krypton and argon metastables by electron impact are given in the following table:

$Xe + e^- \text{----> } Xe^* + e^-$	$\sim 10^{-10}\ cm^3s^{-1}$	(24)
$Kr + e^- \text{----> } Kr^* + e^-$	$4.1 \times 10^{-11}\ cm^3s^{-1}$	(23)
$Ar + e^- \text{----> } Ar^* + e^-$	$2.8 \times 10^{-12}\ cm^3s^{-1}$	(23,24)

it should be noted that the reaction rates are all strongly dependent on electron energy and the above values are therefore averages.

It is not particularly surprising that the lighter rare gases have lower excitation probabilities than for example xenon. For a given electron distribution it is progressively more difficult to excite the lighter rare gases and this helps to explain why experimentally KrF^* and ArF^* lasers require increasingly large partial pressures of the rare gas partner for optimum laser output.

In conclusion, having performed this brief analysis it is difficult to determine a process by which different rare gas partners could drive the halogen donor depletion models at different rates. This treatment has been brief however and their may be some unforeseen subtle process at work that has been overlooked, otherwise it tends to show that for equal concentrations all the rare gases should behave in a similar manner. In a practical system this is not the case however and it has been identified that the lighter rare need to be present in increasingly large proportions for efficient excimer production. This requirement to run the different excimers at differing rare gas partial pressures makes direct comparison more complex.

4.3.3 Experimental Details

It was decided to use the laser system to obtain a feel for the comparative performance of XeF^*, KrF^* and ArF^* under conditions as similar as possible in each case . The purpose behind this was to try and determine the variation in maximum pulse duration between these excimers and confirm that this was due to discharge instability rather than kinetic factors.

XeF^*

The first rare gas fluoride tried was XeF^*. This required the laser head to be passivated with fluorine and pressure windows fitted that were compatible with F_2 and non absorbing at 351 nm.

The laser operating parameters are summarised in the following table:

Pressure Windows	2 x CaF_2 50 mm dia. x 5 mm thick
Mirrors	1 x HR @ 351 nm
	1 x 60% R @351 nm
Electrode Spacing	16 mm

The head vessel was passivated using successive gas fills until the laser performance reached a plateau and maintained this level over a sufficiently long time to allow the experiments to take place; about 20 minutes to half an hour was deemed sufficient. Similarly the charging voltage on the preioniser pulser was increased until the laser output stabilized. Interestingly the preioniser charging voltage required to reach a stable maximum laser output was higher than with $XeCl^*$, probably because of the higher electron attachment coefficient of F_2 compared with HCl, (17).

Once the laser output stabilized and became consistently reproducible a parametric study of laser output duration and pulse energy with varying gas composition and PFN voltage was carried out. The Xe partial pressure was fixed at 10 mbar as previous experiments indicate performance is only weakly dependant on the Xe concentration, (25). This introduces a paradox in that if the rare gas partner does play a major part in the mechanism leading to discharge instability then it may be expected that the laser pulse duration will be strongly dependent on xenon concentration, this has been shown not to

happen in practice except at partial pressures of several tens of Xe. There are other ways in which the xenon concentration can effect the laser performance however such as by optical absorption or by influencing the excimer production kinetic scheme. The experimental results are shown in table 4.3.1.

Each result is an average value taken over a number of shots to ensure that the laser output was consistent and that the values quoted are truly representative. Pulse energies were measured by a Gentec ED-200 calorimeter and are quoted to the nearest mJ. Pulse durations were measured from the laser output temporal profiles obtained using a suitable fast response photodiode and recorded on a Tektronix 2440 digital oscilloscope with a 200 MHz bandwidth; pulse durations are quoted to the nearest ns.

The results show the best performance in terms of pulse duration to be with a mix fairly weak in F_2 with a partial pressure of only 2 mbar. The pulse durations over 80 ns FWHM represent some of the longest XeF^* pulses ever obtained indicating that the laser is working satisfactorily. These pulse durations may be compared with 10-35 ns pulse durations of current commercial discharge pumped XeF^* lasers, (26). The pulse energies however are poor with a specific energy extraction of only around 0.25 Joules per litre. Interestingly gas mixes with higher F_2 partial pressures in some cases produced similar pulse energies but from shorter pulse durations indicating higher gain as a result of improved kinetic efficiency. Unfortunately it seems that this improvement in the excimer formation rate must be traded off against poorer discharge stability in the case of higher halogen donor concentrations.

Table 4.3.1

	PFN Charge (kV)	Pulse Energy (mJ)	Pulse Duration FWHM (ns)
10 mbar Xe, $1\frac{1}{2}$ mbar F_2			
3 bar Ne	20	3	45
	25	5	47
4 bar Ne	20	4	47
	25	5	49
10 mbar Xe, 2 mbar F_2			
3 bar Ne	20	7	82
	25	7	79
4 bar Ne	20	6	77
	25	8	83
10 mbar Xe, $2\frac{1}{2}$ mbar F_2			
3 mbar Ne	20	5	70
	25	6	72
4 bar Ne	20	6	62
	25	9	72
$4\frac{1}{2}$ bar Ne	20	6	53
	25	8	54
10 mbar Xe, 3 mbar F_2			
3 bar Ne	20	6	40
	25	7	44
4 bar Ne	20	6	39
	25	8	42

An example of current and light output waveforms are shown in Fig. 4.1 for an XeF^* gas mix weak in F_2. The lasing turns on at a head current of about 4 kA and off at around 10 kA.

The results obtained with XeF^* serve as a bench-mark against which other fluorine excimers can be compared.

Fig. 4.1

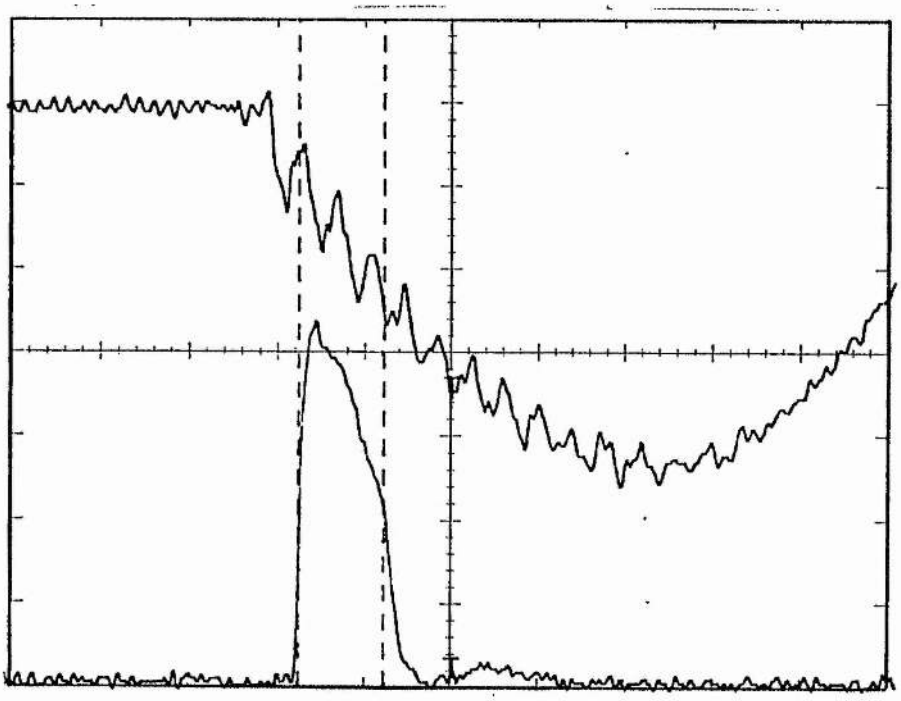

Fig. 4.1 Discharge current and laser light output for a XeF^* laser mix weak in F_2; $1^1/_2$ mbar F_2, 10 mbar Xe, 4 bars Ne; 50 ns/div,4 kA/div

KrF^*

The equipment was switched over to KrF^* making as few changes as possible. All parameters were kept constant except the laser mirrors which were changed for a full reflector and a 60% partial reflector at 249 nm.

Unfortunately it was not possible to maintain all parameters constant between the XeF^* and KrF^* runs. Initial trials with 10 mbar of Kr gave no lasing at all while mixes with as much as 80 mbar Kr lased only poorly. After some trial and error a partial pressure of 60 mbar Kr was adopted as giving best results. This is roughly in agreement with earlier KrF^* parametric studies, (27). With XeF^* the PFN was charged to 20 and 25 kV, with

KrF^* however the PFN needed to be charged to higher voltages to obtain a reliable output, with a PFN charging voltage of 25 kV only a very weak laser output was seen. 28 kV was chosen as the PFN charging voltage, close to the maximum design value of 30 kV. The differences in Kr partial pressure and PFN charging voltage are manifestations of the slightly differing kinetic schemes between KrF^* and XeF^* and their different pumping requirements.

The KrF^* laser was generally more difficult to operate than XeF^* requiring a more precise mirror alignment to achieve reproducible and consistent results. for this reason a smaller but still representative number of results were taken.

Table 4.3.2

	PFN Charge (kV)	Pulse Energy (mJ)	Pulse Duration FWHM (ns)
60 mbar Kr, $2\frac{1}{2}$ mbar F_2			
3 bar Ne	28	14	43
60 mbar Kr, 3 mbar F_2			
3 bar Ne	28	27	40
4 bar Ne	28	22	48
60 mbar Kr, $3\frac{1}{2}$ mbar F_2			
3 bar Ne	28	15	32
60 mbar Kr, 4 mbar F_2			
3 bar Ne	28	5	20

Again it is noted that the longest durations were obtained with gas mixes fairly weak in F_2 although they were all shorter than the equivalent XeF^* pulse durations. Interestingly the pulse energies were much larger than with XeF^*, possibly due to the higher PFN charging voltage and hence bigger discharge current. An example of current

and light output waveforms for 3 mbar F_2, 60 mbar Kr, 3 bars Ne is given in fig. 4.2. This shows that the laser turns on at a head current of 6 kA and turns off at around 10 kA.

Fig.4.2

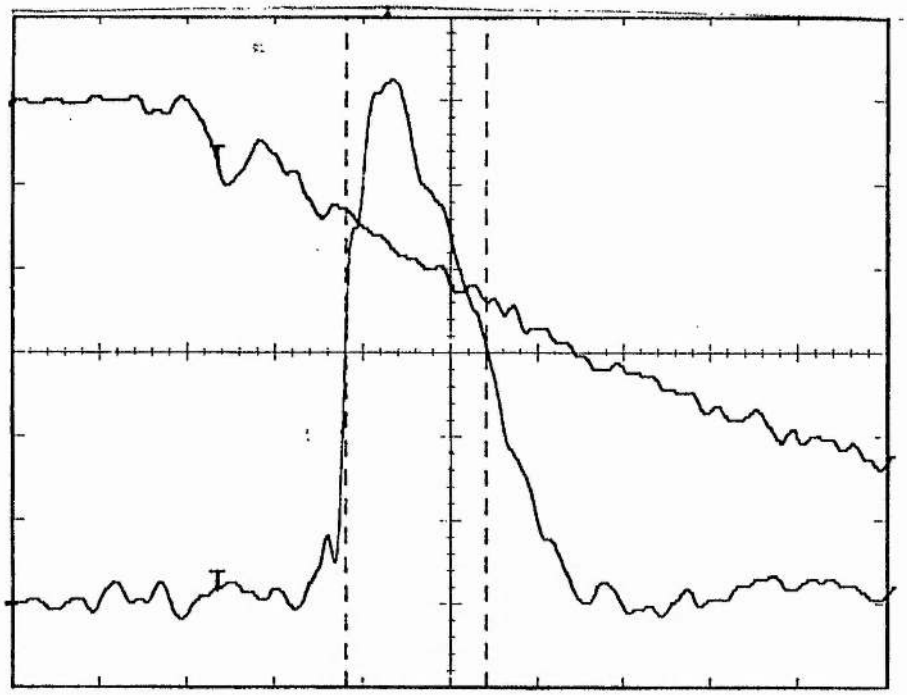

Fig. 4.2 Laser head current and light output waveforms for KrF^* with 3 mbar F_2, 60 mbar Kr and 3 bars Ne, 20 ns/div, 4 kA/div

ArF^*

Having completed the experiments with KrF^* the equipment was then modified again for lasing with ArF^* at 193 nm. Although as few changes as possible were made, operating at this short wavelength does pose special problems. Firstly UV light at 193 nm undergoes significant atmospheric absorption and to counteract this the mirrors forming the optical resonator were placed as close as possible to the pressure windows so as to minimise the proportion of the optical path outside the laser pressure vessel. One high reflector and one 60% reflective output coupler were used.

A further problem with operating at such a short wavelength arises from the fundamental laser physics.The stimulated emission cross-section for a general laser system, (28), is given by the following equation:

$$\sigma = \frac{\lambda^4}{8\pi\tau\Delta\lambda c} \qquad 4.11$$

where λ is the transition wavelength and τ the upper state spontaneous emission time. Following on from this, the pump power density required to produce a unity gain coefficient per unit length is:

$$P = \frac{8\pi hc^2\Delta\lambda}{\lambda^5\eta\phi} \qquad 4.12$$

where ϕ is the quantum efficiency and η is the efficiency of population of the upper laser level.

For the ArF^* system at $\lambda = 193$ nm, with $\Delta\lambda = 1$ mm, (29), and the product of ϕ and η to be ~ 0.05, then the pump power density for a gain coefficient of 0.1 cm^{-1} is found to be 1.1 $MWcm^{-3}$. This is higher that the other excimers considered because of the λ^5 factor, but should still be achievable by using discharge currents approaching 20 kA assuming a V_{ss} of about 1.5 kV.

With due consideration given to the theoretical operational restrictions, experiments commenced. An initial gas mix of 10 mbar F_2, 200 mbar Ar, and 4 bar Ne was used, (30). It is well known that the particular gas proportions are machine dependant and particularly sensitive to variations in the case of ArF^*. Unfortunately no lasing action was obtained. A parametric study of gas proportions was carried out varying the F_2 partial pressure between 6 and 10 mbar and the Ar partial pressure from 120 to 200 mbar, again no lasing was evident.

The inability to produce lasing in ArF^* could be due to the failure to achieve the required pump power density although the available evidence does not support this. A measurement taken with a gas mix of 8 mbar F_2, 200 mbar Ar and 4 bar Ne gave a value for V_{ss} of around 3.5 kV which is larger than with other excimers and implies that the required pump power density of 1.1 $MWcm^{-3}$ was being reached with a head current of

only 9.5 kA. Visual inspection of the discharge, with the mirrors removed, using suitable neutral density filters showed the discharge to be filamentary and inhomogeneous. This is probably a consequence of the high partial pressure of fluorine and also possibly due to the presence of argon, (see chapter 5). In conclusion the most likely reason for no lasing was not the inability to achieve the required pump power density but the failure to produce a sufficiently stable homogeneous glow discharge.

4.3.4 Conclusions

From the experimental evidence it can be deduced that in a practical laser apparatus under pumping conditions as similar as possible in each case, the optical pulse duration will decrease moving from XeF^* to KrF^* and ArF^*. The reasons for this behaviour are not clear cut but some conclusions can be drawn.

It is apparent that the premature termination of lasing in XeF^* and KrF^* and the failure to achieve any lasing at all in ArF^* is the result of discharge instability. In ArF^* in particular the filamentary nature of the discharge could be seen. With XeF^* and KrF^* the laser output terminated while the discharge pumping current was still continuing. With ArF^* the high proportion of F_2 required by the laser kinetics provides a plausible explanation while the reasons for poor performance with KrF^* are more difficult to explain.

It was discovered experimentally that KrF^* required a larger pump power density than XeF^*. As stated previously this could be due to many factors such as the differing reaction rates in the kinetic scheme for the production and quenching of excimer molecules. By equation 4.12 it may be expected that the shorter wavelength of KrF^* will require more intense pumping; it is difficult however to make direct comparisons because the emission line width, $\Delta\lambda$, is also required in the calculation and is made more difficult in the case of XeF^* by the degenerate structure of the laser output in the 351-353 nm region, (31). Even if the other factors in equation 4.2 such as the excimer production efficiency are accurately known the difficulty in assigning a value for $\Delta\lambda$ in XeF^* leaves a large uncertainty.

Having established experimentally that KrF^* requires more intense pumping than XeF^* this can be use to explain why the observed pulse durations are shorter. From fig. 4.2 the measured current at the onset of lasing was slightly larger with KrF^* and the dI/dt during lasing was also greater. This higher discharge current in itself could be responsible for directly driving discharge instability by increasing the electron number density but could also play an important part in driving the mechanisms described in sections 4.2.2 and 4.2.3. In the 'classical' halogen donor depletion model, from eqn. 4.2, the stability time index is dependent on the initial electron number density, $\langle n_{e0} \rangle$, which is in turn related to the discharge current density and electron drift velocity at the onset of the discharge 'burning' stage, see eqn 4.3. While the small proportion of the rare gas partner in the overall gas mix will probably not significantly alter the electron drift velocity the faster turn on of current when KrF^* was operated probably lead to a larger initial electron number density with the consequent acceleration in growth of filamentary instabilities.

References

1 C A Brau; "The Rare Gas Halogen Excimers;" from C K Rhodes (editor);"Excimer Lasers;" Topic in appl. phys. vol 30, 2nd edition, Ch 4, p109, Springe Verlag, New York 1983
2 M M Turner, PhD Thesis, University of St. Andrews, 1990
3 D C Hogan, R Bruzzese, A J Kearsley, C E Webb; "Long Pulse Operation of Discharge Excited XeCl Lasers;" J Phys D, vol 14, L157-61, 1981
4 R S Taylor, K E Leopold; "Microsecond Duration Optical Pulses From a UV Preionised XeCl Laser;" Appl. Phys. Lett., vol. 47(2), p81-3, July 1985
5 Roger A Haas; "Plasma Stability of Electric Discharges in Molecular Gasses;" Phys Rev A, vol 6(2), p1017-43, 1973
6 D Lo, Cheng-En Zheng; "Evolution of Instabilities in an XeCl Laser Discharge;" Opt. Comms. vol 69, p277-80, 1989
7 V Hasson, H M von Bergman; "Spatial Control of Pulsed High-Pressure Pre-ionisation Stabilised Glow Discharges;" J Phys E, vol 13, p632-8, 1980
8 S Sumida *et al* ; "Effect of Preionisation Uniformity on a KrF Laser;" J Appl. Phys, vol 52, p2682-6, 1981
9 R S Taylor; "Preionisation and Discharge Stability Study of a Long Pulse Duration UV-Preionised XeCl Laser;" Appl. Phys. B, vol 41, p1-24, 1986
10 M M Turner, P W Smith; "Modelling of Excimer Laser Glow Discharges;" Proceedings of the 9th International Conference on Gas Discharges and their Applications, p725-9, Venice, 1988
11 D Lo, J Xie; "High Pressure Scaling of a High Current Density XeCl Laser;" J Phys D, vol 24, p1023-4, 1991
12 D Lo; "Electrical Characteristics of a Small Active Volume (1 cm^3) Discharge-Pumped XeCl Laser;" Opt. and Quantum Elect. vol 20, p257-62, 1988
13 R S Taylor, K E Leopold; "Ultralong Optical-Pulse Corona Preionised Excimer Lasers;" J Appl. Phys. vol 65, p22-9, 1988
14 J D Daugherty, J A Mangano, J H Jacob; "Attachment Dominated Electron Beam Ionised Discharges;" Appl. Phys. Lett. vol 28, p581-3, 1976
15 D C Hogan, R Bruzzese, A J Kearsley, C E Webb; "AIP Conference Proceedings 100, 1 (Excimer Lasers) ed. by C K Rhodes, H Egger, H Plummer, Lake Tahoe, Nevada, 1983
16 J Coutts, C E Webb; "Stability of Transverse Self-Sustained Discharge-Excited Long-Pulse XeCl Lasers;" J Appl. Phys. vol 59, p704-10, 1986
17 M R Osborne; "Rare Gas Halide Discharge Stability;" Appl. Phys B, vol 45, p285-91, 1988
18 M R Osborne, J Coutts, M H R Hutchinson, C E Webb; "Output Pulse Termination of a Self Sustained Excimer Laser," Appl. Phys. Lett. vol 49, p7-9, 1986
19 R Slater; "N_2 Production in e-beam Pumped XeF Lasers Containung NF_3;" Appl. Phys. B, vol 42, p17, 1987
20 M Bahr, W Botticher, S Choraba; "The Time Dependent Development of the Macroscopic Instability of a $XeCl^*$ Laser Discharge;" IEEE Transactions on Plasma Science, vol 19 (2), p369-78, 1991
21 M J Kushner; "Microarcs as a Termination Mechanism of Optical Pulses in Electric Discharge Excited KrF^* Excimer Plasmas;" IEEE Transactions on Plasma Science, vol 19 (2), p387-99, 1991
22 J E Velzaco, *et al*; "Quenching rate Constants for Metastable Argon, Krypton and Xenon atoms by Fluorine Containing Molecules and Branching Ratios for XeF^* and KrF^* Formation;" J Chem. Phys, vol 65, p3468, 1976
23 C A Brau; "The Rare Gas Halogen Excimers;" from C K Rhodes (editor);"Excimer Lasers;" Topic in appl. phys. vol 30, 2nd edition, Ch 4, Springe Verlag, New York 1983
24 F Kinnari, A Suda, M Obara, T Fujioka; "Theoretical Simulation of Electron-Beam-Excited Xenon-Chloride (XeCl) Lasers;" IEEE J. Quantum Electrnics, vol 19(10), p1587-600, 1983
25 S A Fairlie; Experiments carried out at AEA Technology, Culham, Oct 1990, Unpublished
26 H W Messenger; "Applications Mark Progress for Excimer Lasers;" Laser Focus World, Sept 1990, p71-82
27 D E Rothe, R A Gibson; "Analysis of Spark-Preionised Large-Volume XeF and KrF Discharge Laser;" Optics Comm, vol 22(3), p265-8, 1977
28 M H R Hutchinson; "Excimers and excimer Lasers;" Appl. Phys, vol 21, p95-114, 1980
29 J M Hoffman, A K Hays, G C Tisone; "High Power UV Noble Gas Halide Lasers;" Appl. Phys. Lett, vol 28, p538-9, 1976
30 M R Osborne, Private Communication
31 C A Brau, J J Ewing; "Emission Spectra of XeBr, XeCl, XeF, KrF;" J Chem. Phys, vol 63, p4640-7, 1975

Chapter 5

The Influence of Buffer Gases on Discharge Stability

5.1 Introduction

It is well known that a buffer gas in a rare gas halide excimer laser plays only an indirect part in the kinetic scheme for the production of excimer molecules. Most excimer molecules are produced either by the ionic recombination of rare gas and halogen ions or by the 'neutral channel' involving dissociative quenching of rare gas excited metastables by halogen donor molecules, (see chapter 1). The only significant part played by the buffer gas in these schemes is that ionic recombination usually takes place in the form of a three body reaction involving a buffer gas atom. Reactions involving complex ions of rare gas and buffer gas atoms that produce excimer molecules do occur but are of lesser importance.

The buffer gas does however fulfil several important functions. For efficient discharge pumping an electrical power density in the region of several hundred $kWcm^{-3}$ needs to be deposited in the laser medium, (1). If the laser gas consisted of only the halogen donor and rare gas partner at a total pressure of several tens of mbar then the discharge self sustaining electric field would be very low. As the pump power deposition in the discharge is given by the product of the self sustaining E field and the discharge current density, unrealistically large current densities would be needed to achieve the required pumping rate. The buffer gas at a total pressure of several bar raises the self sustaining E field sufficiently to make discharge pumping practicable.

It is not possible to make a discharge pumped excimer gas mix solely from a halogen donor and the rare gas partner, even if the total pressure is large enough to satisfy the power deposition requirements. The heavier rare gases interact with electrons such that a high over-voltage is required for breakdown. As the atomic number increases from helium to xenon, both the cross section for ionisation by electron impact and the non-ionising excitation cross section become larger. Unfortunately the non-ionising cross section increases at a faster rate so that for xenon the ratio of the excitation to ionisation coefficients is much larger than in the case of helium, for example. With the heavier rare

gases the threshold energy for inelastic processes is also lower so a higher proportion of the total discharge power is directed into the production of neutral excited states. In the initial stages of the discharge, when the electron number density is small, most of the energy that goes into the production of these excited states is wasted. The neutral excited states are quenched by other neutral species rather than being ionised by subsequent electron impact, as would be the case after breakdown, with the consequent higher electron number densities.

The lower inelastic threshold of the heavier rare gases combined with their preference for the production of excited rather than ionised states leads to a slewing of the electron energy spectrum and fewer high energy electrons. Despite the lower inelastic threshold of the heavier rare gases the smaller proportion of electrons with energies above this threshold results in less of the total discharge power being channelled into ionisation. To counteract this the heavy rare gas is diluted by a large fraction of lighter buffer gas. This causes a reduction in the effective excitation cross section for the gas mix as a whole and hence increases the ionisation cross section relative to the excitation cross section. Consequently the proportion of the electron spectrum above the inelastic threshold is raised and the ionisation efficiency improved.

Kinetic studies using computer modelling, (1), indicate that for xenon diluted with either helium, neon or argon buffer gas the first Townsend coefficient, α, is largest for neon closely followed by helium. Argon appears to result in a value for α of approximately an order of magnitude less at concentrations appropriate for an excimer gas mix. Helium, neon and argon have all been used successfully as the buffer gas in both electron beam and electron beam sustained discharge machines, (2), but argon has been found to give significantly worse performance when self sustained discharge pumping is used. The reason for this markedly inferior performance with argon are therefore probably to do with its influence on discharge stability rather than kinetic factors.

When initially formed, most excimer molecules are in vibrationally excited states yet it is the lower vibrational states, $v = 0,1,...,$which are more favoured as the upper lasing level. The buffer gas performs the important function of collisionally quenching these

higher vibrationally excited states as well as helping to maintain the equilibrium between B and C states where they happen to lie close together in energy, such as in $XeCl^*$.

Although helium is generally accepted as an inferior buffer gas to neon it still finds favour for some applications. Where very high repetition rate operation is desired high velocity gas circulation is usually a necessity. Helium can be advantageous in terms of the engineering requirements as the gas blower power required for a given gas flow is proportional to the mass density of the gas, (3). The lighter mass of helium has been found to allow a five fold reduction in blower power over a similar system using neon as a buffer gas.

There are also financial advantages in choosing helium or argon as buffer gases as the price of these is substantially less than neon. Helium is plentiful as a by-product of natural gas extraction while argon, in common with the other rare gases, must be distiled from air. Argon is approximately 516 times more abundant than neon in the Earth's atmosphere, (4), so that even allowing for normal economic fluctuations, argon will always be substantially cheaper.

In conclusion, although neon is the best buffer gas in terms of kinetic and electrical efficiency there may be advantages in certain cases for using helium and/or argon instead. To determine if this is so requires further studies of the influence of different buffer gases on laser performance and in particular glow discharge stability.

5.2 Studies of Helium Buffered $XeCl^*$ Performance

It was decided to perform a series of experiments to determine the operating characteristics of a helium buffered $XeCl^*$ laser. The laser apparatus available was particularly suitable for such a study as its small active volume meant that the laser gases could be changed rapidly allowing a large number of results to be obtained in a short time; furthermore the simple construction permitted easy measurement of discharge electrical characteristics simultaneously with laser output parameters. By comparison of results obtained with both helium and neon buffer gases it was hoped that an explanation for the inferior performance of helium would become apparent.

5.2.1 Experimental Description

The laser head was fully passivated with HCl and the preioniser driver voltage adjusted until consistent performance was obtained. In the first series of runs the HCl and Xe partial pressures were kept constant and the helium buffer gas pressure increased from 1 bar to 3 bars absolute in 200 mbar increments. At each step the head voltage and laser output temporal profiles were recorded and the laser output pulse energy measured. Head current measurements were also made but were found to be largely invariant across the buffer gas pressure range, a consequence of the head current being determined mainly by the external circuit. The other laser operating parameters were:

Pressure Windows	2 x Herasil (fused quartz)
	50 mm dia. x 9 mm thick
Mirrors	1 x HR @ 308 nm
	1 x 40%R @ 308 nm
Electrode spacing	16 mm
PFN Charging Voltage	20 kV (all cases)

Output energies were measured to the nearest 0.5 mJ for the smaller values and to the nearest mJ for those of 10 mJ and above. The output pulse durations were taken from the light output profiles and are to the nearest nanosecond FWHM. The head voltages were measured from oscilloscope traces and are estimated to be $\pm$ 20 V.

5.2.2 Results

The results for the first experimental run are given in table 5.2.1 and summarised graphically in Fig 5.1

Fig. 5.1

Graphs of pulse duration and output energy against buffer gas pressure for Helium buffered XeCl

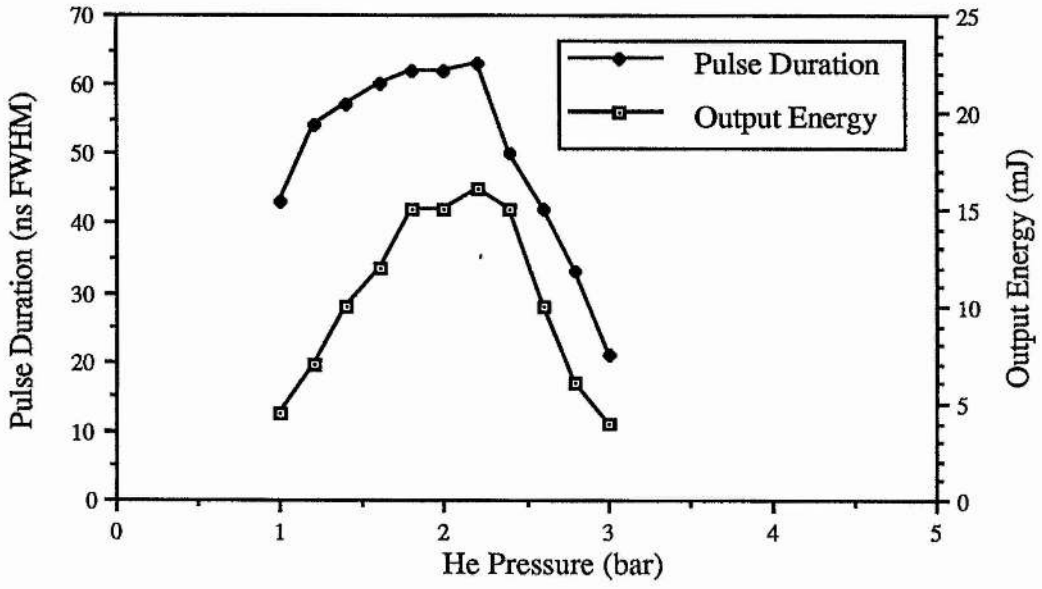

Table 5.2.1

Gas mix 15 mbar Xe, 3 mbar HCl

He Buffer Pressure (bar)	Output Energy (mJ)	Pulse Duration (ns FWHM)	Head Voltage (kV)
1.0	4.5	43	3.39
1.2	7	54	3.54
1.4	10	57	3.84
1.6	12	60	4.07
1.8	15	62	4.43
2.0	15	62	4.48
2.2	16	63	5.02
2.4	15	50	5.16
2.6	10	42	5.49
2.8	6	33	5.60
3.0	4	21	5.66

A problem with the results in table 5.2.1 is that as they were all made using the same gas fill by gradually increasing the helium buffer gas pressure. Despite being careful to minimise the total number of shots, as the experiment took almost one hour to complete and it was suspected that the gas fill may have been partially exhausted towards the later measurements. To check this a further run was made, summarised in table 5.2.2, using larger buffer gas pressure increments to reduce the total number of shots the laser was fired during the course of the experiment.

Table 5.2.2

15 mbar Xe, 3 mbar HCl

He Buffer Pressure (bar)	Output Energy (mJ)	Pulse Duration (ns FWHM)	Head Voltage (kV)
1	4	42	3.45
2	17	68	4.72
3	8	34	6.20
4	No Lasing Recorded		

Fig. 5.2

Light output and laser head voltage profiles from the experiment summarised in table 5.2.2. Head voltage (upper traces) 2.95 kV/div, laser light output (lower traces) in arbitrary units, all traces 50 ns/div

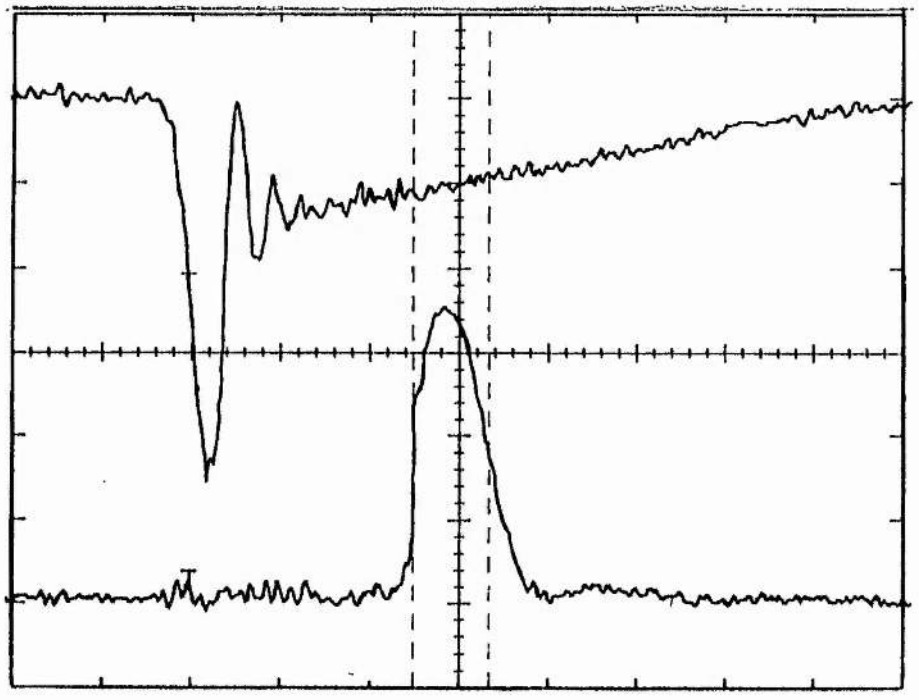

15 mbar Xe, 3 mbar HCl, 1 bar He; PFN charge 20 kV

Fig. 5.2. (cont.)

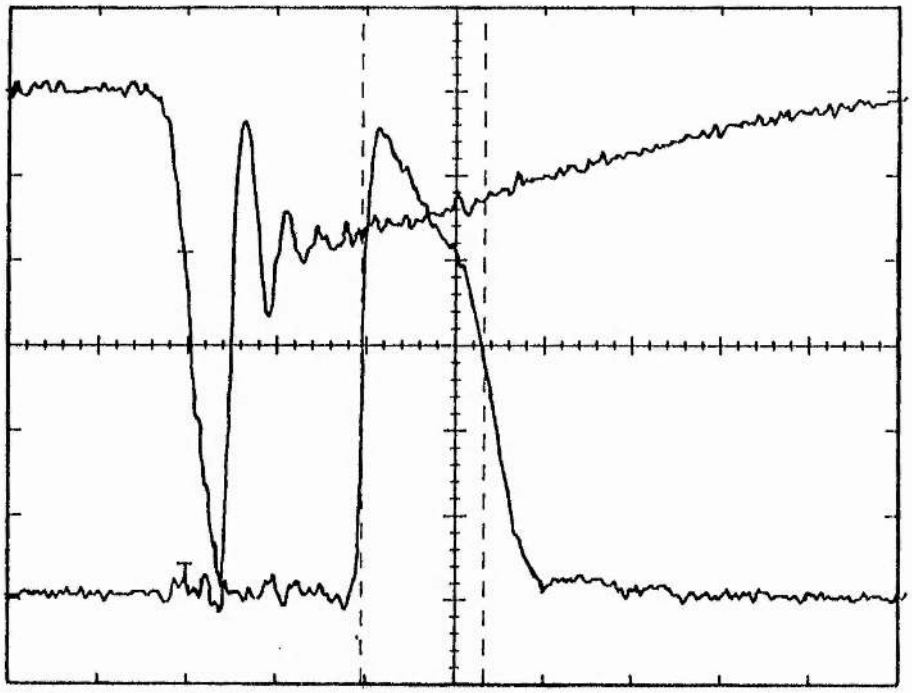

15 mbar Xe, 3 mbar HCl, 2 bar He; PFN charge 20 kV

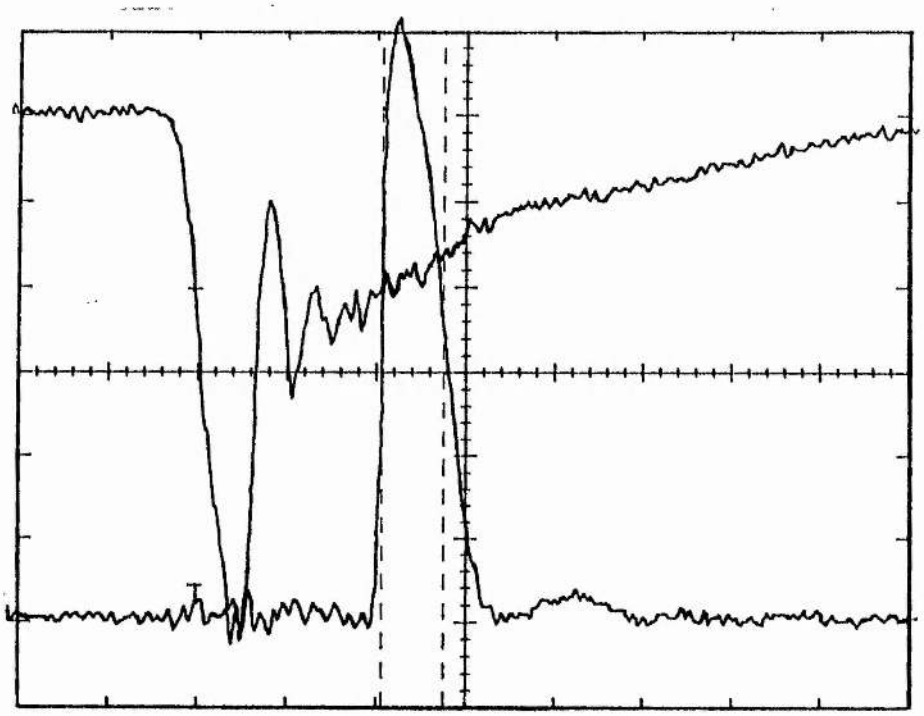

15 mbar Xe, 3 mbar HCl, 3 bar He; PFN charge 20 kV

Comparison of tables 5.2.1 and 5.2.2 shows fairly good agreement at the lowest buffer gas pressure but as expected table 5.2.2 gives higher pulse energies and shorter pulse durations as buffer gas pressure is increased. The use of the two sets of data in conjunction with each other allows a truer picture of the laser performance. Light output and head voltage profiles for the results in table 5.2.2 are given in Fig. 5.2.

For the sake of completeness a further run was made using a higher HCl partial pressure. In this case the shot to shot reproducibility of the laser was not as good but the results were still recorded and are given in fig. 5.3.

Fig. 5.3
Graphs of pulse duration and output energy against buffer gas pressure for helium buffered XeCl
15 mbar Xe, 4 mbar HCl

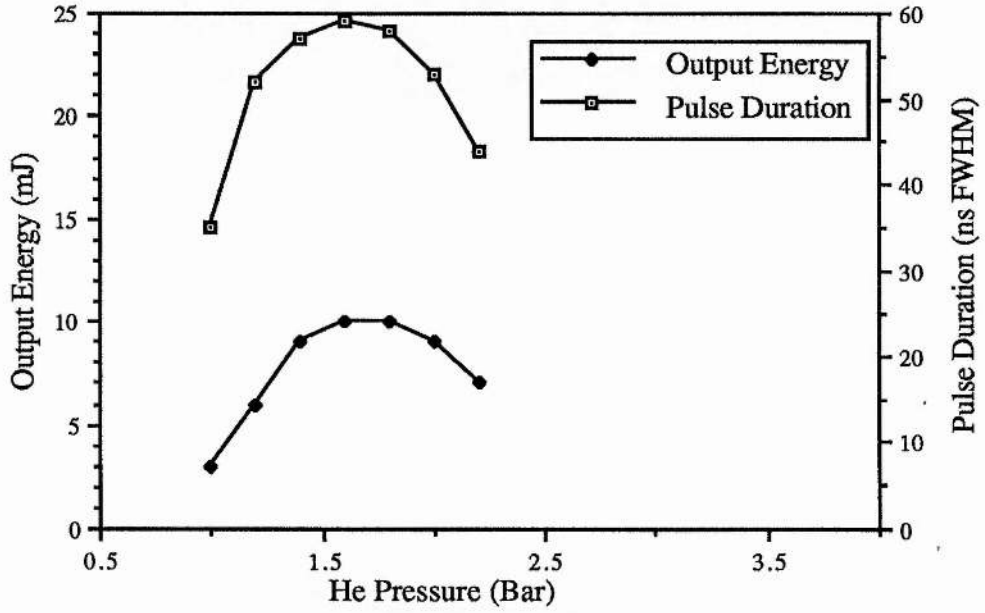

5.2.3 Discussion of Results

The results from these experiments raise several important points worthy of further discussion. It can be seen from fig. 5.1 that the maximum pulse duration is obtained with a buffer gas pressure of around 2.2 bar and that above this pressure the pulse duration falls off rapidly. The light output profiles in fig. 5.2 show however that despite the pulse duration declining at higher buffer gas pressures the peak amplitude of the laser output

continues to increase. This is probably due to the higher specific pump power deposition in the gas at higher buffer gas pressures and the increased efficiency of the excimer formation processes resulting in higher gain. This helps to confirm that the laser termination is due to the instability of the glow discharge rather than causes related to kinetic factors responsible for the production of excimer molecules.

Comparison of results between helium buffered $XeCl^*$ and the experiments described in chapter 2 using neon as the buffer gas, confirm that pulse durations are much shorter when helium is used. From the fundamental properties of helium discussed earlier it is to be expected that helium will give slightly worse performance than neon; the longest pulse durations obtained with helium however are only around half that achieved with neon. This can be explained by the much lower buffer gas pressures used with helium. The rates of the favourable reactions in which the buffer gas plays a part not surprisingly all increase with greater buffer gas pressure. As stated previously the most important of these are the quenching of vibrationally excited excimer molecules and the ionic recombination channel for excimer production which is a three body reaction involving a buffer gas atom. With a lower overall buffer gas pressure these processes would proceed at a slower rate resulting in a reduced rate of production for excimer molecules in the upper laser state. It is presumed that if the discharge stability could be improved to the same level as with neon with helium buffer gas at pressures in the range of 3 to 4 bar then laser performance in terms of specific energy extraction would be similar. It seems that there is some feature of helium that induces glow discharge instability earlier and at lower pressures than neon.

Fig. 5.4
Graph of Head Voltage Against Buffer Gas Pressure for Helium Buffered XeCl

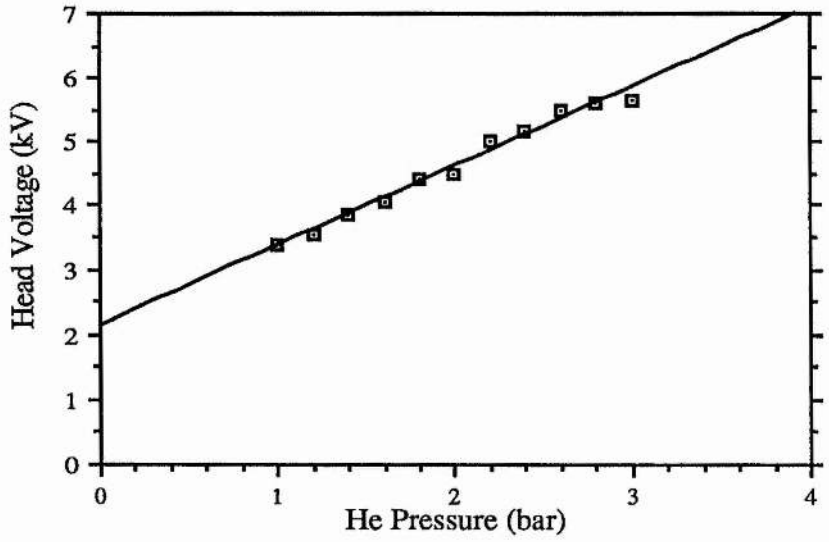

In addition to laser output parameters throughout these experiments the laser head voltage was also measured. The variation in measured head voltage with buffer gas pressure taken from the data in table 5.2.1 is plotted in fig. 5.4. It should be noted that the points plotted are the experimentally measured values of head voltage and that no correction has been applied for the additional voltage generated by head inductance effects. The points all lie on a straight line with the gradient proportional to the reduced electric field, E/P, which according to discharge theory should remain constant. Extrapolation gives an intercept at 2.1 kV and this may be taken as the contribution to the measured head voltage from the head inductance. Correcting for this gives an E/P of 0.79 $kVcm^{-1}bar^{-1}$. Analysis of the self sustaining voltages of an equivalent gas mix of 15 mbar Xe and 3 mbar HCl but with a neon buffer gas in the pressure range 2 to 5 bar gives an E/P of only 0.31 $kVcm^{-1}bar^{-1}$. The use of helium as the buffer gas therefore significantly increases the value of the self sustaining electric field.

The reduced electric field is determined by the balance between the electron generation and electron loss mechanisms and may be interpreted as a measure of the energy gained by an electron between atomic collisions. The E/N (or E/P) is therefore an indicator of the electron temperature within the discharge. It is physically sensible that discharges in

helium should have a high electron temperature because of the high energy threshold for inelastic processes, below this threshold electrons in collision with helium atoms can only interact elastically and the energy lost in each collision will be smaller than in a typical inelastic collision. As the total gas pressure increases the electric field increases to maintain a constant reduced electric field. This implies that the electron temperature will rise with increasing gas pressure because the energy gained on average between collisions remains constant but collisions occur more frequently and below the inelastic threshold energy only a small amount of energy is lost by the electrons in each collision with a helium atom. All of this however implies that the production of electrons by the ionisation of helium, wether directly or via excited states, must be significant. This is in contradiction to the assumption made by Webb and others that for $XeCl^*$ the only significant electron production mechanism is by ionisation of Xe* states.

Returning to the discharge stability theory proposed by Bahr *et al* , (5), (see section 4.2.3) the electron temperature is known to be important for balancing the electron production and attachment processes believed to operate. At high electron temperatures the dominant electron attachment mechanism of dissociative electron attachment to vibrationally excited HCl molecules is less favourable. It is also known that the main free electron production mechanism , the ionisation of Xe^* metastables, proceeds at a faster rate with increasing electron temperature. It is therefore proposed that as the discharge sits at a higher reduced electric field the energy deposition in the gas is greater than for an equivalent gas mix based on a neon buffer. This causes an increase in the electron temperature so that electron attachment processes can no longer keep pace with the increased electron production rate. As this happens the electron density will tend to run away leading to the accelerated growth of filamentary instabilities and discharge collapse. This mechanism therefore provides an explanation for the experimentally observed inferior performance of helium buffers that is based upon discharge stability rather than the excimer production kinetic scheme.

5.3 The Use of Argon as a Buffer Gas

As discussed earlier, although argon is kinetically an inferior buffer gas to either neon or helium it has been used successfully in electron pumped machines, (2). The use of argon in discharge pumped excimer lasers has been less successful as argon appears to significantly reduce glow discharge stability compared with other buffer gases. A series of experiments were conducted to assess the performance of argon as a buffer gas in a discharge pumped $XeCl^*$ laser.

5.3.1 An Argon Buffered $XeCl^*$ laser

The laser system was used in the same way as described in the previous section but with the helium buffer substituted by argon. Argon buffer pressures in the range of 1 to 4 bar with 15 mbar of xenon and 2 to 4 mbar of HCl were tried but no lasing action was obtained. Visual inspection of the discharge with the laser mirrors removed showed it to be filamentary and inhomogeneous. Problems were also experienced with parasitic arcing between the hot electrode and the walls of the laser head vessel. Why this should be so is unclear as the distance to the grounded electrode is shorter however it was suspected that the path taken did involve surface tracking across the polyethylene insulating support for the hot electrode. This problem was cured by the inclusion of some Mylar™ insulating sheet inside the laser head vessel.

The failure to achieve any lasing at all with pure argon buffer gas was disappointing and naturally restricted the scope of the experiments that could be performed. Instead it was decided to study the influence of buffer gases containing mixtures of different proportions of helium and argon.

5.3.2 The Use of Helium / Argon Mixtures as a Buffer Gas

It was suspected that using a mixture of helium and argon as the buffer gas in a discharge pumped XeCl laser may result in longer pulse durations and higher pulse energies than when either of the gases is used alone at the same pressure. Work carried out by Hiramatsu and Goto, (6), showed that a discharge pumped $XeCl^*$ laser could give

higher output energies at total gas pressure of 1.7 bars if a neon / argon buffer gas was used instead of pure neon, although in this case the laser pulse durations were only around 8 ns (FWHM). Other workers have also reported that at buffer gas pressures below 2 bars an argon / helium mixture can produce higher output energies than either pure helium or pure argon at the same total pressure, (7,8).

This behaviour was investigated using a large volume, discharge pumped, X-ray preionised machine, (9), and found to hold to a limited extent. When small quantities of argon were added to an otherwise pure helium buffer, laser performance in terms of output energy and pulse length were found to increase. Why this should be so is unclear but the most likely explanation probably lies in the argon producing an improvement in the efficiency of the kinetic scheme.It was tentatively suggested that Penning ionisation of xenon atoms by argon excited states may be responsible; it is known however that many of the excited states of argon are not sufficiently energetic to ionise xenon. The large active volume of this machine and its consequently high gas consumption unfortunately restricted the number of experiments that could be carried out.

It was decide to use the small volume laser to further study this effect. The laser operating parameters remained unchanged from the earlier helium only and argon only experiments, that is:

Pressure Windows	2 x Herasil (fused quartz)
	50 mm dia. x 9 mm thick
Mirrors	1 x HR @ 308 nm
	1 x 40%R @ 308 nm
Electrode spacing	16 mm
PFN Charging Voltage	20 kV (all cases)

Runs were made with 15 mbar Xe and 3 mbar HCl starting with helium buffer gas pressures of 1, 1.5, 1.75 and 2 bar. Argon was added in small increments and at each stage profiles of the laser light output, the head voltage and the discharge current were recorded and the pulse energy was measured. The results are given in table 5.3.1.

Table 5.3.1

15 mbar Xe, 3 mbar HCl

Buffer Gas Composition	Pulse Energy (mJ)	Pulse Duration (ns FWHM)	Head Voltage (kV)
1 bar He	3.5	41	3.48
+ 200 mbar Ar	4.5	38	3.92
+ 300 mbar Ar	4	36	3.84
+ 450 mbar Ar	2.5	34	4.07
1.5 bar He	10	64	3.30
+ 60 mbar Ar	11	68	3.36
+ 130 mbar Ar	10	53	3.36
+ 200 mbar Ar	6	43	3.07
1.75 bar He	12	74	4.37
+ 100 mbar Ar	11	65	4.43
+ 200 mbar Ar	pulse energy	36 (average)	4.72
+ 300 mbar Ar	erratic	29 (average)	4.43
2 bar He	12	56	4.43
+ 100 mbar Ar	8-25	50-75	4.50

It can be seen that at the lower helium buffer pressures the addition of small quantities of argon does improve pulse energies and in one case improves the pulse duration also. In all cases however the pulse energies and durations were poor when compared with a neon buffered gas mix. The addition of larger quantities of argon resulted in a rapid decline in laser performance, furthermore the outputs from the helium / argon mixtures were usually inferior to those obtained from a pure helium buffer at the equivalent total pressure. It was also noted that at higher helium pressures the addition of argon produced wildly erratic laser outputs with very large shot to shot variations.

The light output profiles, head voltage and discharge current traces for the addition of argon to a 1.5 bar helium buffer are shown in fig. 5.5. It can be seen that the addition of argon causes an increase in the peak light output, presumably a result of higher laser gain.

Fig. 5.5

Light output profiles (bottom traces), head voltages (middle traces) and discharge currents (top traces) for the addition of argon to a 1.5 bar helium buffered XeCl gas mix 15 mbar Xe, 3 mbar HCl. All traces 50 ns/div. Head voltages 2.8 kV/div. Discharge currents 4.2 kA/div. PFN charge 20 kV.

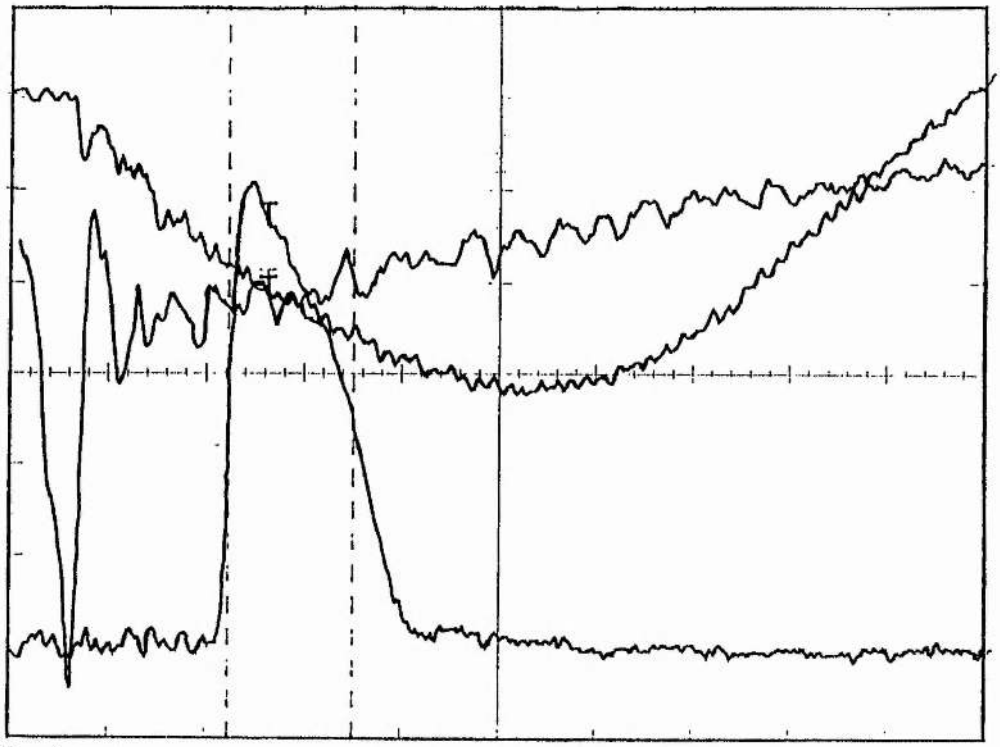

No additional argon

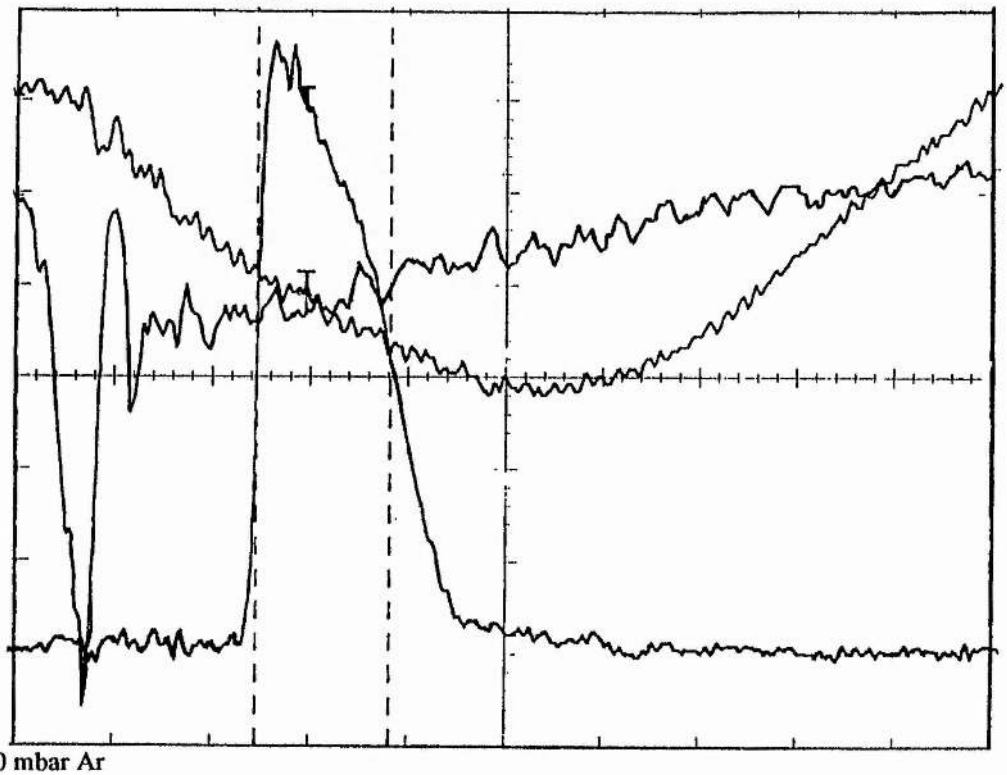

Plus 60 mbar Ar

Fig. 5.5 (cont.)

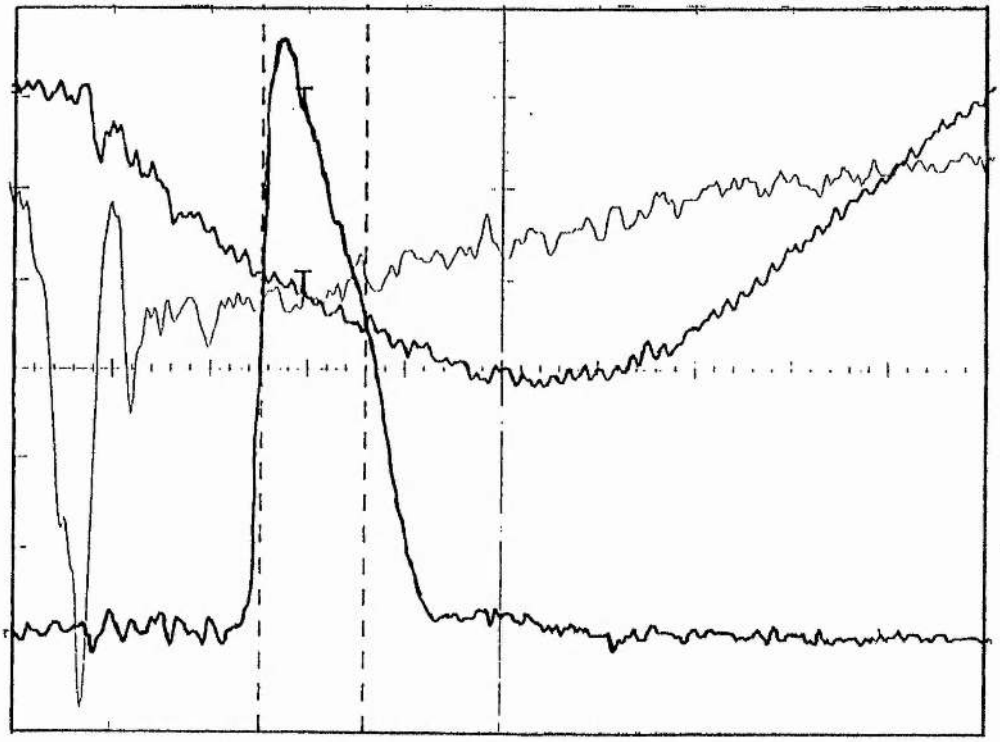

Plus 130 mbar Ar

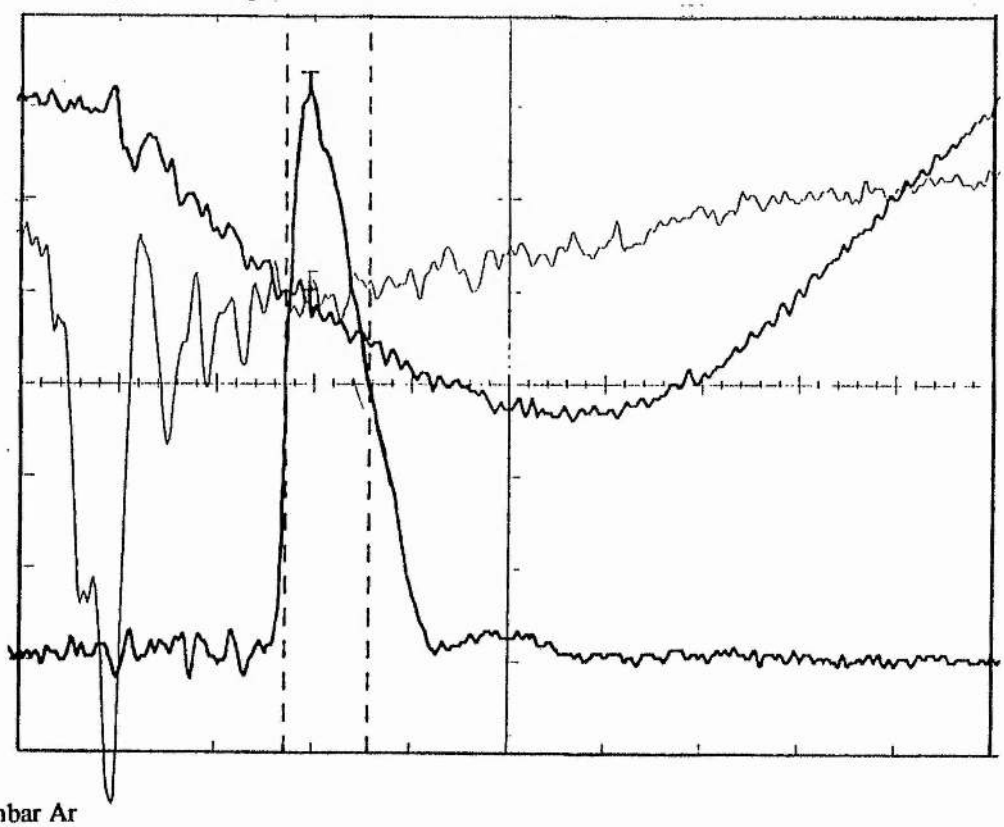

Plus 200 mbar Ar

There is no appreciable difference in the discharge current between the traces and only a very slight increase in the discharge self sustaining voltage so the power deposition in the gas is essentially constant, the increase in gain must therefore result from an improvement in kinetic efficiency. As argon partial pressure is increased the gain stays high but the pulse duration falls, presumably because of the earlier onset of discharge collapse.

The increase in gain with the addition of argon is to be expected when it is considered that that all the buffer gas mixtures were at total pressures below that shown to be optimum for a helium only buffer, (see section 5.2.2). The addition of any buffer gas, ignoring discharge stability factors, would therefore be expected to result in higher gain by improvements in the efficiency of the kinetic scheme such as an increase in the rate of vibrationally excited B state relaxation.

This experimental evidence therefore indicates that argon is an acceptably efficient buffer gas as part of the excimer production kinetic scheme but it unfortunately tends to accelerate the growth of discharge instabilities resulting in premature discharge collapse and laser termination. This is consistent with previous work where short laser pulse durations were also observed, (6).

5.3.3 Possible Explanations for the Poor Discharge Stability of Argon Buffered Excimer Discharges

Having identified that the use of argon as a buffer gas in discharge pumped $XeCl^*$ lasers is detrimental to discharge stability explanations for this are considered. A full theoretical treatment of why this should be so is beyond the scope of this thesis and therefore this section will be restricted to identifying some properties of argon that may have a bearing on discharge stability.

In all the current discharge stability theories for excimer discharges the dominant electron production mechanism is identified as the multistage ionisation of the rare gas partner, (5, 10-12), although doubt has been cast on the validity of this assumption here as it has been shown that E/N is influenced by the buffer gas composition. In the case of $XeCl^*$ it is believed that the excitation of Xe atoms proceeds by electron impact to produce

Xe^* metastables followed by their ionisation to Xe^+ ions by subsequent electron impact. The production of free electrons by ionisation of the buffer gas is generally accepted to be too energetic to be significant. This may not be true however in the case of argon. The first ionisation potential of argon is 15.68 eV compared with 21.47 eV for neon and 24.46 eV for helium, (4), and in view of the large partial pressure of the buffer gas electron production by single and multi-stage ionisation may be appreciable.

An analysis of electron impact ionisation of rare gases is given by Rapp and Englander-Golden, (13), but perhaps the treatment of ionisation of rare gas excited metastables by Ton-That and Flannery is more useful, (14). It is shown that the multi-stage ionisation of rare gases via excited metastables is more favourable than direct ionisation under the physical and electrical conditions of excimer laser discharges. Not only are the ionisation cross sections for metastables larger in the case of argon than for example neon but also the ionisation potentials of excited states of argon are lower than their neon equivalents implying that ionisation can be accomplished by lower energy electrons. Without detailed knowledge of the electron energy spectrum an exact comparison between the electron production rates due to ionisation of the various rare gases used as buffers can not be made. It can be deduced however that the higher E/N values found with gas mixes containing helium and the consequent higher electron temperature will drive these ionisation processes faster than with a predominantly neon buffer.

The contribution played by argon in driving glow discharge instabilities remains difficult to explain and is worthy of further investigation.

References

1 M M Turner, PhD. Thesis, University of St Andrews, 1990
2 S E Moody *et al* ; "Measurement of Lasing Performance and Efficiency of e-Beam pumped Xenon Chloride;" IEEE J. Quantum Elect. vol 17(9), p1856-60, 1981
3 J Fieret; "Aerodynamics of a High Repetition Rate Excimer Laser;" Eureka Excimer Definition Phase Report, Culham Laboratory, (1987), Unpublished
4 Handbook of Chemistry and Physics, Chemical Rubber Company
5 M Bahr *et al* ; "The Time Dependent Development of the Macroscopic Instability in $XeCl^*$ Laser Discharge;" IEEE Transactions on Plasma Science, vol 19(2), p369-78, 1991
6 M Hiramatsu, T Goto; "Efficient Low-Pressure Operation of a Discharge-Pumped XeCl Laser Using Ne/Ar Diluent;" Phys. Lett. A, vol 112A, p385-8, 1985
7 C G Christov, I V Chaltakov, I V Tomov and V L Lyutskanov; "An Efficient and compact Discharge-Excited XeCl Laser;" J Phys. D, vol D17, p247, 1984
8 M Hiramatsu, T Goto, S Hattori, C Yamabe; "Improved Performance of Discharge-Pumped XeCl Laser Using Ar/He Diluent;" Japan J Appl. Phys, vol 23, p1223, 1984
9 M H Plummer, University of St Andrews, Private Communication
10 J Coutts, C E Webb; "Stability of Transverse Self-Sustained Discharge-Excited Long-Pulse XeCl Lasers;" J Appl. Phys. vol 59, p704-10, 1986
11 M R Osborne, J Coutts, M H R Hutchinson, C E Webb; "Output Pulse Termination of a Self Sustained Excimer Laser;" Appl. Phys. Lett. vol 49, p7-9, 1986
12 M J Kushner; "Microarcs as a Termination Mechanism of Optical Pulses in Electric Discharge Excited KrF^* Excimer Plasmas;" IEEE Transactions on Plasma Science, vol 19(2), p387-99, 1991
13 D Rapp, P Englander-Golden; "Total Cross Section for Ionisation and Attachment in Gases by Electron Impact;" J. Chem. Phys. vol 43(5), p1464, 1965
14 D Ton-That, M R Flannery; "Cross Sections for Ionisation of Metastable Rare Gas Atoms (Ne^*, Ar^*, Kr^*, Xe^*) and of Metastable N_2^*, CO^* Molecules by Electron Impact;" Phys. Rev. A, vol 15, p517-26, 1977

Chapter 6

Techniques for Studying the Growth of Discharge Instabilities

6.1 Introduction

All the current theories of glow discharge instability explain discharge collapse by the growth of filamentary inhomogeneities. There is some difference of opinion however as to the exact mechanism by which these inhomogeneities grow and take over the discharge volume.In work presented by R.S. Taylor, (1) photographs of the discharge evolution indicate that filaments originate at the surface of both electrodes, but especially at the cathode, and grow inwards to consume the discharge volume. The local halogen donor depletion model of Coutts and Webb, (2) and the subsequent development by M.R. Osborne, (3) implies that under conditions where this mechanism is dominant, inhomogeneities should grow anywhere in the discharge volume where an initial disturbance to the halogen donor concentration occurs. It is noted however that most of these initial hot spots from which larger features emerge tend to be at or near to electrode surfaces; this is because these points tend to be subject to small variations in the local E field during the initial stages of discharge formation due to electrode surface imperfections.

The more recent theories of discharge stability by Bahr *et al* , (4) and the similar theory by Kushner, (5) both rely on the growth of initially small local variations in species populations to produce larger features that consume the glow discharge, although the growth mechanisms are different to that originally given by Coutts and Webb. In common with the earlier theories both these mechanisms depend on localised electric field variations as initiators of instabilities. The microarc theory of Kushner is particularly interesting in that it proposes that lasing is terminated by a disruption to the optical homogeneity of the laser medium due to a large number of small arcs, each on a scale of 10-100 μm, originating from hot spots on the electrode surfaces. The small size of these features means that they probably could not have been resolved in the photographs taken by Taylor.

It is not clear therefore if the discharge instabilities that cause the termination of lasing originate in the bulk of the plasma or at the electrode surfaces and if so whether the

cathode is favoured over the anode. The rate at which these instabilities grow to encompass the whole discharge is also difficult to determine. To try and answer these questions, some experiments were carried out to gain more information about the nature of discharge collapse.

6.2 Laser Output Spatial Profiles

6.2.1 Description of Experimental Method

Although the amount of equipment available was restricted and hence the complexity of the diagnostic techniques that could be used was limited, it was still possible to devise a simple experiment to measure the laser temporal profiles across the width of the laser beam output. In this way both the optical pulse duration and the laser amplitude due to specific regions of the active medium could be recorded at all points between the electrodes to determine their variation spatially across the laser beam profile.

Fig. 6.1

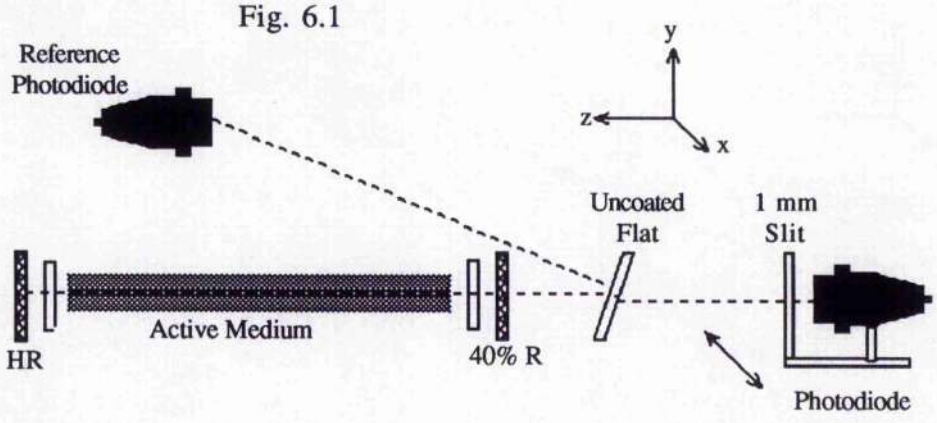

Experimental set-up for measuring the variation in laser light output across the width of the XeCl* laser beam profile

The experimental apparatus, shown in fig 6.1, consisted of a fast photodiode in front of which was positioned a 1 mm wide vertical slit. The photodiode was fixed to an optical mount which could be traversed horizontally so that the slit could be positioned to pick out a 1 mm wide vertical strip of the laser output at any position between the electrodes. Further refinement was added to ensure consistency by use of a second, reference photodiode. This was necessary to take account of the small shot to shot

variations characteristic of the laser and also to monitor the decline in the total laser output as the gas fill aged. An uncoated quartz flat was placed between the laser output and the slit to partially reflect a small proportion of the laser beam into the reference photodiode. In this manner the performance of the laser as a whole could be monitored simultaneously with the first photodiode looking at only a narrow strip. The first photodiode was moved across the beam width in increments to obtain a complete spatial profile.

6.2.2 Use with neon buffered XeCl*

Initially the experiment was conducted using neon buffered XeCl* gas mixes. The 1mm slit was moved in 1mm increments across the width of the laser output so that in all 16 readings were taken for each beam profile. It was discovered, not surprisingly, that the mirror alignment strongly influenced the spatial uniformity of the laser output and consequentially great pains were taken to carefully align the laser mirrors before each experiment to give the highest possible pulse energy.

A summary of the experimental parameters is given below:

Pressure Windows	2 x Herasil (fused quartz)
Mirrors	1 x HR @ 308 nm
	1 x 40% R @ 308 nm
Electrode Spacing	16 mm
PFN Charging Voltage	20 kV

The photodiode was moved in 1 mm increments from the cathode (hot) to the anode (grounded electrode).

The experiment was performed using gas mixes containing 15 mbar Xe, 3 and 4 mbar HCl and 3 and 4 bar neon buffer. An example of the oscilloscope traces obtained is given in Fig 6.3 for a gas mix consisting of 15 mbar Xe, 4 mbar HCl and 3 bars Ne. A graph showing the variation in pulse duration (FWHM) across the beam profile for three of these gas mixes is shown in fig 6.2.

Fig. 6.2
Graphs of Local Pulse Duration Against
Distance Across Beam Profile

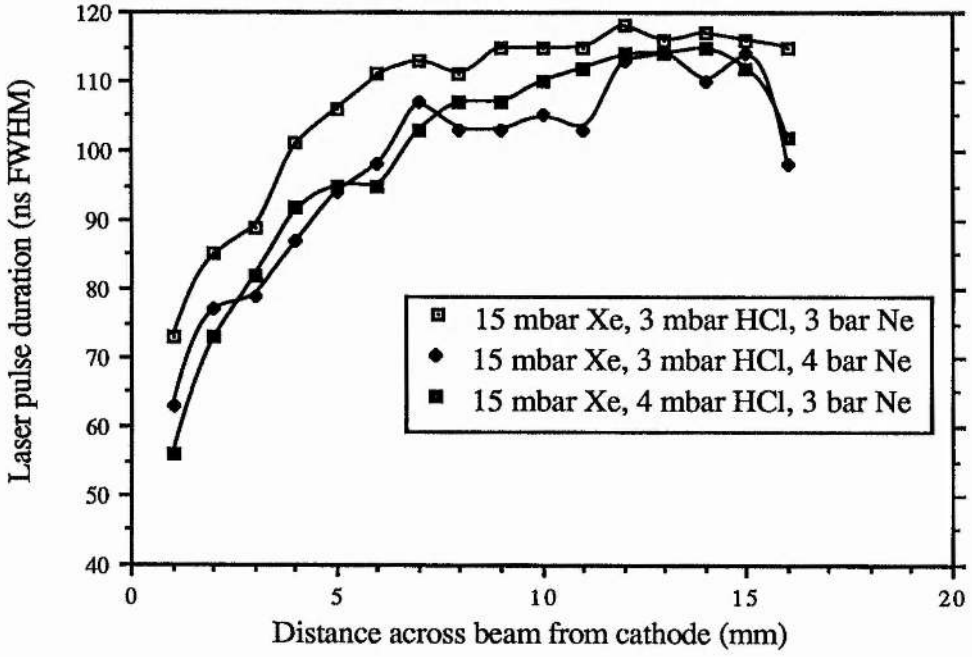

Fig. 6.3

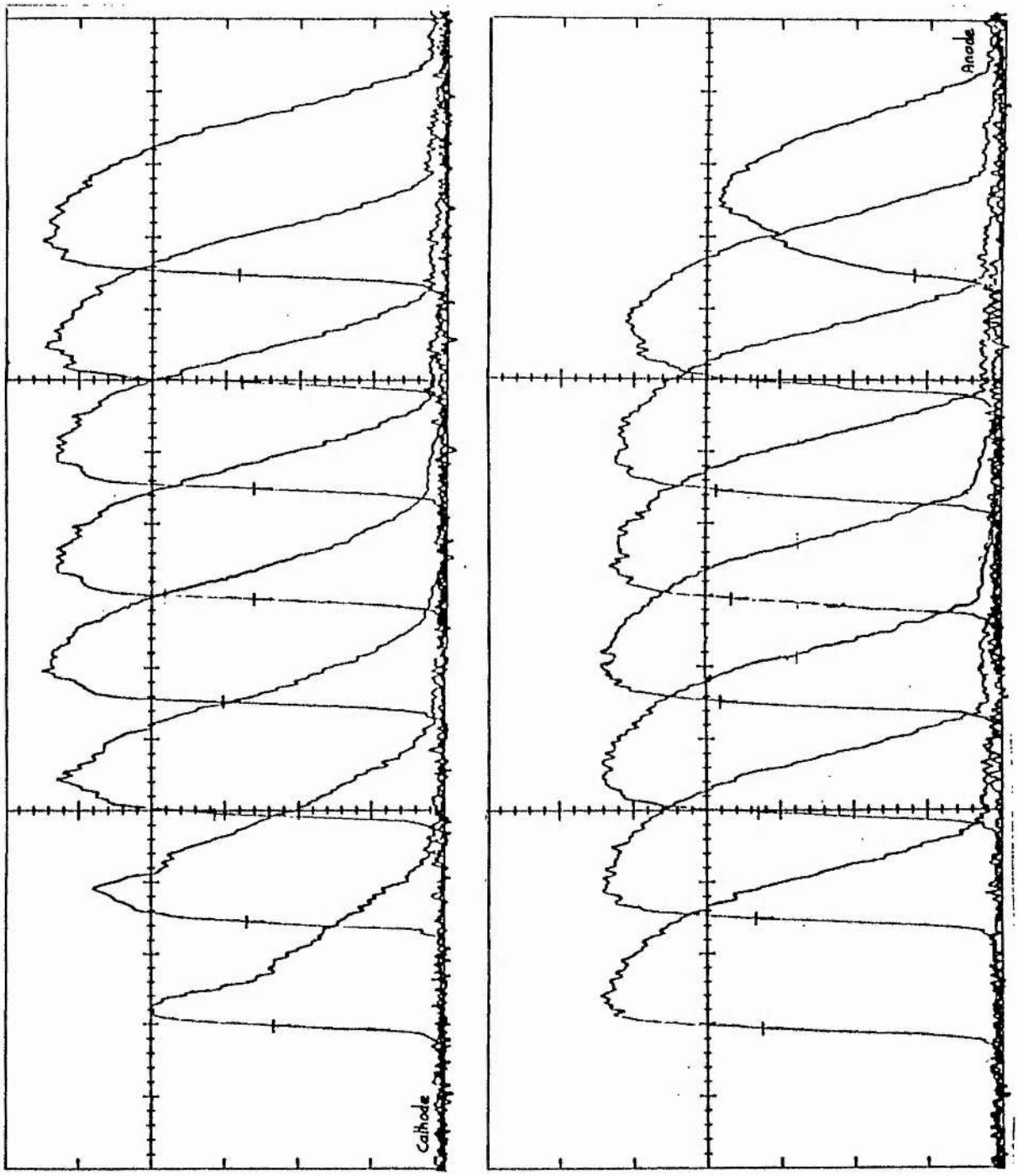

Fig. 6.3. Laser output profiles for neon buffered $XeCl^*$ moving in 1 mm wide vertical strips from the cathode (top left) to the anode (bottom right), gas mix 15 mbar Xe, 4 mbar HCl, 3 bars neon.

By reference to figs. 6.2 and 6.3 it can be seen that the optical pulse duration tends to be shorter near to both electrodes but most especially the cathode. The magnitude of the laser output and pulse duration tend to be fairly constant across the beam profile away from the electrodes. It is therefore probable that instabilities grow into the discharge volume from both electrodes but those originating at the cathode surface take effect earlier and grow faster than those at the anode.

From fig. 6.2 the laser output waveforms close to the cathode show a sharp truncation of the laser output power rather than the more normal, rounded profile away from the cathode. This indicates that the laser termination mechanism acts in this region before the maximum gain is reached. This is further evidence that discharge instabilities originate at the cathode and progress towards the anode.

This cathodic origin for discharge instabilities is partially in contradiction with the microarc theory of Kushner, (5). The microarc theory implies that filaments will be initiated from hot spots on both electrode surfaces where the electric field is locally enhanced on a microscopic scale. In this apparatus the anode surface takes the form of a fine mesh and it may be expected that this would provide many more hot spots from which filaments could grow than the solid faced cathode. This seems however not to be the case.

6.2.3 Use with Helium Buffered XeCl*

The experiment was continued using helium as the buffer gas in place of neon. The purpose of this was not only to collect more data generally but also to compare the behaviour of both helium and neon.No changes to the apparatus or experimental method were required. Runs were made with gas mixes containing 15 mbar Xe, 3 mbar HCl and the buffer gas was varied from 1.5 to 2.5 bar He.

A representative set of light output profiles for the gas mix 15 mbar Xe, 3 mbar HCl and 2 bar He is given in fig. 6.4

Fig. 6.4

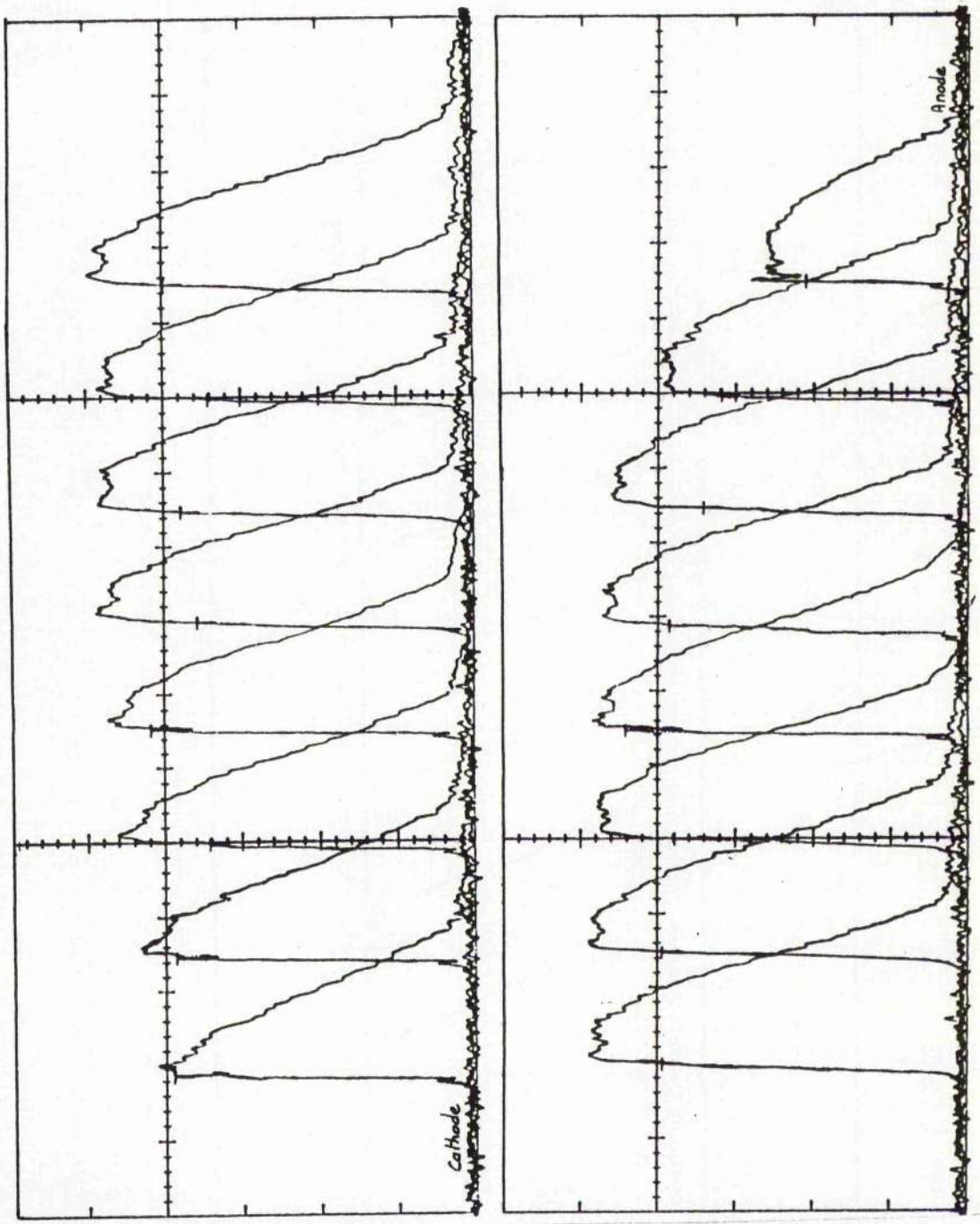

Fig. 6.4 Laser output profiles for Helium buffered $XeCl^*$ moving in 1 mm wide vertical strips from the cathode (top left) to the anode (bottom right), gas mix 15 mbar Xe, 3 mbar HCl, 2 bars helium.

Graphs of the output pulse duration (FWHM) against the distance across the beam profile from the cathode are given in fig.6.5.

Fig. 6.5
Graph of Local Laser Pulse Duration
Against Distance Across Beam Profile

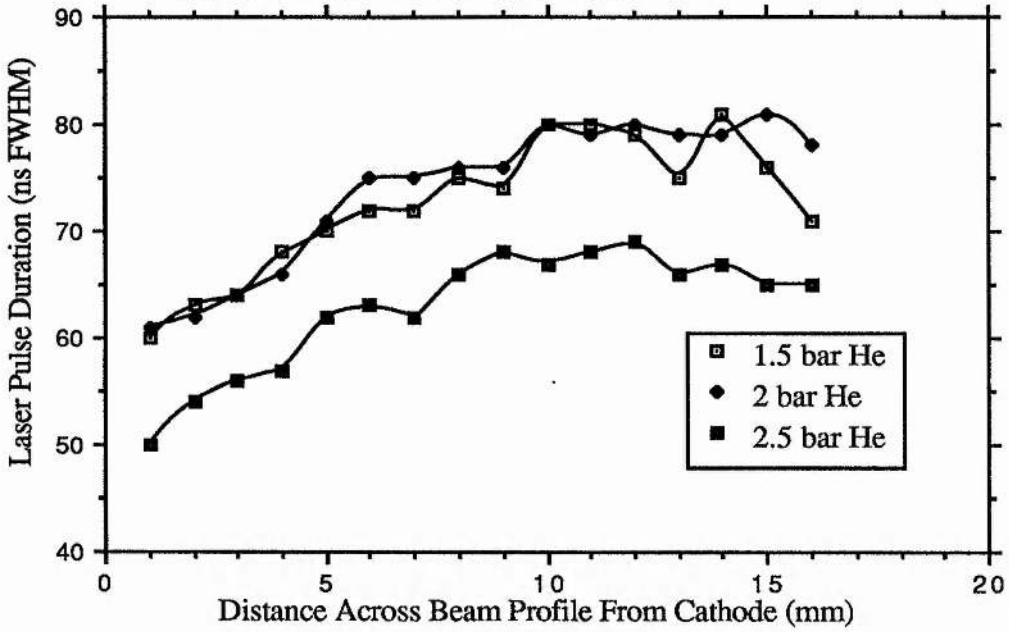

In general the behaviour of helium buffered gas mixes appears to be similar to that of neon. The optical pulse duration is shorter moving towards the cathode with a smaller fall-off near the anode; this again implies that the inhomogeneities responsible for the termination of the laser output originate at the cathode and propagate towards the anode. the most significant feature however is that the pulse durations measured close to the cathode with helium are very similar to that obtained with neon, i.e. in the region of 60 ns FWHM. This is surprising as with neon the pulse durations measured in the centre of the beam were much larger, >110 ns compared with ~80 ns, when helium was used. It is therefore probable that for both helium and neon the discharge instabilities at the cathode take a similar amount of time to evolve to the point where they disrupt lasing, ~ 50 to 60 ns, where upon they rapidly grow towards the anode, at an increasing rate, until lasing stops throughout the entire discharge volume. The rate of growth after this initial formation stage

seems to be much faster with helium than with neon, taking only about 20 ns to envelop the whole discharge as opposed to approximately 50 ns for a typical neon buffered mix.

6.3 The Monitoring of XeII Emissions as an Indicator of Discharge Stability

The technique of monitoring the emissions from high lying XeII states has been used successfully by several workers as a measure of the growth of high density filaments in excimer glow discharges. A theoretical explanation of the method is given by Coutts and Osborne, (6) while accounts of its application to studying $XeCl^*$ lasers have been published, (7,8)

The basis of the technique relies on the monitoring of the XeII ($6p^4D^0_{7/2}$ - $6s^2P_{5/2}$) transition at 484 nm as an indicator of the population of ionised xenon in the $6p^4D^0_{7/2}$ state. It is known that this state is only significantly populated in regions of a discharge with a very high electron density, i.e. filaments and arcs. In regions of homogeneous glow discharge the population of this state is very small. The spontaneous decay lifetime of the transition has been estimated at around 10 ns, (6) and the emission wavelength lies in a spectral region of low continuum discharge radiation further helping to make this a useful means of determining the nature of the laser discharge. The rise in emissions at 484 nm should therefore act a reliable indicator of the growth of discharge inhomogeneities. One problem however is that the technique can only be used with the $XeCl^*$ laser as broad-band emissions from XeF^* ($C \rightarrow A$) centred on 483 nm prevents its use with XeF^*.

Although not a new technique it was considered worthwhile to pursue as a means of obtaining more information about the nature of discharge evolution in helium and neon buffered $XeCl^*$ gas mixes. It was also considered useful to verify the method so that it could be used as a diagnostic tool in subsequent experiments.

6.3.1 Experimental Method

The discharge end light was monitored under non-lasing conditions, that is with the 308 nm optical resonator removed. A dielectric mirror with a nominal 100% reflectivity at 483 nm, originally intended for use with XeF^* ($C \rightarrow A$), was available and was used as a back reflector at one end of the laser cavity. At the output end of the laser head the light was focussed down by means of a simple telescope and aligned with the input to a Hilger and Watts 25 cm monochromator which used a simple triangular prism as the dispersion element.. By careful alignment and narrowing down of the monochromator input and output slits, the output bandwidth was estimated as about 3 nm; this was considered sufficient to isolate the 484 nm XeII line from other features in the neighbourhood. The monochromator was calibrated against a standard, low power HeNe laser at 633 nm. The experimental apparatus is shown schematically in fig. 6.6.

Fig. 6.6

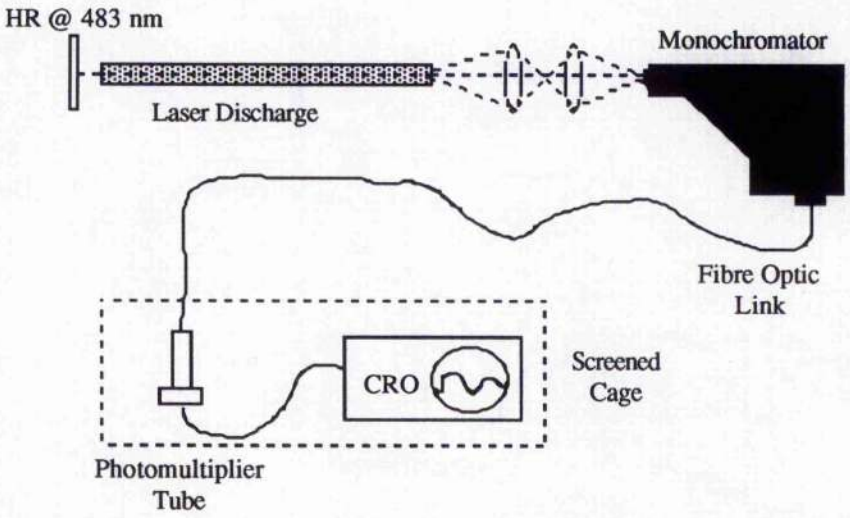

Schematic diagram showing the apparatus used for the monitoring of XeII emissions at 484 nm originating in the $XeCl^*$ laser discharge

The narrow bandwidth output from the monochromator was particularly dim and required detection by means of a photomultiplier tube. Unfortunately the photomultiplier tube could not be directly fitted to the output of the monochromator because of electrical

noise problems due to the proximity of the laser pulsed power; a typical output from the photomultiplier of around 100 mV was completely lost in the ambient noise. A solution was implemented by channelling the monochromator output by optic fibre several metres across the laboratory to a screened box, inside which were the photomultiplier tube and the oscilloscope connected by as short a cable as possible. This arrangement significantly improved the signal to noise ratio making the experiment possible.

6.3.2 Experimental Results

The method was first tested on a neon buffered $XeCl^*$ gas mix of 15 mbar Xe and 3 mbar HCl with the buffer gas pressure varied in 4 stages between 1.5 and 4 bars of neon. The PFN charging voltage was kept constant at 20 kV and the optical alignment and photomultiplier bias voltage were not altered so that each trace obtained was under a consistent set of conditions. Synchronisataion between traces was provided by comparison with the laser head voltage which was measured simultaneously in each case. To further reduce noise to as low a level as possible and to smooth out the effects of laser shot to shot variations, all traces were formed by using a special feature of the oscilloscope to electronically average 8 individual shots to form each trace.

The oscilloscope traces obtained from this experiment are shown in fig. 6.7. It can be seen that after the head breakdown the growth of XeII emissions, and hence high current density filaments, is small. After a few tens of nanoseconds however the growth rate increases rapidly and begins to run away in an exponential like manner. This rate of this running away seems to be larger at higher buffer gas pressures confirming the results from previous experiments that the growth of instabilities proceeds faster with increasing pressure.

Fig. 6.7

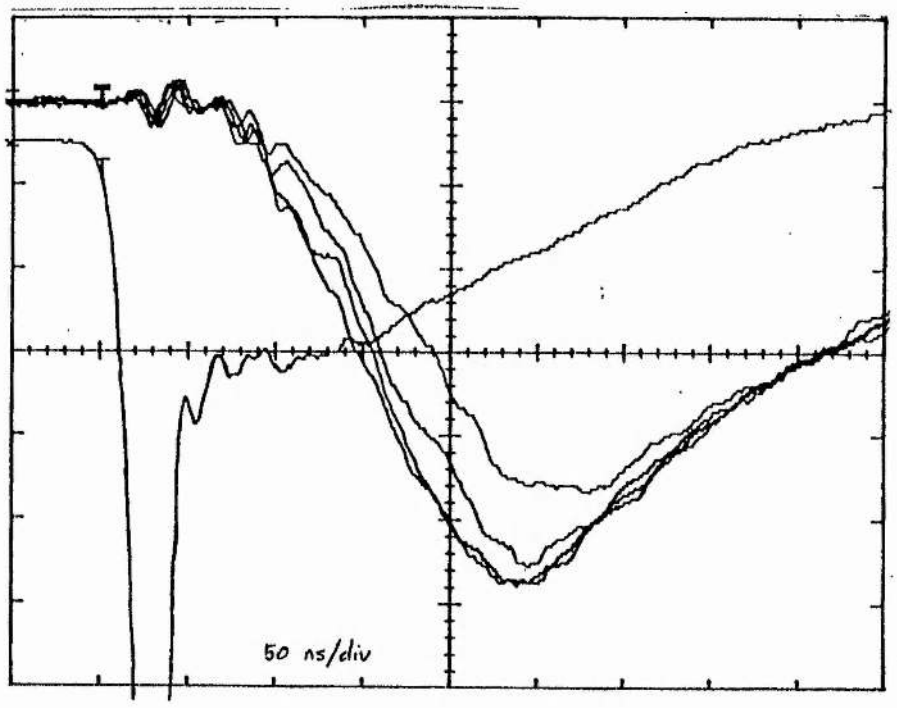

Rise in XeII (484 nm) emissions for neon buffered $XeCl^*$ (upper traces) synchronised with laser head voltage (lower trace). Showing the earlier rise in XeII emissions with increasing buffer gas pressure. Head voltage 1.4 kV/div, gas mix 15 mbar Xe, 3 mbar HCl, moving right to left 1.5, 2, 2.5, 3 bars neon.

The experiment was repeated using helium as the buffer gas in place of neon. Again 15 mbar Xe and 3 mbar HCl were used with the buffer gas pressure varying between 1.5 and 3 bars so that direct comparison could be made with the neon results. All other experimental parameters remained unaltered. The traces obtained are shown in fig. 6.8.

Fig. 6.8 shows the behaviour of helium buffered $XeCl^*$ to be very similar to that with neon, with the oscilloscope traces exhibiting the same basic features. The rate of growth of the XeII emissions from helium does seem however to proceed at a faster rate than with neon, at a given pressure, once the initial growth is under way. This helps confirm the observation made in section 6.2.3 that once initiated, filaments grow faster in helium buffered gas mixes.

Fig. 6.8

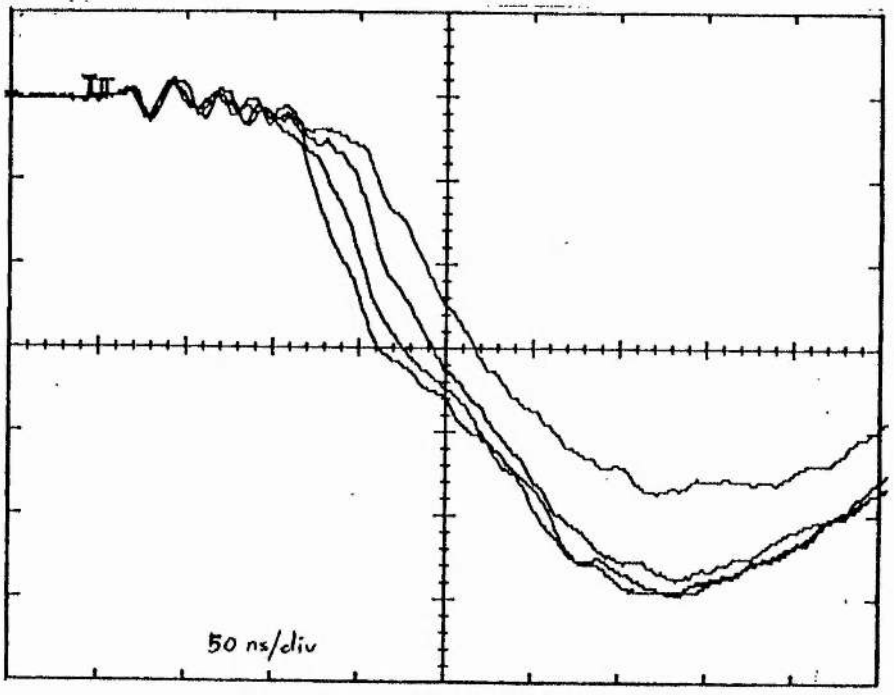

Rise in XeII (484 nm) emissions for helium buffered $XeCl^*$ showing the earlier rise in XeII emissions with increasing buffer gas pressure. Gas mix 15 mbar Xe, 3 mbar HCl, moving right to left 1.5, 2, 2.5, 3 bars helium.

More unexpected, however, is the observation that when helium and neon buffered traces are taken together and synchronised with the point at which the laser head breaks down, the time taken for the XeII emissions to run away in the case of a helium buffer is greater than with neon. This result was unforeseen as under the same conditions neon always gives longer pulse durations than helium. The possibility that this could be due to some experimental error can not be ruled out although this is unlikely as the effect seemed to be consistent over several runs. The XeII emission at 484 nm is known to only reflect the presence in the discharge of regions of very high electron density, i.e. filaments, and the precise mechanism by which these filaments are formed should have no direct bearing on the workings of the experiment. The only experimental uncertainties that may be considered significant therefore is random errors in the oscilloscope traces. Although these were minimised as far as possible by averaging out a number of individual shots to produce each trace the inherent randomness of discharge instability processes and the shot to shot

variation between laser pulses characteristic of the equipment can not be ignored. These random errors can not be quantified precisely and so the best conclusion that can be reached is that it is possible that the time taken from breakdown to the rapid rise of XeII emissions is the same or slightly greater for helium rather than neon buffered $XeCl^*$ gas mixes. This area clearly warrants further study.

6.4 Conclusions

The two experiments described in this chapter helped to increase the accumulated knowledge of the nature of discharge evolution in helium and neon buffered $XeCl^*$ gas mixes. The experiments furthermore confirmed the usefulness of these techniques as diagnostic tools for use in other experiments that may be required to be carried out.

Summing up, the laser spatial profiles experiment confirms the observations of Taylor, (1) that discharge inhomogeneities tend to grow into the discharge volume mainly from near the cathode surface. It is also interesting that despite the use of a mesh anode with its consequent local E field enhancement, the initiation of instabilities close to the anode does not present as much of a restriction as previously thought.

Both the spatial profiles and the XeII experiments indicate that the initiation of filamentary instabilities in both neon and helium buffered gas mixes takes place on a similar time-scale but that once formed instabilities consume the discharge volume and terminate lasing faster when a helium buffer gas is used. These observations however lack corroboration from other sources.

Lastly, the anomalous results obtained with helium in the XeII emission experiments, if true, are difficult to explain and indicate behaviour contradictory to the conclusions of all other studies. It is not therefore proposed to provide a theory to explain the results as doing so would merely involve a large degree of speculation. The experiment does however serve to illustrate the complex nature of discharge instability processes and the difficulties in both designing experiments to study discharge evolution and interpretation of the results.

It may have been desirable to combine both both techniques into an experiment that could look at the XeII emission in each of a series of vertical slices across the discharge volume. In this way the relative delay before the onset of arc formation could be determined for various positions across the discharge. Although such an experiment was considered, it was unfortunately found to be beyond the capabilities of the equipment available. The spatial profiles experiment was carried out under lasing conditions but the XeII emission experiment involved the monitoring of incoherent spontaneous emission. In order to ensure that the light reaching the monochromator only originated from a specific region of the discharge volume, extra collimating optics would have been required. This would have drastically cut down the amount of light available at the monochromator and it was judged that the resultant output would be too faint to detect. Even when the XeII emission from the entire discharge volume was measured, as described, the signal was only just comfortably detectable above the ambient electrical noise and restricting the size of the output signal by looking at only a small region of the discharge would have resulted in an unacceptablely low signal to noise ratio.

References

1 R S Taylor; "Preionisation and Discharge Stability Study of Long Optical Pulse Duration UV-Preionised XeCl Lasers;" Appl. Phys B, vol 41, p1-24, 1986

2 J Coutts, C E Webb; "Stability of Transverse Self-Sustained Discharge-Excited Long-Pulse XeCl Lasers;" J Appl. Phys. vol 59, p704-10, 1986

3 M R Osborne; " Rare Gas Halide Discharge Stability;" Appl. Phys. B, vol 45, p285-91, 1988

4 M Bahr, W Botticher, S Choroba; "The Time Dependent Development of the Macroscopic Instability of a $XeCl^*$ Laser Discharge;" IEEE Transactions on Plasma Science, vol 19, p369-79, 1991

5 M J Kushner; "Microarcs as a Termination Mechanism of Optical Pulses in Electric-Discharge-Excited KrF Excimer Lasers;" IEEE Transactions on Plasma Science, vol 19, p387-99, 1991

6 J Coutts, M R Osborne; "Emissions From High-Lying States as a Probe of Excimer Laser Discharge Character;" Journal of Modern Optics, vol 34, p1513-24, 1987

7 M R Osborne, J Coutts, M H R Hutchinson, C E Webb; "Output Pulse Termination of a Self-Sustained Excimer Laser;" Appl. Phys. Lett, vol 49(1), p7-9, 1986

8 M R Osborne, M H R Hutchinson; "Long Pulse Operation and Premature Termination of a High-Power Discharge-Pumped XeCl Laser;" J. Appl. Phys, vol 59, p711, 1986

Chapter 7

Magnetic Stabilisation of Excimer Laser Discharges

7.1 Theory of Magnetic Stabilisation

This chapter concerns the study of the influence of externally applied magnetic fields on excimer laser discharge behaviour. The purpose of this investigation was to try and determine if applied magnetic fields have any positive benefits in terms of improved discharge stability.

The stabilisation of laser discharges by external magnetic fields was first demonstrated by Seguin, Capjack, Antoniuk and Nam for a high power CO_2 laser, (1). The theory of the technique, as described in their paper, involves using a d.c. solenoid to produce a magnetic field in the inter-electrode space. It is believed that a suppression of the glow to arc transition mechanism and improved discharge stability results from a smoothing out of inhomogeneities by highly sheared velocity mixing due to the interaction

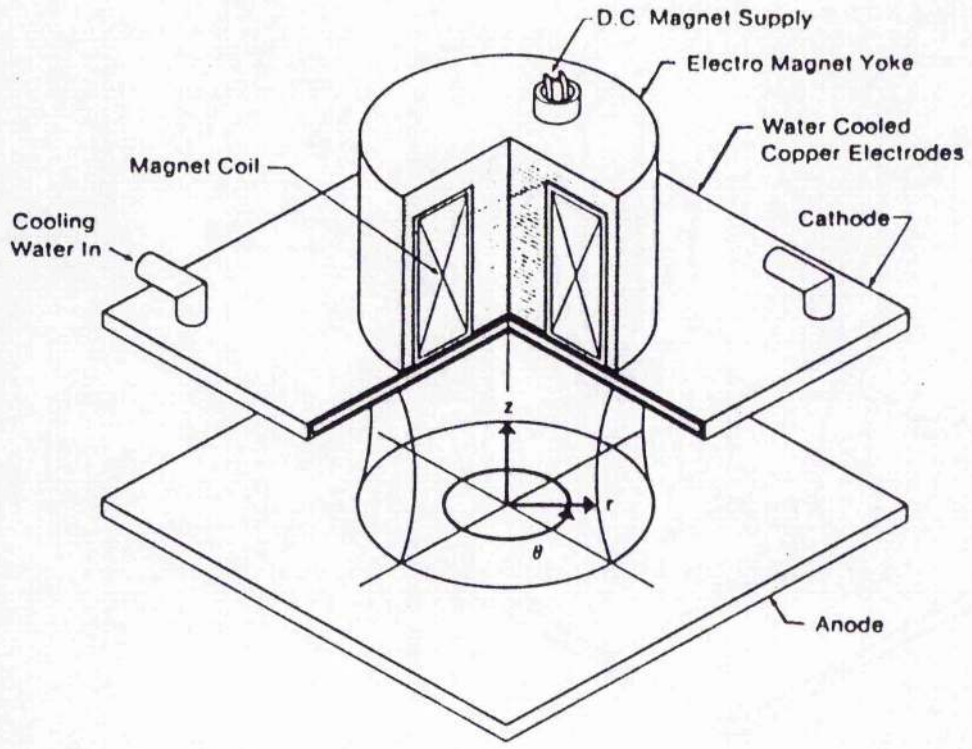

Fig. 7.1. Experimental arrangement used in the experiments described by Seguin *et al*, from refs. 1&2

between the magnetic field and the discharge plasma. A more precise description of the nature of these interactions is described in a subsequent paper, (2), and the extension of the technique to coaxial geometry has also been undertaken, (3).

It can be seen that charged species moving in the direction parallel to the z axis under the influence of the applied electric field will be subject to a Lorentz force by their interaction with the radial component of the magnetic field, $\mathbf{B}_r$. This will impart a component of velocity v_θ, which will cause the charged species to rotate about the z axis. It can be seen however that once the electrons and ions have a rotational motion v_θ, they will also interact with the axial component of the magnetic field, $\mathbf{B}_z$, causing the discharge plasma to be confined into a diffuse rotating cylinder parallel to the z axis. The size of the velocity components resulting from the action of the magnetic field will depend upon the particle velocities due to the electric field in a particular region of the discharge. The strong spatial variations of the electric field close to the discharge electrodes will give rise to a strongly sheared flow system in these regions with a consequent inhibition of the mechanisms for the formation of discharge instabilities.

More quantitatively the equations of motion for the discharge plasma can be derived by applying the law of conservation of momentum.

$$mn\frac{d\mathbf{v}}{dt} = \rho_q(\mathbf{E} + \mathbf{v} \times \mathbf{B}) + \mathbf{J} \times \mathbf{B} - \nabla P - m_i n\nu(\mathbf{v} - \mathbf{v}_n) + \mu_i \nabla^2 \mathbf{v} \qquad 7.1$$

$$m_n n_n \frac{d\mathbf{v}_n}{dt} = -\nabla P_n - m_i n\nu(\mathbf{v}_n - \mathbf{v}) + \mu_n \nabla^2 \mathbf{v}_n \qquad 7.2$$

where $m = m_e + m_i$ is the sum of the electron and ion masses, $\mathbf{v}$ the charged fluid velocity, $\mathbf{v}_n$ the neutral gas velocity, n the charged particle number density , n_n the neutral gas number density, ρ_q the fluid electric charge density, $P = P_e + P_i$ the sum of electron and ion scalar pressures, P_n the neutral gas pressure, $\mathbf{J}$ the current density, $\mathbf{B}$ the magnetic field, ν the effective collision frequency for momentum exchange, μ_i the ion viscosity coefficient, and μ_n the neutral gas viscosity coefficient. The term $m_i n_n \nu(\mathbf{v} - \mathbf{v}_n)$ represents the rate of

momentum transfer from the charged to the neutral fluid, while $\mu\nabla^2\mathbf{v}$ accounts for viscous boundary layer and drag effects. The current density is given by applying Ohm's Law:

$$\mathbf{J} = \hat{\sigma} \bullet \mathbf{E}_T \qquad 7.3$$

where $\hat{\sigma}$ is the conductivity tensor in the cylindrical polar coordinate frame used here.

A complete solution to this system of equations is cumbersome, however some approximations can be made. By noting that the system has θ symmetry all quantities will be independent of θ. As a consequence the steady state θ component of eqn. 7.2 can be written as:

$$m_i n\nu(v_{n\theta} - v_\theta) - \mu_n \nabla^2 v_{n\theta} = 0 \qquad 7.4$$

It can be inferred from this that the motion of the neutral gas particles is strongly coupled to the motion of the charged species, hence $v_{n\theta} \approx v_\theta$. Furthermore by taking the net plasma charge density as zero (only true away from the cathode fall region) the θ component of equation 7.1 can be simplified to:

$$\sigma_\perp(\mathbf{E}_z - v_\theta \mathbf{B}_r)\, \mathbf{B}_r - m_i n\nu(v_\theta - v_{n\theta}) + \mu\nabla^2 v_\theta = 0 \qquad 7.5$$

By neglecting viscosity effects the rotational plasma velocity can be approximated thus:

$$v_\theta \approx \mathbf{E}_z / \mathbf{B}_r \qquad 7.6$$

By inserting appropriate values into equation 7.6 Seguin *et al* estimate that rotational velocities in the region of 10^3 ms^{-1} should be realised which is considered sufficient to prevent the growth of electro-thermal instabilities which normally occur on a timescale of several milliseconds, (4).

Although it is suggested, (1), that this method can be applied to excimer discharges there are many important differences that must be considered. Although both CO_2 and excimer lasers operate by discharge pumping a gaseous active medium, they do so in very different regimes of gas pressure and discharge current density. The gas lasers considered

in references (1-3) typically operate in a c.w. mode at pressures of a few tens of mbar and with discharge current densities less than one amp per cm^{-2}. Under these conditions the discharge instability mechanisms responsible for termination of the laser output in CO_2 lasers differ from those considered to be dominant in excimer discharges, evolving over much longer time-scales. As well as, (4), a further description of discharge stability and the characteristic behaviour of a typical CO_2 laser discharge is given by Denes and Lowke, (5). As a result of these differences in operating regimes the mechanism describing the interaction between the magnetic field and the discharge plasma may not hold. In particular the short lifetime of excimer discharges may prevent the spiralling outwards of discharge filaments into a diffuse cylinder as observed in CO_2 discharges. In view of the apparent dissimilarity between CO_2 and excimer discharges the direct applicability of magnetic stabilisation techniques according to Seguin *et al* may therefore be questioned.

Referring back to the excimer discharge stability theories discussed in chapter 4, (6-10), it is apparent that as discharge instabilities form, whatever their cause, these features tend to persist throughout the evolution of the discharge. In particular, Bahr, (9), points out that localised spatial distributions of both electron temperature and excited species populations tend to remain intact due to the absence of any discharge stabilising feedback or mixing mechanisms in the direction perpendicular to the discharge E field. Without any such mechanisms to provide spatial mixing of populations then the processes that drive the formation and growth of instabilities will proceed unchecked. It may therefore be worthwhile to study the application of external magnetic fields to excimer laser discharges in the hope that the consequent motion of the discharge electrons in directions perpendicular to the discharge E field, and the resultant extra mixing of species distributions, have effects that are beneficial for discharge stability.

Before an experiment could be considered it was necessary to make an estimate of the size of the additional electron motion required to produce the desired effect and the strength of the magnetic field needed to produce that motion. Only electrons are considered as it is assumed that ions with masses substantially larger than that of an electron will not be significantly influenced by any applied magnetic fields over the lifetime of the discharge

and may therefore be considered stationary, (10). The uncertainty of the precise processes expected to be involved makes these estimates of additional electron motion somewhat subjective. The size of the applied magnetic field should however be larger than the intrinsic magnetic field associated with the action of the discharge current in the loop formed by the electrodes and their supporting current feeds. This was estimated by considering the discharge and the electrode assemblies as forming a pair of single turn solenoids with half the total current flowing in each. This assumes that the current flow back to the thyratron divides equally between the top and bottom ground return paths. Each of these imaginary solenoids is therefore 25 cm long with a single turn. By applying the standard expression given in equation 7.7:

$$B = N' I \mu_0 \sin\theta \qquad 7.7$$

with N' the number of turns per unit length and θ half the angle subtended at the coil centre by the solenoid length, the magnetic field due to the discharge current was estimated as of the order of a few mT for typical values of the laser discharge current. It was decided to try a magnetic field approximately 10 times larger than this as a starting point for some rough calculations. This is similar to the magnitude of the magnetic fields used by Seguin *et al.* By using a value for the radial component of the applied magnetic field of 3×10^{-2} Tesla in equation 7.6 and taking the electric field as around 10^5 Vm^{-1} the rotational plasma velocity can be estimated as 3×10^3 ms^{-1}. This implies that for a typical discharge lifetime of 100 ns the rotational motion will lead to a displacement of 300 μm.

Looking at the problem from another angle, according to Kushner, (10), discharge characteristics are dominated by features, initially on a scale of 10's to 100 μm. As a first approximation a significant effect should therefore be apparent from a magnetic field capable of producing a displacement of greater than 0.1 mm in electrons on a timescale comparable with the filament growth rate. It has been shown that the electron drift velocity in a typical excimer laser discharge is of the order of 10^4 ms^{-1}, (11), however the distribution of velocities of individual electrons will be much larger than this, say 10^5 - 10^6

ms^{-1}. Calculation of the Lorentz force on electrons with this range of velocities suggests that the desired displacement will result from applied magnetic fields with strengths in the region of a few tens of mT. This size of magnetic field is similar to that used with beneficial results by Seguin *et al*, (1,3).

In conclusion, although an applied magnetic field will probably not interact with an excimer discharge plasma in exactly the same manner as that observed with CO_2 discharges the technique shows sufficient promise to justify further investigation. An experiment was therefore designed to determine if the application of such a magnetic field has any measurable effect on excimer discharges or laser performance.

7.2 Initial Experiments

7.2.1 Experimental Apparatus and Method

For the first series of experiments a simple solenoid was constructed to provide the magnetic field. The coil was built with 10 turns on a rectangular former 35 cm x 11 cm x 2 cm wide, (see fig. 7.2). The coil was designed to fit inside the laser head adjacent to the grounded anode; initial plans to place the coil outside the laser head were dropped because it was considered that the magnetic screening effect of the laser head would be too much of a problem to overcome. By mounting the coil in this manner the magnetic field in the inter-electrode space should consist of components both radial and parallel to the electric field in the same way as the experiments carried out by Seguin *et al.* A suitable thyratron-switched pulse generator using a 0.5 μF, 20 kV capacitor was built to provide the required current pulse.

The approximate magnetic field at the centre of the coil was calculated by treating it as a short solenoid and using equation 7.7. With $N' = 500\ m^{-1}$ and $\sin\theta = 1/5$ equation 7.7 gives an approximate B field of 130 $mTkA^{-1}$. This calculation is not particularly accurate and only gives the B field at the centre of the coil, the fall-off in field moving away from the coil can only be estimated. It does provide a rough guide however and serves as a starting point for further measurements.

Fig. 7.2

Experimental Apparatus

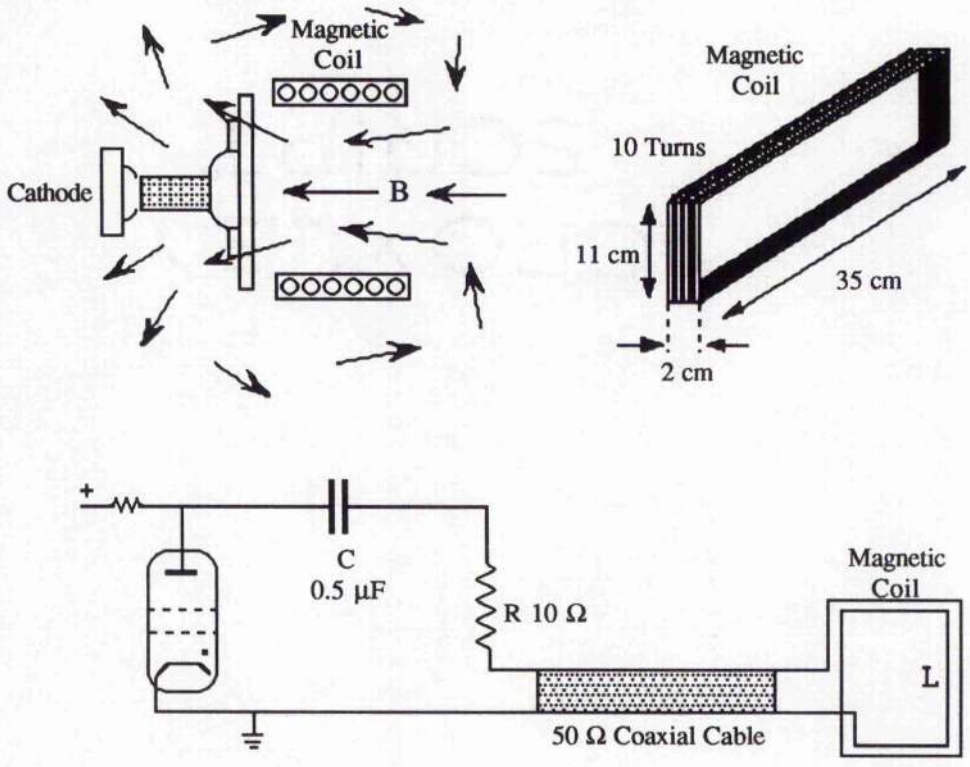

Fig. 7.2. Diagram showing the arrangement of the magnetic coil in relation to the laser discharge and the circuit used to drive the coil.

A reliable method of measuring the B field due to the coil was sought. A Hall probe was tried and found to be unsuitable because of sensitivity to electrical noise generated by the thyratron switching circuit and so an alternative method was devised using a simple search coil. A search coil gives a voltage response proportional to the rate of change of B with respect to time by the following expression:

$$V = N A \frac{dB}{dt} \qquad 7.8$$

where N is the number of turns on the search coil and A is the search coil area. Simultaneous measurement of the magnetic coil current and the search coil voltage using a dual beam oscilloscope allowed the measurement of both the magnetic coil dI/dt and the resultant dB/dt at any instant in time. As the dB/dt at a particular point is proportional to the

magnetic coil dI/dt this allows the proportionality constant relating these quantities to be determined.

$$\frac{dB}{dt} = k\frac{dI}{dt} \qquad 7.9$$

integrating gives:

$$B = kI + c \qquad 7.10$$

but when I = 0, B = 0 also, therefore c = 0 and

$$B = kI \qquad 7.11$$

Hence, by using an oscilloscope trace and simultaneously measuring the magnetic coil current, the magnetic coil dI/dt and the output voltage from the search coil the magnetic field at any instant is given by:

$$B = \frac{VI}{NA\left(\frac{dI}{dt}\right)} \qquad 7.12$$

This method allowed a more accurate determination of the magnetic coil B field and its distribution in space. The main error arose from the slightly nonlinear response of the search coil to the magnetic field because of the integrating effect of stray capacitances in the search coil but this effect was small. The search coil gave a value of 85 $mTkA^{-1}$ for the B field at the centre of the magnetic coil.

It can be shown by the application of Laplace transform techniques that the current from a capacitor discharge through an inductive load, L, such as the magnetic coil, with a series resistance, R, is given by:

$$i(t) = \frac{V_0}{\omega L}\exp(-\alpha t)\sin(\omega t) \qquad 7.13$$

Where $\alpha = \frac{R}{2L}$ and $\omega^2 = \left(\frac{1}{LC}\right) - \left(\frac{R}{2L}\right)^2$

It therefore follows that while the resultant B field is proportional to the number of turns per unit length of the coil the peak current is proportional to the reciprocal of the coil inductance which is in turn proportional to the square of the number of turns per unit length of the coil. To obtain the maximum possible B field it is advantageous to use a coil with as few turns as possible so that the coil current is maximised. For this reason the magnetic coil was wound with only 10 turns, the minimum number estimated to be required to obtain the desired B field distribution.

The discharge circuit driving the magnetic coil included a series resistance to provide damping and prevent current reversal that might otherwise have damaged the thyratron. This series resistance used high-power carbon-composition resistors and was made up to a value of about 10 Ω. The magnetic coil drive circuit produced a current pulse of about 4 μs FWHM, passive delay lines allowed the synchronisataion of the laser pulse with the peak of the magnetic current pulse.

7.2.2 First Experimental Results

With the magnetic coil in place, mounted in the vertical plane behind the grounded anode, (see fig. 7.2), the search coil was used to measure the B field in the inter-electrode space. The search coil was also mounted in the vertical plane. An average of a number of readings from the search coil gave a value for the magnetic field of about 6.6 ± 0.3 $mTkA^{-1}$ at the mid-point between the electrodes. This is a considerably smaller field than was measured at the centre of the magnetic coil in free space, This can be attributed to the screening effect of the stainless steel anode body and the rapid fall in magnetic field strength with distance.

The experiments commenced using $XeCl^*$ with a helium buffer gas. Helium was chosen as the buffer gas as it produces shorter optical pulse durations than neon as a result of the faster evolution of discharge instability processes. For this reason it was hoped that any discharge stabilising effects of using a magnetic field would be more pronounced in a helium buffered gas mix than with neon.

The experiments were conducted using a gas mix of 15 mbar Xe, 3 mbar HCl and 2, 2.5 and 3 bars of helium. The PFN charging voltage was 20 kV and a nominal 40% reflectivity output coupler was used. The magnetic coil current during lasing was 900 Amps corresponding to a B field of 6 mT. The variation in laser pulse durations is given in the following graph, fig. 7.3.

Fig. 7.3
Graph of laser optical pulse duration against He buffer gas pressure with and without an externally applied magnetic field

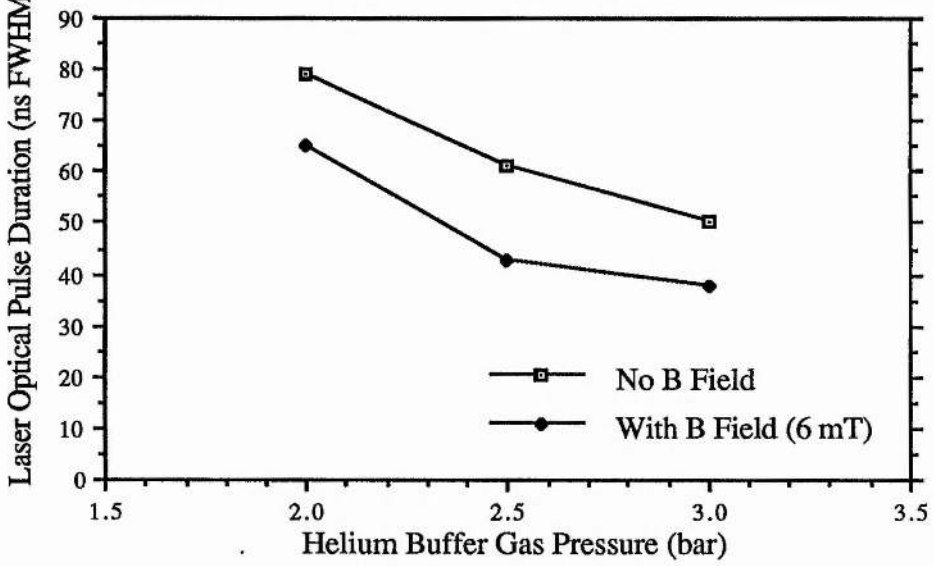

The results showed that the presence of the magnetic field seemed to significantly reduce the optical pulse duration. The experiment was repeated several times by simply turning on and off the magnetic field and in each case the optical pulse duration was shorter with the field in place. One experimental difficulty however was the large shot to shot variation in pulse duration, as much as 10 ns between pulses, resultant from using helium as the buffer gas at the relatively high pressure of 3 bar.

It was decided to determine how the strength of the applied magnetic field effects the laser output. With a gas mix of 15 mbar Xe, 3 mbar HCl, 3 bar He, the optical pulse

duration at various applied magnetic fields was measured. The results are reproduced in fig. 7.4.

Fig. 7.4
Graph of optical pulse duration against applied magnetic field strength

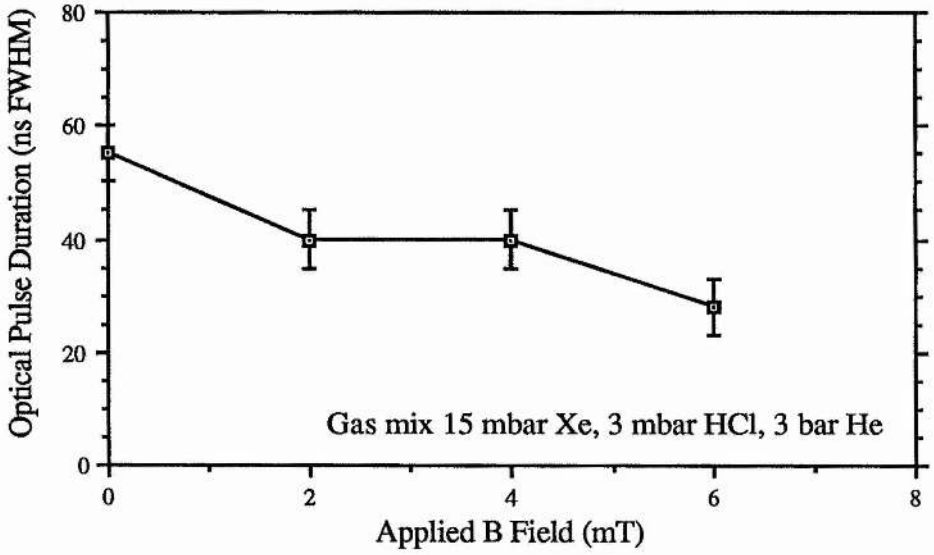

Although the results do not fit into a particularly straight line the downward trend in the laser pulse duration with increasing magnetic field is apparent.

The experiment was repeated using neon as the buffer gas in place of helium. The gas mix was 15 mbar Xe, 3 mbar HCl, 3 bars neon with all other parameters unchanged. Despite varying the applied magnetic field between zero and 6 mT only a very small reduction in the optical pulse duration was noted. The effect, if genuine, was difficult to distinguish from the normal random shot to shot variations of the laser. All pulse durations fell in the range 118 - 122 ns FWHM. This tends to imply that any effects due to the applied magnetic field are less pronounced with neon buffered gas mixes.

To test if the magnetic field polarity had any effect the polarity was reversed by swapping over the connections to the magnetic coil. This made no perceptible difference to the laser output.

7.2.3 Initial Conclusions

The limited scope of the initial experiments made it difficult to draw any firm conclusions but did provide pointers for further investigation. The biggest effect was seen with helium buffered gas mixes at relatively high buffer gas pressures which have already been shown not only to suffer from short laser pulse durations but also to produce unreliable and erratic behaviour, (see chapter 5). It was therefore concluded that to produce a larger and more consistent response the size of the applied magnetic field should be increased and that gas mixes with either neon as the buffer gas or helium at lower pressures should be used.

7.3 Further Experiments Using an Applied Magnetic Field

The experiments were continued to provide more information and hopefully to determine if the reduction in laser output pulse duration was a genuine effect or not. In this section further experiments are described using a magnetic field provided by a coil driven by a current pulse in such a way that the magnetic field could again be considered as constant throughout the laser pulse. The application of the investigative techniques used in chapter 6 to discharges with and without magnetic fields are also described. Experiments were also carried out using a magnetic field with a rise-time comparable to that of the laser pulse so that the turn-on of the magnetic field could be synchronised with the laser pulse. The purpose of this was to determine if the magnetic field was influencing the discharge behaviour by disturbing the preionisation electron distribution in some or the effects obtained were due to an interaction with the discharge directly.

7.3.1 Experiments Using a Larger Magnetic Field

A new magnetic field coil was constructed, essentially similar to the last coil but with dimensions 30 cm x 6 cm x 2 cm wide and with 12 turns.This time the coil was placed in the horizontal plane above the inter-electrode space to reduce the magnetic screening effect of the stainless steel electrodes, see fig. 7.5. Naturally this also changed the shape of the magnetic field distribution but the manner in which the magnetic field spread out from

the coil ensured that significant components of magnetic field both parallel to and transverse to the E field were present.

Fig. 7.5
Experimental Apparatus

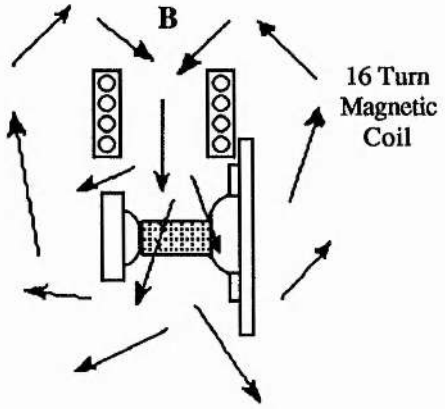

Fig. 7.5 Schematic diagram showing the arrangement of the magnetic coil above the laser discharge in order to obtain a larger magnetic field in the inter-electrode space.

Measurement of the B field between the electrodes using the search coil in the horizontal plane gave a calibration of 30 $mTkA^{-1}$; this was much larger than with the magnetic coil aligned vertically behind the anode. The same pulse generation circuit as before was use to produce the magnetic coil current.

Using an $XeCl^*$ mix with helium as the buffer gas, the variation in laser pulse duration with various values of applied magnetic field was investigated. The laser operating parameters were kept the same as in the previous experiments with a 40% reflectivity output coupler and a PFN charging voltage of 20 kV. The results for a gas mix of 15 mbar Xe, 3 mbar HCl and $1\frac{3}{4}$ bars helium were typical and are reproduced in fig. 7.6.

Fig. 7.6
Graph of laser pulse duration against applied magnetic field
15 mbar Xe, 3 mbar HCl, 1.75 bar He

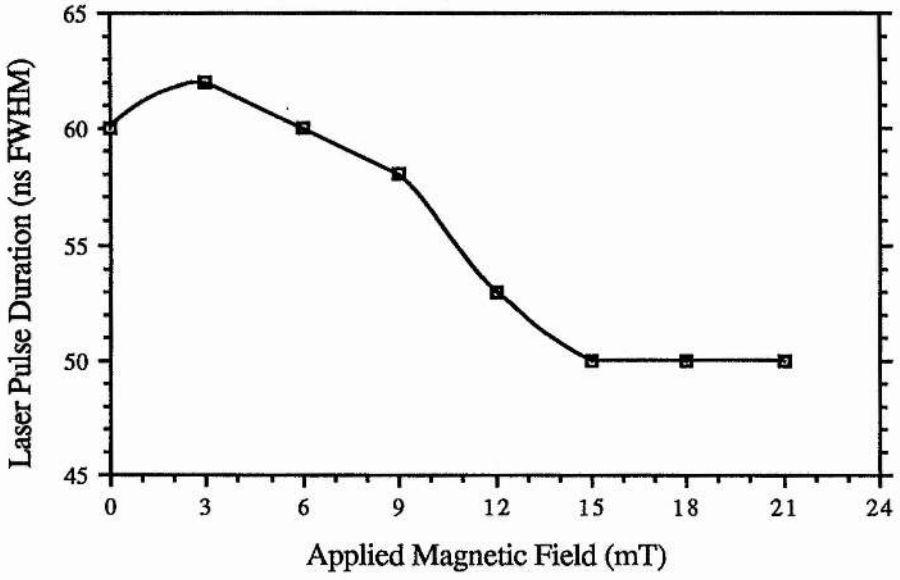

All readings were taken from averages of 8 individual shots to minimise the random errors due to shot to shot variations in laser performance. Using more than 8 shots would have further reduced these random errors but would possibly have increased the systematic error in the data due to earlier exhaustion of the gas fill. It was estimated that the pulse durations quoted are ± 2 ns.

It is difficult to get any quantitative information from these experiments but the results clearly show a fall-off in laser pulse duration with increasing magnetic field. It is also interesting that there is evidence of a saturation in the effect at higher magnetic fields.

7.3.2 The use of the Laser Spatial Profiles Technique with Applied Magnetic Fields

The laser spatial profiles technique, as described in chapter 6, with a moving slit to isolate vertical strips of the laser output, was used to further investigate the behaviour of laser discharges under the influence of applied magnetic fields.

The method used was exactly as before with a 1 mm slit moved in 16 increments of 1 mm across the beam output profile from the cathode to the anode. Readings were taken

with and without the applied magnetic field at each stage in the hope that more would be revealed about the way in which the magnetic field influenced discharge behaviour.

Fig. 7.7 shows the variation in laser pulse duration across the beam profile with and without the applied magnetic field. The laser pulse duration was not measured as FWHM but instead in terms of a 'pulse duration index' which was defined as the time duration, in ns, for which the light output, as measured on the oscilloscope traces, was in excess of 1 cm in height. This parameter is therefore arbitrary in the sense that it depends on the photodiode and oscilloscope being used. It was chosen as it was felt that it provided a more reliable measure of the output pulse duration than the FWHM time, being less dependent on the laser gain and more closely related to the pulse base width. The true base width of the pulses could not be accurately measured because of problems with definition in view of the electrical noise present. The gas mix used was 15 mbar Xe, 3 mbar HCl, 2 bars He; the PFN charging voltage was 20 kV and the inter-electrode spacing 16 mm.

Fig. 7.7
Graphs of optical pulse duration against distance across the discharge from the cathode with and without an applied B field

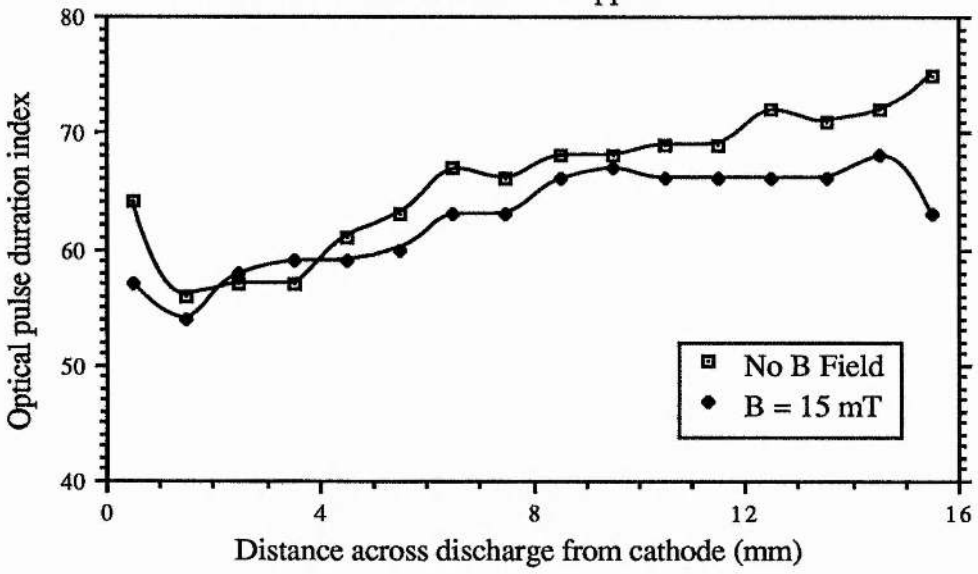

The form of fig.7.7 again shows that the magnetic field produces a reduction in the laser pulse duration and that this is fairly evenly spread across the beam profile. It is difficult to tell from this experiment if this reduction is due to the magnetic field initiating

instability processes earlier in the discharge evolution or whether the magnetic field accelerates their growth once they have been formed. The random spread of the data points made it impossible to reach a more accurate conclusion.

The experiment was also carried out using neon buffered $XeCl^*$ gas mixes but any effects that may have been present were very small and impossible to record with any degree of certainty.

7.3.3 The Use of the XeII (484 nm) Emission Technique to Study the Effects of Applied Magnetic Fields

The technique of using the light from XeII emissions at 484 nm to monitor the growth in discharge filaments, was applied to the study of the influence of magnetic fields on discharge evolution. The method used was as described in chapter 6. A variety of $XeCl^*$ gas mixes using both neon and helium as the buffer gas were tried but without much success. Any differences in the growth of the XeII emissions that may have been present with and without the magnetic field were generally too small to detect above the ambient noise and random experimental variations inherent in the method.

The only results obtained with any reliability were acquired using a gas mix of 15 mbar Xe, 3 mbar HCl, and the high buffer pressure of 3 bars helium. As shown earlier in section 7.2.2 this gas mix showed large reductions in the optical pulse duration when a magnetic field was applied. The oscilloscope traces obtained are given in fig. 7.8 and show that the rise in XeII emissions proceeds at a faster rate when the magnetic field is in place. This implies that the magnetic field accelerates the rate of growth of discharge filaments. Any more detailed conclusions than this are difficult to reach.

Fig. 7.8

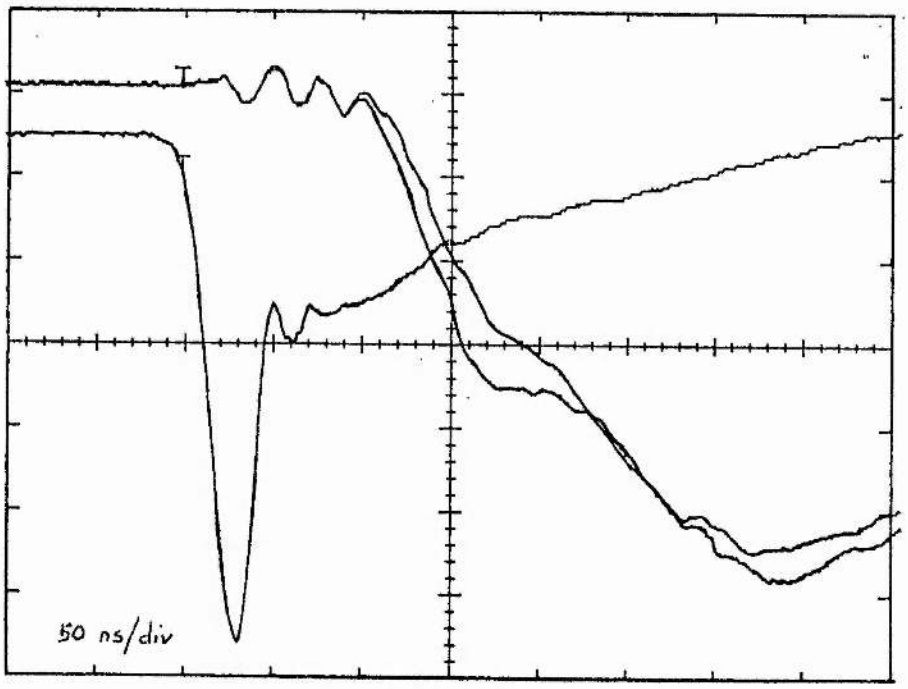

Oscilloscope traces showing the growth of XeII (484 nm) emission with (left) and without (right) an applied magnetic field of approx. 21 mT, gas mix 15 mbar Xe, 3 mbar HCl, 3 bars helium. Also for reference purposes the laser head voltage (lower trace), 3.55 kV/div

7.3.4 Synchronising the Magnetic Field Pulse with the Laser Pulse

It is well known that the failure to produce a sufficiently uniform preionisation electron distribution results in the formation of inhomogeneous glow discharges with poor stability. It was therefore decided to investigate whether the applied magnetic field was producing the acceleration in discharge instability by its influence on the preionisation distribution or the glow discharge itself. To do this the magnetic current pulse was synchronised with the laser pulse by a variable delay box allowing the switching on time of the magnetic pulse to be adjusted with respect to the laser pulse. In this way the magnetic field could be turned on before, during, and after the laser pulse and its effects studied. The duration of the magnetic field pulse was however, in all cases much longer, than the laser pulse durations.

It was found to be necessary to modify the magnetic coil driver circuit to produce a more rapid turn-on of current. A 0.85 nF peaking capacitor was inserted into the circuit as closely as possible to the magnetic coil, see fig. 7.9, to produce a ringing current waveform with a peak amplitude of about 1300 Amps but more significantly a rise-time from zero to 1000 Amps of around 250 ns. Ideally a 'top hat' magnetic coil current pulse was required but this was not possible on the time-scale of 10's of ns considered here. With a current of 1300 Amps corresponding to a magnetic field of 30 mT, and magnetic fields of only a few mT having been shown earlier to produce a significant effect, it was possible to synchronise the onset of the magnetic field with the turn-on of lasing to remove any influence the magnetic field may have over the preionisation distribution yet still retain a significant magnetic field during the laser pulse.

Fig. 7.9

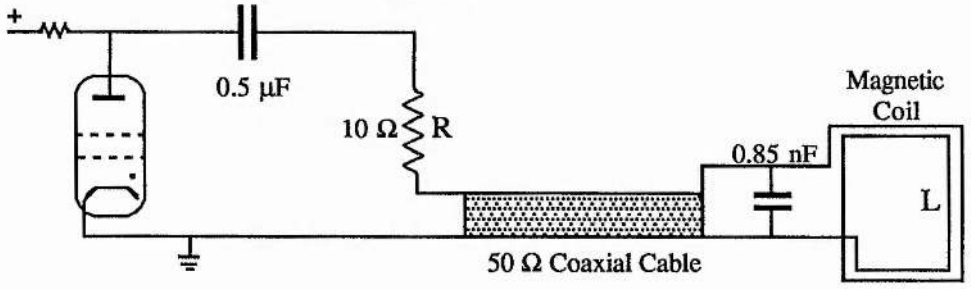

Magnetic coil drive circuit designed to give a ringing current waveform.

Various XeCl* gas mixes, with both helium and neon as the buffer gas, were used with the turn-on of the magnetic field before, during and after the the laser pulse. In all cases the reduction in laser pulse duration was noted when the magnetic field was synchronised with the laser pulse rather than with the preionisation phase. This tends to show that the reduction in laser pulse durations was due to the influence of the magnetic field on the development of the discharge itself rather than by disturbing the preionisation distribution. A more conclusive experiment would have been to produce a magnetic coil current pulse with a very fast turn-off. In this way the magnetic field could be set to be active during the preionisation phase only and to turn off immediately before the start of the

laser pulse. Current pulses such as this are used in the driving of recombination lasers and can be produced by more advanced pulsed power techniques using nonlinear magnetic materials, (12) or by the use of a second thyratron as a 'crow bar' to divert the discharge current at the required instant. Unfortunately the equipment required to produce such a current pulse by either method was not available and so this experiment could not be carried out.

7.3.5 Conclusions

Several conclusions may be drawn from this set of experiments. The use of a constant applied magnetic field up to 21 mT tends to show an increase in the pulse shortening effect as the magnetic field increases, there is however evidence that the amount of pulse shortening may saturate at higher magnetic fields. The measurement of the laser pulse duration moving across the beam profile tends to show that the magnetic field reduces the optical pulse duration at all points across the beam profile. The technique was not sufficiently accurate to provide any more reliable information. Similarly the monitoring of Xe II emissions served only to suggest that the presence of the magnetic field may be acting to increase the rate of filament growth although again the experiment was inconclusive. Lastly, changing the timing of the magnetic field pulse with respect to the laser pulse showed that the magnetic field was most likely changing the laser output by its influence over the discharge itself rather than by disturbing the preionisation distribution.

Other conclusions were that the reduction in the laser pulse duration is larger when helium is used as the buffer gas in place of neon and that the effect is larger at higher buffer gas pressures. These are the conditions that were identified earlier as driving discharge instability without an applied magnetic field.

It is difficult at this stage to propose an explanation as to why a constant applied magnetic field should drive discharge instability processes. It was originally expected that a magnetic field should impart an additional component of motion on to the discharge electrons helping to produce extra mixing and the homogenization of electron temperature and excited species distributions. This, it was hoped, would help to improve discharge stability. As this is clearly not the case it is possible that the opposite is happening and that

the magnetic field is helping to spatially confine electrons. In this way an increasing magnetic field would cause the electrons to traverse an increasingly tight spiral trajectory. Intuition however suggests that if this is the case then a reversal of the magnetic field polarity should tend to cause the electrons to spiral outwards, experiments however show this not to be the case.

7.4 The Influence of Spatially Variant Magnetic Fields on Excimer Laser Discharges

All the experiments carried out so far used magnetic fields that could be considered both temporally and spatially constant. Any changes in the applied field between different points in the discharge volume were small and on a spatial scale comparable with to the discharge itself. An individual electron was therefore subjected to much the same magnetic field as its neighbours. It was proposed that a better mixing effect may be obtained if the applied magnetic field could be made to vary in both direction and magnitude, on a mm scale, throughout the discharge. In this way electrons that were initially close in space would experience different Lorentz forces. Although this is a vague notion it was considered sufficiently plausible to justify experimental investigation.

7.4.1 Experimental Apparatus

The production of a spatially variant magnetic field in the laser discharge volume was not a trivial matter. Any device inserted into the laser head had to be sufficiently close to the discharge to produce the required magnetic field distribution yet not so close to the electrodes that it could cause voltage flash-over problems.

It was decided to produce a spatially variable magnetic field by means of an array of small magnetic coils placed as closely as possible above the discharge. An array of small permanent magnets was also considered but rejected because of the difficulty in turning off the magnetic field to provide a control experiment. The design of the array, shown in fig. 7.9, was with 16 rectangular coils, 15 mm x 25 mm, with 10 turns each. The coils used 0.56 mm diameter enamelled copper wire and were connected in parallel with the currents

in adjacent coils flowing in opposite senses. The whole array was encapsulated in epoxy resin to prevent voltage flash-over and provide mechanical strength. The decision to connect the coils in parallel was taken to keep the overall inductance of the array as small as possible although this did mean that the total current would be shared equally between the coils. The overall self inductance of the parallel combination was measured as 600 nH. The current pulser circuit was similar to before but the series resistance was reduced to 4.7 Ω; this gave a maximum current pulse of 2400 A in total or 150 A in each coil.

The magnetic field from a single coil in the array was measured using a Hall effect probe with the coil being driven from a d.c.power supply. The magnetic field measured at the centre of the single coil, in air, was 300 μTA^{-1} so that the peak magnetic field produced by a current of 150 A was about 45 mT. This allowed a rough estimate of the form and size of the magnetic field due to the coil array to be inferred.

Fig. 7.10

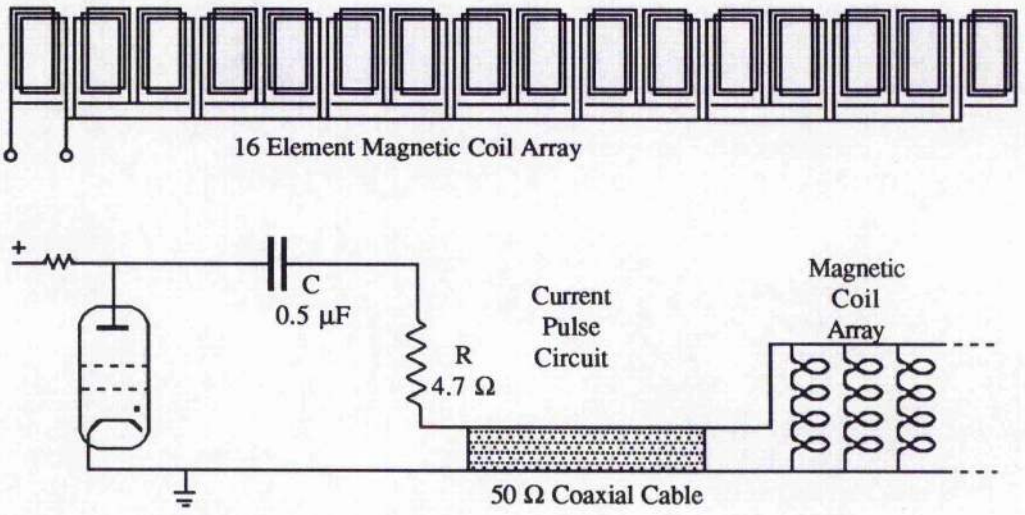

Magnetic coil array and the circuit used to drive it.

7.4.2 Results Using XeCl* with a Neon Buffer Gas

A full parametric survey of the influence of the magnetic coil array was carried out for neon buffered XeCl* gas mixes. In all cases the electrode separation was 16 mm and the PFN charging voltage was maintained at 20 kV. The optical resonator was formed from

a nominal 100% back reflector and a 40% reflectivity output coupler. The partial pressure of xenon was kept constant at 15 mbar but the HCl partial pressure was varied between 2 and 6 mbar in 1 mbar increments. Total buffer gas pressures of 3, 4 and 5 bars neon were used. For each gas mix the optical pulse duration, FWHM, was measured with and without the applied magnetic field produced in the coil array by a total current of 2400 A. The magnetic field pulse was sufficiently long so that the magnetic field could be considered temporally constant throughout the laser pulse.

The magnetic coil array produced little or no effect on the gas mixes with a neon buffer gas pressure of 3 bars but at higher buffer gas pressures the presence of the magnetic field tended to produce longer duration laser pulses. This effect was not particularly large but was consistent and reproducible. The difference between the pulse durations with and without the magnetic field was largest with gas mixes at high buffer gas pressures and with high partial pressures of HCl; these are the gas mixes that have been shown previously to be susceptible to poor discharge stability. The optical pulse durations with and without the applied magnetic field for gas mixes at 4 and 5 bars total neon buffer gas pressure are plotted in fig 7.11 and an example of one of the pairs of oscilloscope traces obtained is given in fig. 7.12.

Fig. 7.11
Graph of optical pulse duration against HCl partial pressure with and without applied magnetic field from 16 coil array

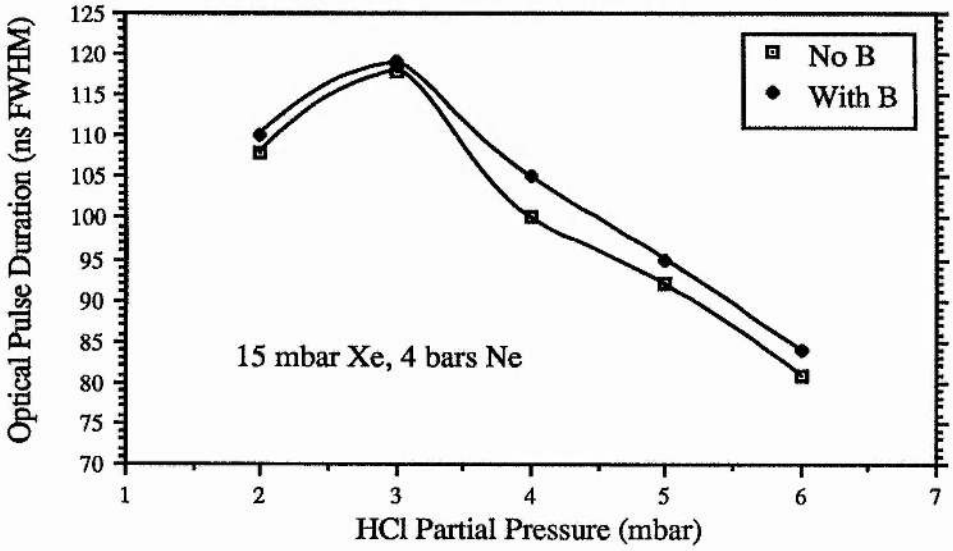

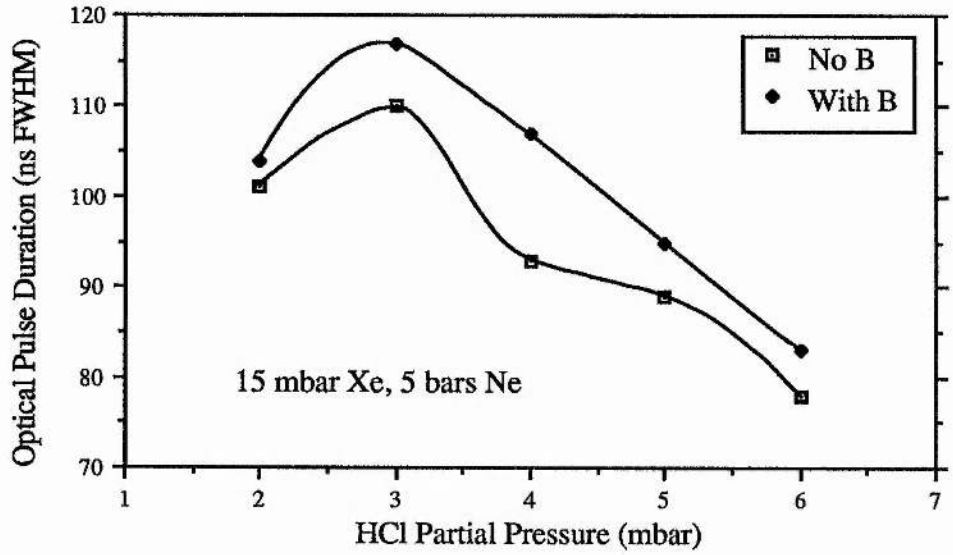

Fig. 7.12

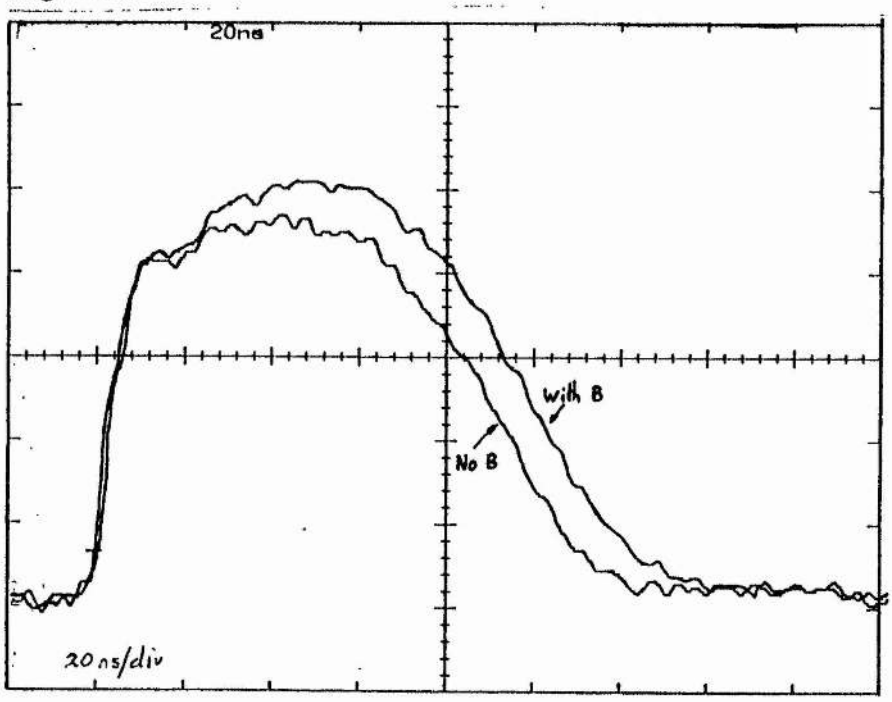

Fig. 7.12. Oscilloscope traces showing the laser output profiles with and without an applied spatially variant magnetic field due to a total current of 2300 A in the 16 element magnetic coil array. Gas mix 15 mbar Xe, 5 mbar HCl, 5 bars neon 20 ns/div.

7.4.3 Results Using XeCl* with a Helium Buffer Gas

The experiment was repeated exactly as before but substituting helium for neon as the buffer gas. Again a similar effect was obtained in that the spatially variant magnetic field extended the optical pulse durations. The laser pulse durations with and without the applied magnetic field for a gas mix of 15 mbar Xe, 3 mbar HCl and $1^1/_2$ 10 3 bars helium are plotted in fig. 7.13. As an example, the waveforms for 15 mbar Xe, 3 mbar HCl and $2^1/_2$ bars helium are given in fig 7.14. From fig. 7.14 it can be seen that the shape of the light output traces makes the measurement of the pulse durations in terms of FWHM very difficult and so the pulse durations used in fig 7.13 were nominally defined as the time in ns for which the oscilloscope traces exceeded the 1 Volt level.

Fig. 7.13
Graph of Optical Pulse Duration (Arbitrary Units) Against Helium Buffer Gas Pressure With and Without an Applied Spatially Variant Magnetic Field

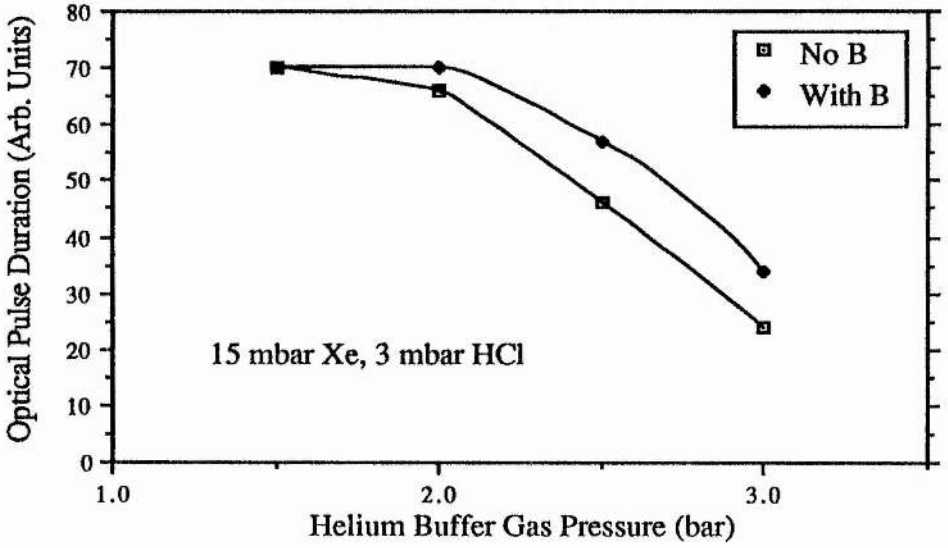

Fig. 7.14

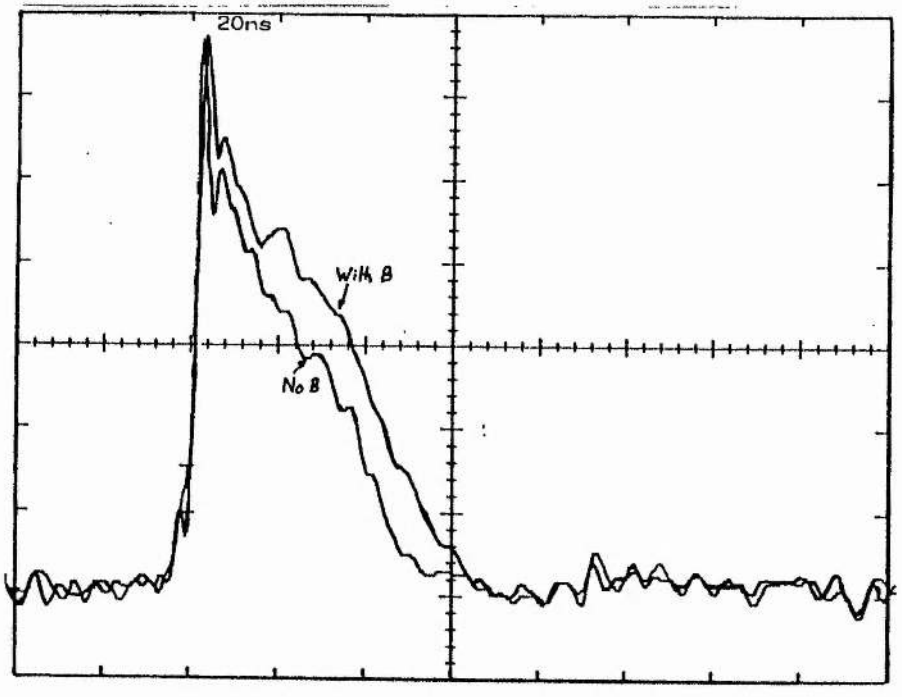

Fig. 7.14. Oscilloscope traces showing the laser output profiles with and without an applied spatially variant magnetic field due to a total current of 2300 A in the 16 element magnetic coil array. Gas mix 15 mbar Xe, 3 mbar HCl, 2.5 bars helium, 20 ns/div.

7.4.4 Further Experiments

Having shown that the use of the magnetic coil array produces longer duration optical pulses than with no magnetic field some further experiments were carried out to confirm this effect.

It was suspected that the presence of the magnetic coil array may have been influencing the form of the laser discharge in some way when switched off. With the current pulse circuit inactive the coils still remained connected across the 0.5 μF capacitor in its discharged state. This could possibly have allowed some form of ringing current flow in the resultant tuned circuit perhaps induced by the magnetic field associated with the discharge current. To find if the coil array made any difference to the laser performance the laser output was monitored with the magnetic current pulse circuit simply switched off, the 0.5 μF capacitor disconnected and again with the input to the magnetic coil array short circuited. In each case no difference to the laser performance was noted. Comparison of the laser output parameters measured with the magnetic coil array switched off and those obtained earlier with no magnetic coil, (see chapter 2), showed the laser to be operating consistently. It was therefore concluded that the presence of the magnetic coil array, when switched off, in no way influences the operation of the laser.

At this stage the magnetic coil current pulse circuit was further modified by reducing the series resistance from 4.7 Ω to 2 Ω. This produced a peak current of 4400 A but unfortunately also resulted in an under-damped waveform with considerable current reversal. Prolonged use of this circuit would have damaged the thyratron, a type CX 1685 without a hollow anode structure, and so only a small number of experiments were possible.

By using this higher current circuit configuration it was possible to obtain some important results with specific gas mixes but it was decided that to extend the life of the thyratron it would be unwise to perform parametric studies over a wide range of gas mixes. The XeII emission at 484 nm was measured with and without the magnetic field due to the 16 coil array with a total current of 4400 Amps. The gas mix used was 15 mbar Xe, 3 mbar HCl, 5 bars Ne. The waveforms, reproduced in fig. 7.15, clearly show that the rise in XeII

emissions, and presumably the growth of high current density filaments, occurs later in the discharge when the magnetic field is applied. It is difficult to get any quantitative information from the waveforms but they do serve to show that the applied magnetic field suppresses the rate of filament growth. The connection can be made between the longer laser pulse durations and the suppression of filament growth by presuming that the longer laser pulses are a consequence of the suppression of filament growth processes. The XeII emission technique therefore provides evidence to support the supposition that the longer duration laser pulses obtained with an applied magnetic field are due to an improvement in discharge stability and not by the magnetic field influencing the laser output in some other, unforeseen way.

Fig. 7.15

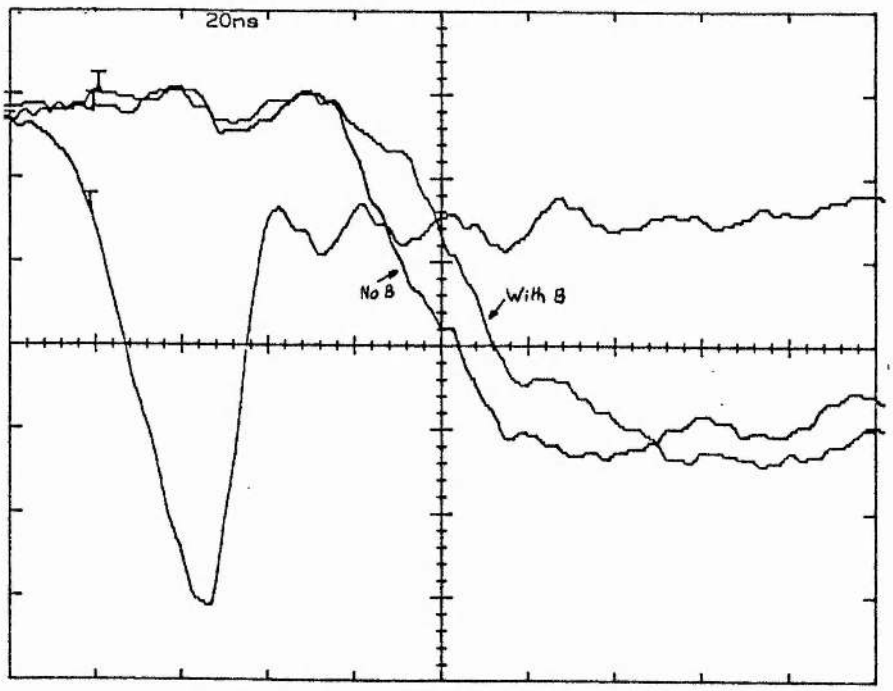

Fig. 7.15. Oscilloscope traces showing XeII (484 nm) emissions with (right) and without (left) an applied magnetic field from the 16 coil array described in the text. The laser head voltage (lower trace) is also shown for synchronisation purposes. Gas fill, 15 mbar Xe, 3 mbar HCl, 5 bar Ne; 20 ns/div; head voltage 3.6 kV/div; total current in magnetic coil array 4400 A.

Another significant effect of an applied spatially variant magnetic field was discovered accidentally. A gas mix containing 15 mbar Xe, 4 mbar HCl and 5 bars neon was operated for several hundred shots, to ensure passivation of the laser head and to align the optical resonator, until the gas fill became exhausted. As before a nominal 100% back reflector and a 40% reflectivity output coupler were used with an electrode separation of 16 mm and a PFN charging voltage of 20 kV. With no applied magnetic field the laser output was weak and erratic with some shots producing no lasing while others resulted in pulses of durations, at best, 20 ns FWHM.

Fig. 7.16

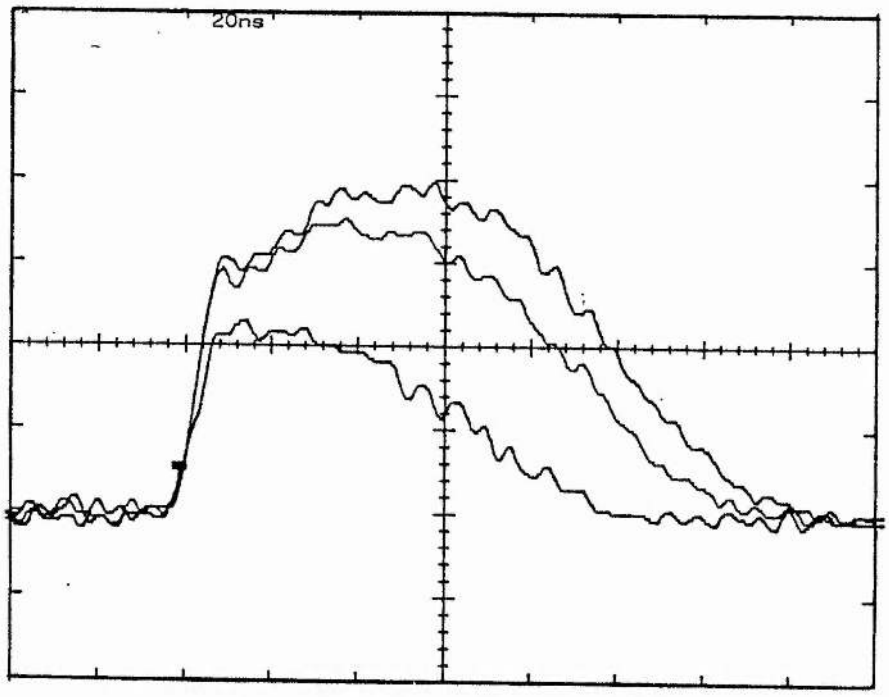

Fig. 7.16. Laser output profiles showing the result of the application of a magnetic field from the 16 coil array described in the text to a partially spent XeCl gas fill at three different values of magnetic coil current. Total magnetic coil currents 3400 A (lower trace) 4000 A (middle trace) 4400 A (upper trace). 15 mbar Xe, 3 mbar HCl, 3 bar Ne; 20 ns/div. No applied magnetic field resulted in erratic laser performance with pulse durations < 20 ns.

When the magnetic coil array was switched on the laser outputs dramatically improved in terms of both pulse duration and shot to shot reproducibility. Typical laser

output waveforms obtained with three different values of total magnetic coil current are given in fig. 7.16. As can be seen the longest pulse duration of 96 ns FWHM was obtained with the largest magnetic coil current of 4400 Amps and this pulse duration is close to or better than what would be expected from a fresh gas fill with no applied magnetic field, (see fig. 7.11). This experiment was repeated several times using other spent gas fills with consistent results although the number of shots for which the magnetic field was used was limited by the need to prevent damaging the thyratron. It was concluded that what was being seen was most probably a genuine effect and not the result of some unforeseen experimental error.

Why the application of a spatially variant magnetic field should produce a much larger improvement in laser pulse durations with a partially spent gas fill is difficult to explain. It is well known that in an $XeCl^*$ gas mix using hydrogen chloride as the halogen donor degrades by the failure of all of the dissociated HCl molecules to recombine after each shot. A significant proportion of the H^+ and Cl^- ions tend to reform as either H_2 or chlorine containing molecules and reactions between Cl^- ions or Cl^* radicals and the laser head materials may also be significant. In order to aid the shifting of the chemical equilibrium towards the reformation of HCl it has long been a common practice to add a small partial pressure of H_2 to the gas mix, (13), and it has also been shown that periodic injections of HCl extend gas lifetimes and produce more reliable laser outputs, (14). Recent studies have also accurately assessed the most common gas degradation products in $XeCl^*$ lasers and their influence on laser performance, (15).

The main difference between a spent and a fresh gas fill may therefore be taken as the presence in the spent gas fill of molecular contaminants. This is not particularly helpful in explaining how the applied magnetic field influences the laser output when it is considered that over the duration of a typical excimer discharge most atomic and molecular species can be considered to be stationary, (10). The magnetic field can therefore be taken to influence only electrons and the lightest of ions. A mechanism to explain the interaction of the magnetic field with heavier species is difficult to propose with any certainty.

7.4.5 Conclusions to Section 7.4

The application of spatially variant magnetic fields to $XeCl^*$ excimer laser discharges produced some interesting and unexpected results. It seems that such fields produce a small extension in laser pulse durations with the largest improvements being with gas mixes rich in HCl and at high buffer gas pressures. Monitoring of XeII emissions at 484 nm tends to show that this improvement in pulse duration is due to improved discharge stability rather than kinetic factors. The most likely cause of this effect that can be proposed at this stage is that the magnetic field introduces an extra mixing mechanism into the motion of the discharge electrons helping to homogenise electron temperature and excited species distributions.

The enhanced effect obtained with partially spent gas fills, if confirmed, is very difficult to explain and requires further investigation.

7.5 Suggestions For Further Work

The application of external magnetic fields to excimer laser discharges appears to produce a number of interesting effects, all of which however require further investigation and verification. In particular the application of spatially variant magnetic fields to laser discharges could prove to be commercially useful, not only by producing longer duration laser pulses but perhaps more importantly by extending gas fill lifetimes. This requires more experimentation, perhaps with a laser head designed from the outset to incorporate magnetic coils into the electrode structures rather than as a separate addition as used here. It should also be possible to reproduce the magnetic field distributions used in these experiments by using permanent magnets although these might pose difficulties in providing a suitable control experiment to assess the effect with and without the magnetic field in place.

References

1 H J J Seguin, C E Capjack, D M Antoniuk, K H Nam; "High Power Laser Discharge Stabilisation With Magnetic Fields" Appl. Phys. Lett, vol 37, p130, 1980

2 C E Capjack, D M Antoniuk, H J J Seguin; "Dynamics of Magnetically Stabilised Laser Discharge;" J Appl. Phys, vol 52, p4517-22, 1981

3 H J J Seguin, C E Capjack, D M Antoniuk, V A Seguin; "A Magnetically Stabilised Radial Discharge for a High Powered Laser" Appl. Phys Lett, vol 39, p203-5, 1981

4 W L Nighan, W J Wiegand; "Causes of Arcing in C.W. CO_2 Convection Laser Discharges;" Appl. Phys. Lett, vol 25, p633, 1974

5 L J Denes, J J Lowke; "V-I Characteristics of Pulsed CO_2 Laser Discharges;" Appl. Phys. Lett, vol 23, p130-2, 1973

6 R S Taylor; "Preionisation and Discharge Stability Study of a Long Pulse Duration UV-Preionised XeCl Laser;" Appl. Phys. B, vol 41, p1-24, 1986

7 J Coutts, C E Webb; "Stability of Transverse Self-Sustained Discharge-Excited Long-Pulse XeCl Lasers;" J Appl. Phys. vol 59, p704-10, 1986

8 M R Osborne; "Rare Gas Halide Discharge Stability;" Appl. Phys B, vol 45, p285-91, 1988

9 M Bahr, W Botticher, S Choraba; "The Time Dependent Development of the Macroscopic Instability of a $XeCl^*$ Laser Discharge;" IEEE Transactions on Plasma Science, vol 19 (2), p369-78, 1991

10 M J Kushner; "Microarcs as a Termination Mechanism of Optical Pulses in Electric Discharge Excited KrF^* Excimer Plasmas;" IEEE Transactions on Plasma Science, vol 19 (2), p387-99, 1991

11 M M Turner; PhD Thesis, University of St Andrews, 1990

12 A K Kidd; "A Method of Rapidly Terminating the Current Pulse Applied to Recombination Lasers;" Pulse Power for Lasers II, p35-42, SPIE, Los Angeles, 1989

13 T J McKee, D J James, W S Nip, R W Weeks; "Lifetime Extension of XeCl and KrCl Lasers with Additives;" Appl. Phys Lett, vol 36(12), p943-5, 1980

14 S Ogura, Y Kawakubo, K Sasaki, Y Kubuto, A Miki; "Output Power Stabilization of a XeCl Excimer Laser by HCl Injection;" Gas and Metal Lasers and Applications, p123-8, SPIE, Jan 1991

15 G M Jursich, W A Von Drasek, K Mulderink, V Olchowka, J Reid, R K Brimacombe; "Influence of Gas Composition on XeCl Laser Performance;" Gas and Metal Lasers and Applications, p113-22, SPIE, Jan 1991

Conclusions and Suggestions for Further Work

It has been shown that discharge instability and the difficulty in maintaining a uniform high pressure glow discharge are the major causes of the failure of practical rare gas halide excimer lasers to achieve theoretical performance predictions. Studies of the laser kinetics and plasma chemistry of these systems predict pulse durations and efficiencies far in excess of those currently achievable with discharge pumping and this can be attributed to the difficulty in maintaining an even power deposition into the active medium. In chapter 3, despite the use of a pulsed power scheme capable of closely meeting the theoretical ideal of a fast voltage turn-on, fast rate of rise of current and a steady maintaining of the optimum power deposition density, the laser pulse duration was actually worse than with a less sophisticated pulse power circuit. This was attributed to the inadvertent driving of discharge instabilities.

Having established the necessity of good discharge stability and the importance of suppressing the glow to arc transition it became apparent that the factors that influence discharge stability are both numerous and complex. In consequence it has not been possible to reach any grand overall conclusion but a number of useful facts have emerged. It has long been known that both preionisation conditions and the presence of the electronegative halogen donor strongly influence discharge stability but it has now been shown that the rare gas partner is also important with the lighter rare gasses producing less stable discharges. It has also been possible to show that the inferior performance of helium buffered gas mixes as compared with neon is most likely due to an earlier collapse of the glow discharge rather than kinetic factors. Strong evidence has also been presented to show that argon is a satisfactory buffer gas except for its unfortunate tendency to induce very poor discharge stability.

The results of the experiments in magnetic stabilisation of excimer discharges are somewhat enigmatic. Although the application of a constant magnetic field was expected, according to theory, to improve discharge stability by a suppression of the glow to arc transition mechanism performance seemed to deteriorate, although this was not proved

conclusively. In contrast a magnetic field that was temporally constant but spatially variant throughout the discharge volume seemed to improve discharge stability and lead to longer duration laser pulses. It is unfortunate that the scope of this work was restricted by constraints on time and equipment availability as further investigation would be useful for resolving these matters.

The nature of high pressure glow discharges and the glow to arc transition are difficult to understand fully and there are many questions that remain to be answered in the quest to improve excimer laser performance. Not only does the arc formation mechanism remain to be understood but perhaps more significantly the question should be asked that given the favourability of arc formation why when a glow discharge collapses do relatively few arcs form; a glow discharge is after all simply a mass of avalanche events so closely spaced that they interact and may be considered as a uniform mass.

Appendix 1

The design of an all solid state trigger circuit for a CX 1625 ceramic thyratron.

This appendix describes the design of an all solid state trigger unit to drive an EEV type CX 1625 ceramic thyratron. This work was carried out in collaboration with Andrew R Dick as part of his MSc. in Pulsed Power and Laser Engineering, University of St. Andrews, 1991.

The manufacturers of the CX 1625, EEV, recommend that for maximum current switching rate performance the thyratron should be driven by a circuit capable of meeting the following specification.

Grids 0 and 1 Current Driven (priming)

	min	typical	max	units
Grid 1 drive current (peak)	50	100	150	A
Unloaded grid 1 drive pulse	300		2000	V
Grid 1 pulse duration	2.0			μs
Grid 1 pulse dV/dt	1.0			$kV\mu s^{-1}$

Note: grid 0 current should be about 10% of grid 1 value

Grid 2 Voltage Driven (control)

	min	typical	max	units
Unloaded grid 2 drive pulse	600		2000	V
Grid 2 pulse duration		0.5		μs
Grid 2 pulse dV/dt	10			$kV\mu s^{-1}$
Grid 2 pulse delay wrt. grid 1	0.2		3.0	μs
Loaded grid 2 bias voltage	-100		-300	V

Information taken from ;"Hydrogen Thyratrons, EEV Product Data"

Subsequent conversations with EEV suggested that the above published data was somewhat conservative, in particular for maximum current switching speed a priming grid current of 50 amps is now generally accepted to be sufficient.*

In the past large thyratrons such as the CX 1625 have been triggered using pulse generators incorporating smaller thyratrons. It was realised however that advances could be made in size, weight and reliability if advantage was taken of modern semiconductor technology and high voltage thyristors (SCRs) were used instead. In general, thyristors capable of holding off voltages in the kV range and conducting currents of many tens of amps tend to be physically large, their main application being in power supplies and motor control circuits. As a consequence of this these devices tend to have slow turn on times with current rise-times of only a few hundred As^{-1}. The thyristor chosen for the thyratron drive circuit therefore represents a compromise between switching speed, current handling capability and voltage hold off.

Fig. A1.1

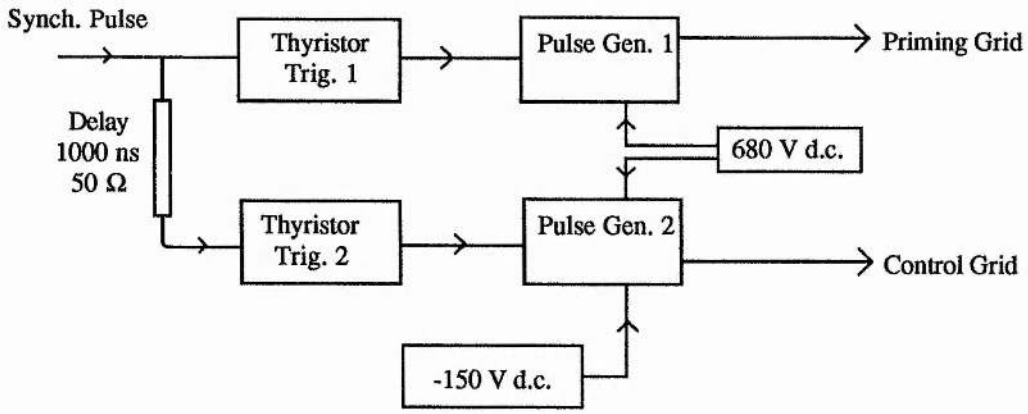

Block Diagram of the All Solid State Thyratron Trigger Unit

A block diagram of the layout of the thyratron trigger unit is given in Fig. A1.1. The two pulse generator modules, each containing a single thyristor, were charged from a

* L. Kettle, EEV, Private communication.

680 V d.c. power supply; the pulse generator intended to drive the control grid was biassed by a seperate -150 V d.c. supply. The thyristors in each pulse generator module were themselves triggered by a pair of low voltage trigger circuits.

The tyristor chosen as the main switching element of the pulse generator modules was the type ACR25U8LG supplied by MEDL. This device has a voltage hold off of 800 V and can handle peak currents of up to 370 A when used in single shot applications such as here. The device is capable, with careful circuit design, of switching on currents at up to 2 $kA\mu s^{-1}$ but has no reverse blocking capability and must be used in conjunction with a suitable protection diode.

Fig. A1.2

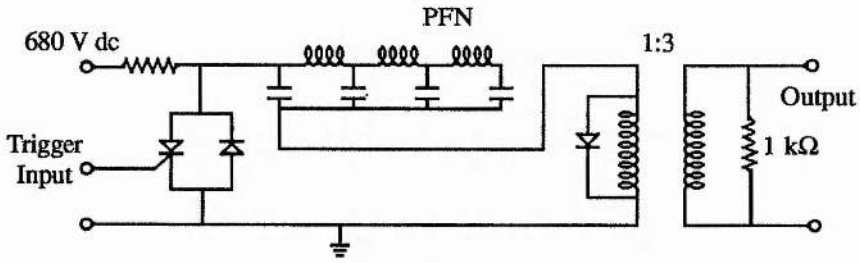

Circuit Diagram of the High Voltage Pulse Generator Modules

The circuit diagram of the pulse generator modules is shown in fig. A1.2. Their operation is straightforward in that the thyristor discharges the pulse forming network (PFN) through the 3:1 voltage step up transformer. The PFN was constructed from suitable high voltage (1 kV) capacitors and wire wound, air cored inductors to generate a pulse of about 1 μs duration. The 1 kΩ resistor at the output was provided to give a load for the pulse generator to fire into should it be inadvertently be operated open circuit.

Fig. A1.3

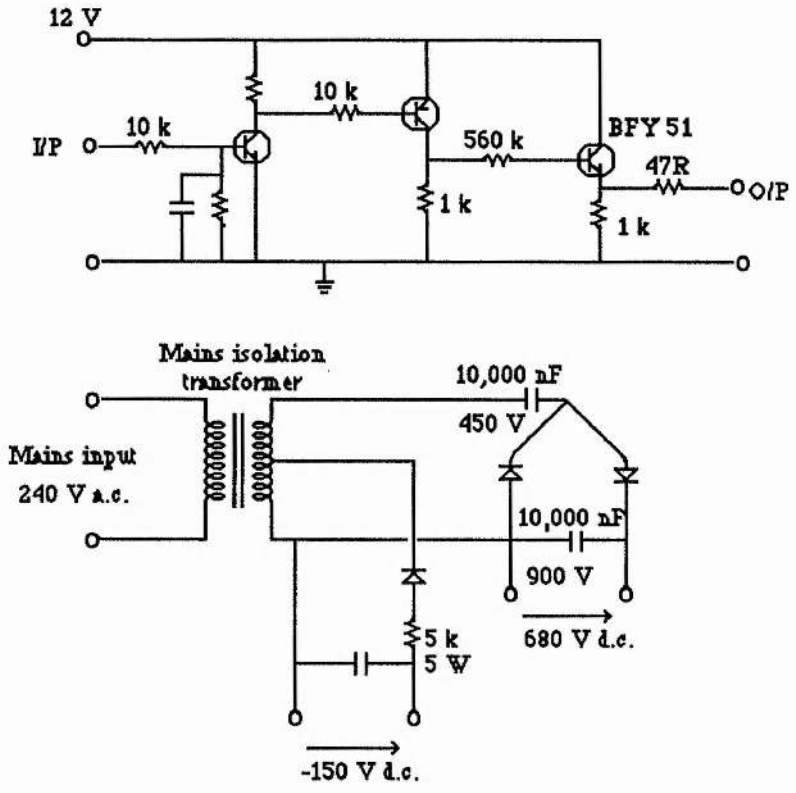

The other elements of the trigger unit are shown in fig. A1.3 and are straightforward using proven technology. In service the trigger generator required some minor modifications, mainly to the low voltage thyristor trigger pulse circuits to prevent spurious triggering from electrical noise. It was also discovered that during operation high voltage pulses were being reflected back into the control grid pulse generator circuit, possibly from the impedance mismatch at the thyratron, causing permanent damage to the thyristor. This was cured by using suitable varistors (zenamics) is series with the control grid output to 'soak up' any voltage spikes.

Appendix 2

Specialist current and voltage diagnostic equipment

A2.1 High Voltage Oscilloscope Probes

There are few commercially available attenuating high voltage probes suitable for the measurement of fast voltage pulses with amplitudes of up to 30 kV. The only commercially available probe available for the work described here is the Tektronix type P6015 which has an attenuation factor of 1000:1 and is suitable in terms of response time and working voltage. It suffers from the disadvantage however that it must be matched to the oscilloscope by a special cable terminating in a compensation box plugged directly into the high impedance oscilloscope input. The oscilloscope used for the majority of the results presented here was a Tektronix 2440 digital storage oscilloscope which possessed many useful features but because of its high content of low voltage integrated circuits was prone to picking up electrical noise. Furthermore to prevent damage by voltage transients it was desirable to keep the oscilloscope as remote as possible from the laser, in an adjoining room supplied by a separate mains phase. This need for remote operation ruled out the direct use of the Tektronix probe for measurement of laser electrical parameters. Instead a series of home made liquid filled high voltage probes with a 50Ω output impedance were constructed permitting connection to the oscilloscope through standard 50Ω coaxial cable.

An example of a liquid filled probe is shown in photograph A2.1 and a schematic diagram in fig A2.2.

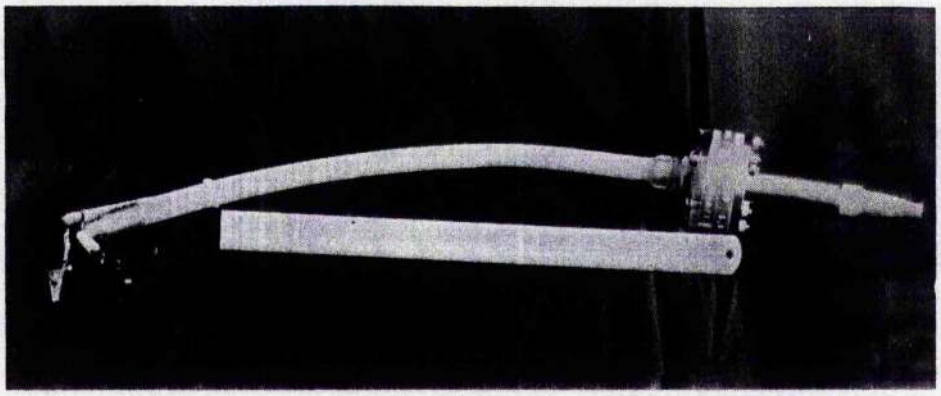

Photograph showing a liquid filled high voltage probe, 30 cm rule gives scale

Fig. A2.2

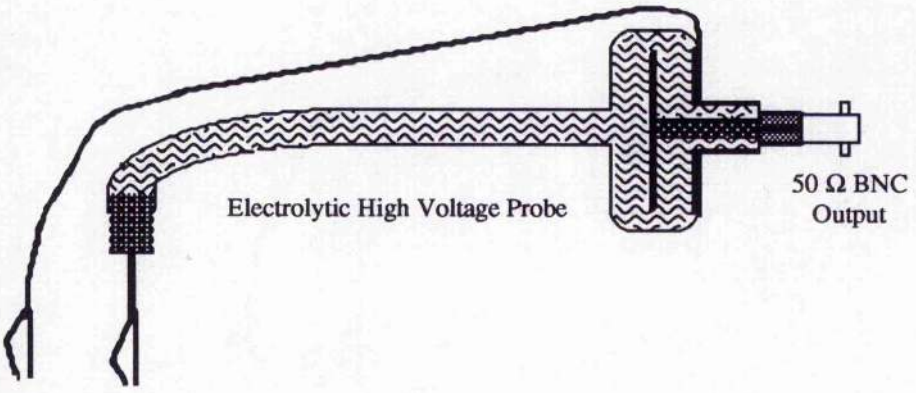

To ensure voltage rise-times of less than 10 ns it has been found necessary to not only maintain the ratio of the resistive elements of the attenuator arms but also the reactive elements due to stray capacitance. Too much capacitance restricts the response time to the relevant time constant while failure to maintain the ratio of the reactances due to the stray capacitances the same as the ratio of the resistances results in pulse distortion. These ratios automatically remain fixed in a liquid filled probe due to the nature of its construction. A disadvantage of this probe design is that it can only be used under pulsed conditions where the voltages are applied for times short in relation to the time taken for significant ion migration. For the work carried out here these probes are entirely satisfactory in this respect.

The probes were initially filled with copper sulphate solution, the concentration of which was adjusted to give an impedance as close as possible to 50Ω in the low impedance leg of the probe to ensure impedance matching between the probe and the coaxial cable. The attenuation factor of the probe is therefore dependent on the length of the polyethylene tube and each probe was calibrated against a Tektronix probe under pulsed conditions using a suitable high voltage source. To ensure that the resistance of the low impedance leg was as far as possible due only to the resistance of the copper sulphate solution, the ohmic resistance of the metal contacts to the centre of the 50Ω output was kept as small as possible. Any significant resistance in this leg would cause the resistive and the reactive

components of the two halves of the probe not being in the same ratio and would lead to pulse distortion.

It was found that over a period of several weeks the copper sulphate took part in an exchange reaction with the constituents of the stainless steel internal components resulting in the formation of a brown precipitate. This required the probes to be regularly refilled and calibrated. To solve this problem copper sulphate was substituted by sodium thiosulphate with improved lifetime between recalibrations. Even so recalibration was done routinely about every 2 to 3 months or before accurate work.

A2.2 Current Measurement

The laser head current was generally measured using a very low value ohmic resistance inserted in one of the two current return paths of the driving circuit. This current viewing resistor was a commercial design made by T & M Research Inc. and is shown in photograph A2.3. The resistance value was nominally 5 mΩ and the value of the current flowing through it was given by the voltage generated across the standard BNC output. The resistor was specially designed for pulse current measurements and was constructed to have an extremely low inductance so that any voltages generated across this stray inductance due to time varying currents will be vanishingly small. This low inductance feature is particularly important as for example with a single thyratron drive circuit switching current at a rate of 10^{11} As^{-1} the voltage generated across a stray inductance of only 1 nH will be 100 V; this can be compared with a calibration factor of 5 VkA^{-1} for the resistor. The manufacturers claim a current rise-time of less than 1 ns can be resolved.

Photograph A2.3

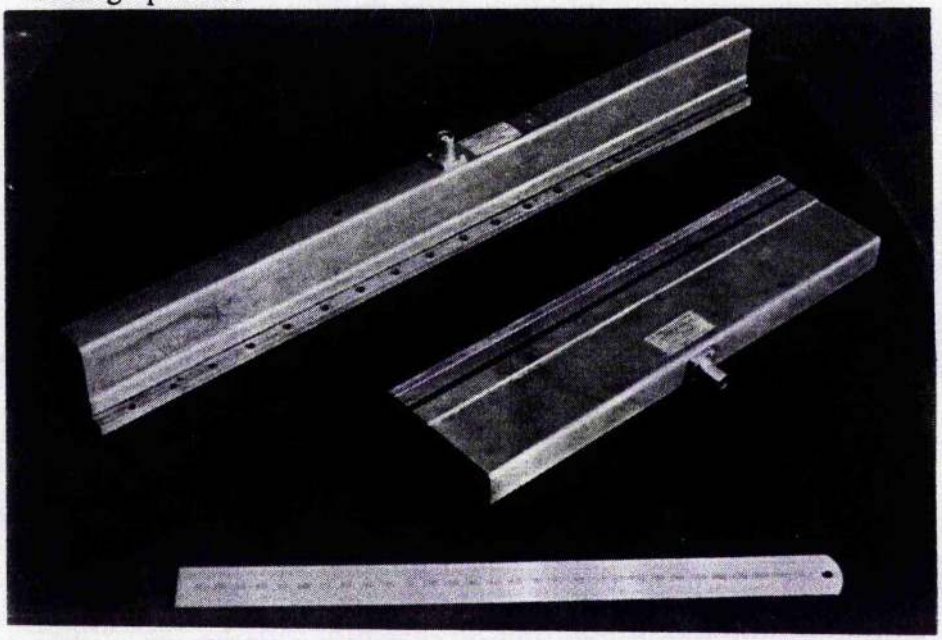

T &M Research current viewing resistors, the smaller of the two shown here was built into the low inductance current return path to allow measurement of the laser discharge current.

Unfortunately only one suitable current viewing resistor was available, ideally an identical pair of resistors, one in each current return path, would have been used so that the total current would be give by the sum of the voltages across each resistor. As this was not possible the resistor available was inserted into one path only and was calibrated against other current measuring methods. It was not sufficient to say that the total current would divide equally between the two return paths because of the slightly differing resistances presented by the two paths.

The current viewing resistor was calibrated against a Pearson Electronics Inc. type 410 current measuring transformer. This instrument is highly accurate but suffers from the disadvantage that it can only be used at a maximum current of up to 5 kA and all currents measured must pass through the half inch diameter central hole; this makes it unsuitable for inclusion in wide, low inductance current feed geometries. The minimum current rise-time of these devices is around 20 ns. Further cross calibration was possible during the testing of the pulse forming network into the resistive dummy load described in chapter 2.

Appendix 3

This appendix contains photographs of the laser system and its associated apparatus.

Fig. A3.1

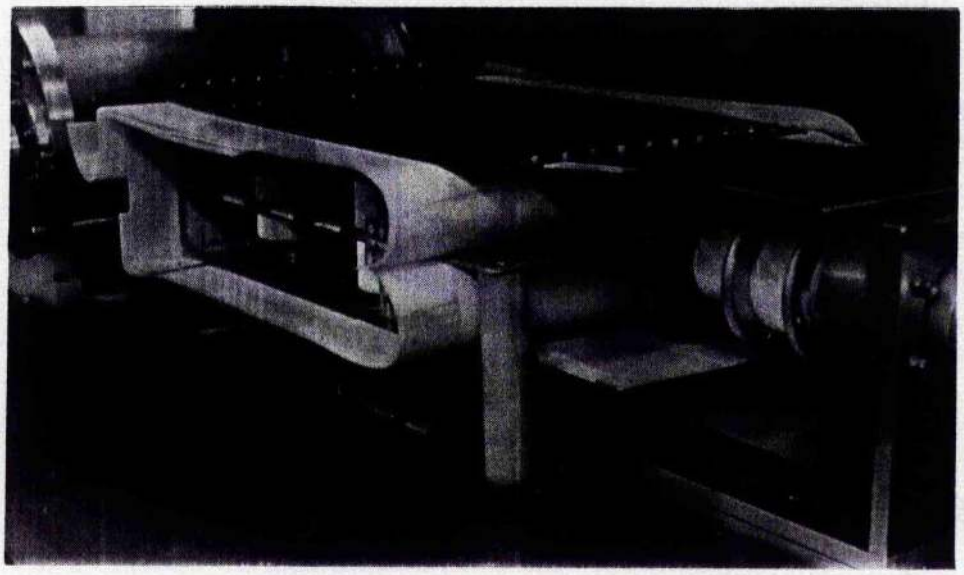

General view of the laser pulsed modulator showing the PFN and the ceramic thyratron mounting.

Fig. A3.2

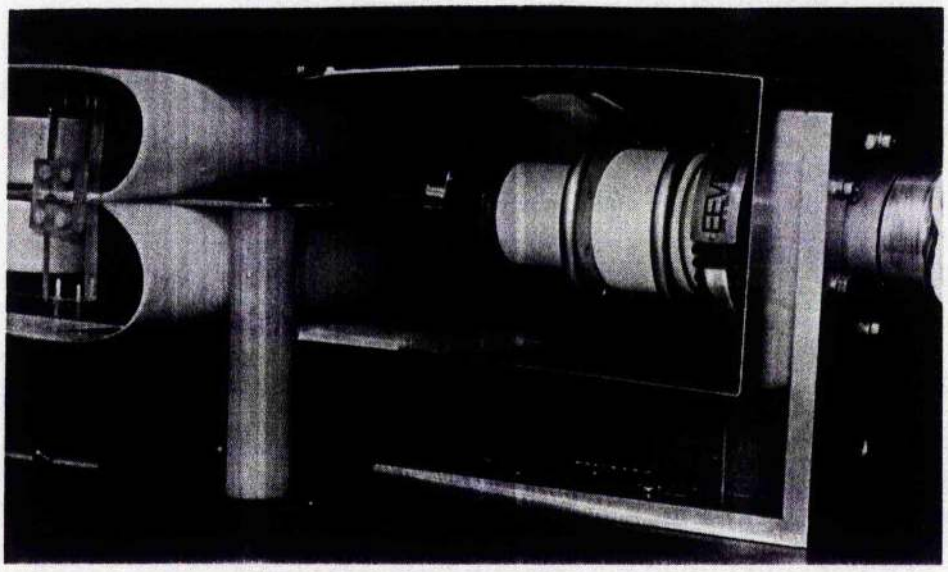

View showing the mounting of the CX 1625 ceramic thyratron.

Fig. A3.3

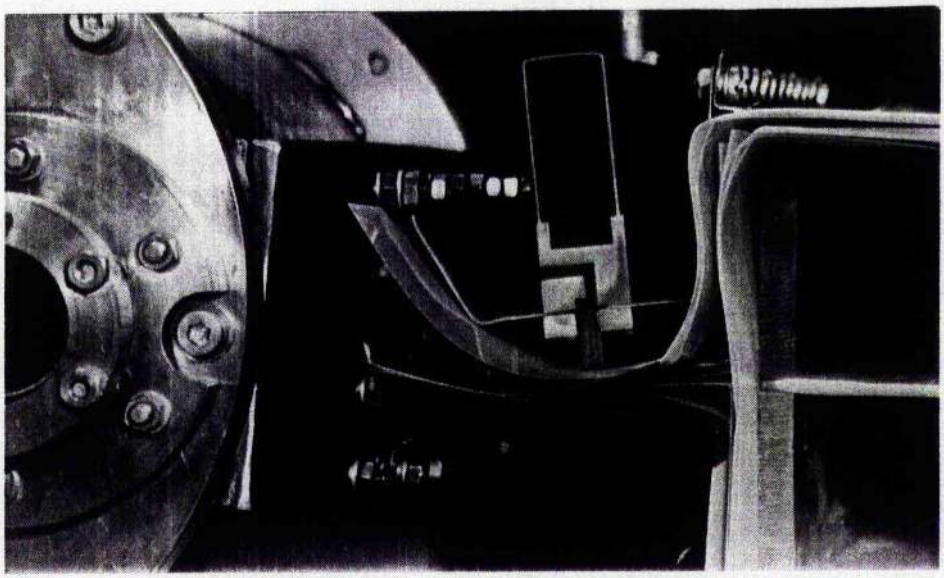

The current feeds to the laser head showing the current viewing resistor used to monitor the laser discharge current.

Fig. A3.4

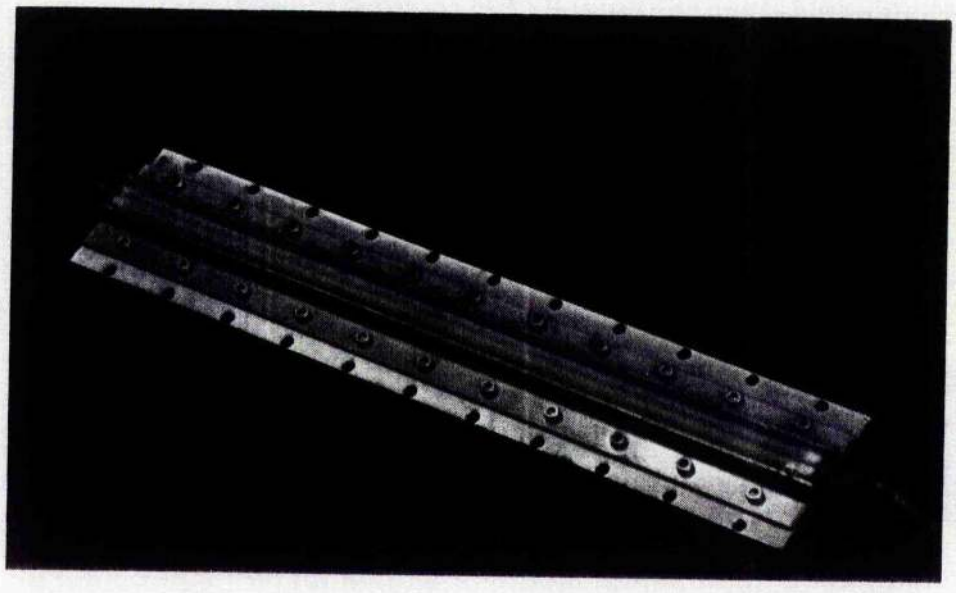

The laser anode incorporating the corona preioniser.

Fig. A3.5

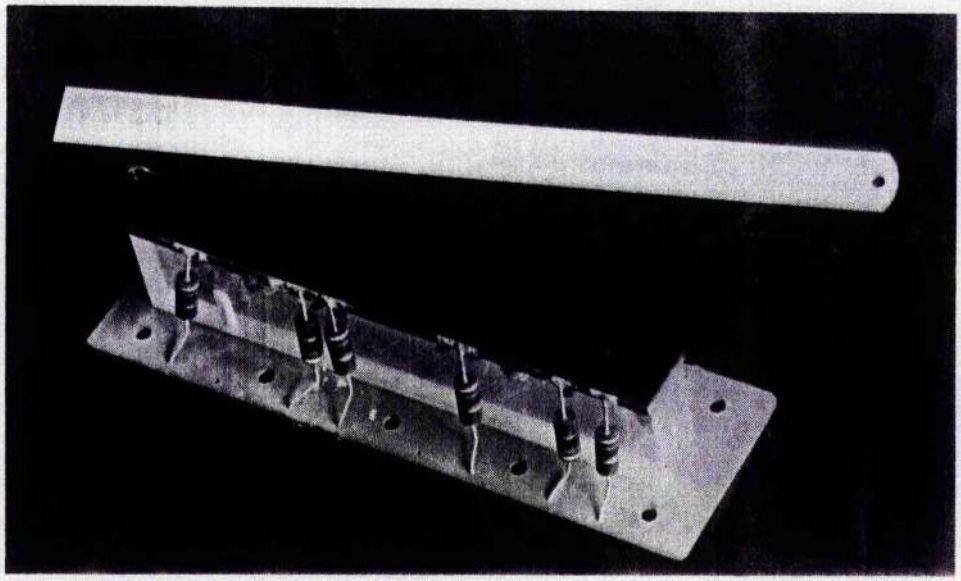

The 4Ω resistive dummy load used in place of the anode for testing the PFN characteristics as described in chapter 2. The electrically conducting rubber pad necessary to provide a good contact with the cathode can be seen on the top face.The resistors are of moulded carbon construction to minimise the inductance of the load.

Fig. A3.6

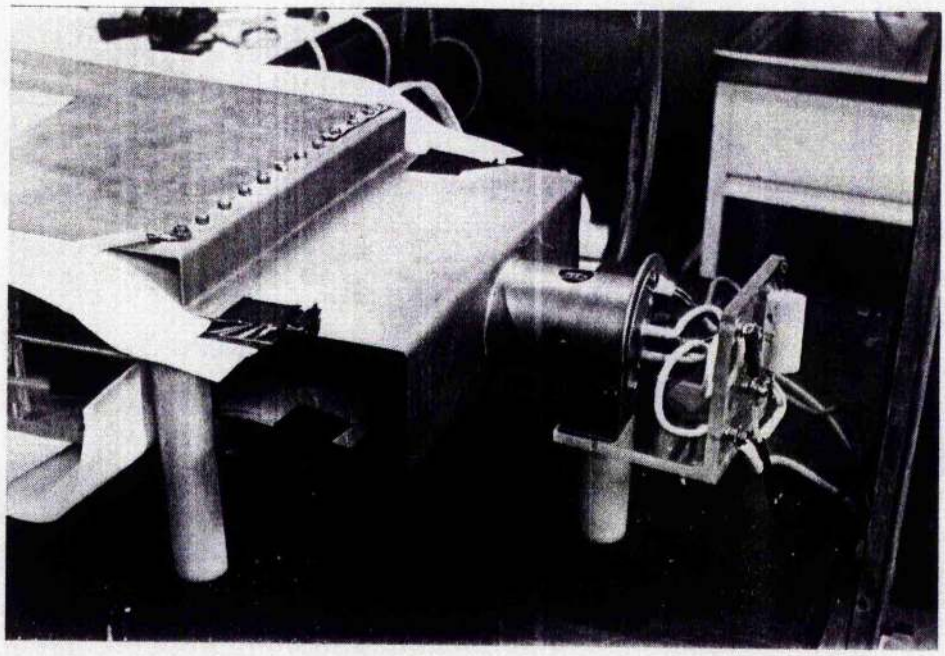

The low inductance housing for the CX 1785 glass thyratron used in the nonlinear capacitor experiments described in chapter 3.

Fig. A3.7

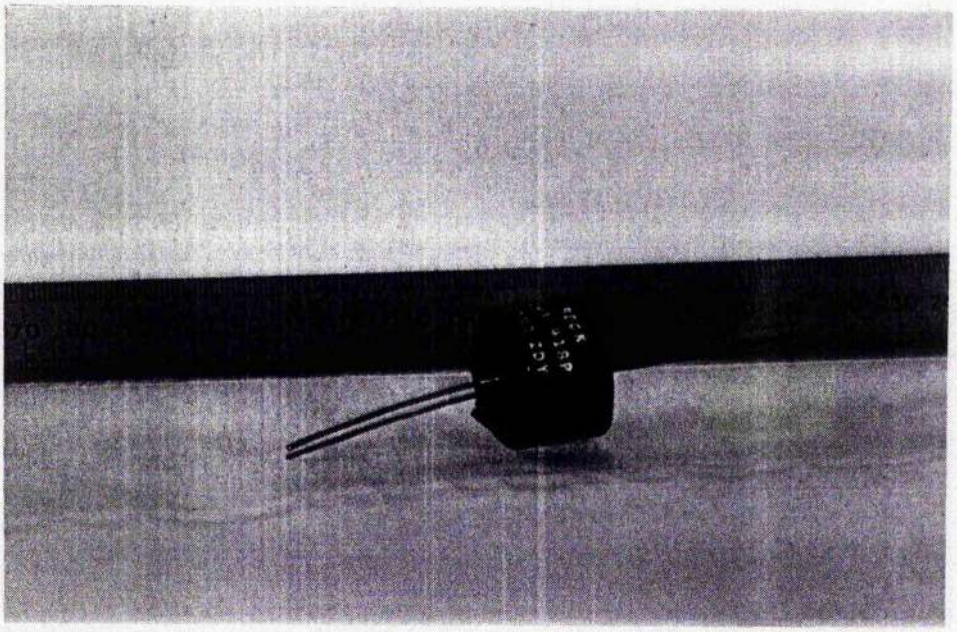

A nonlinear dielectric capacitor as used in the pulse sharpening experiments described in capter 3. The ruler gives the scale in millimetres.

Fig. A3.8

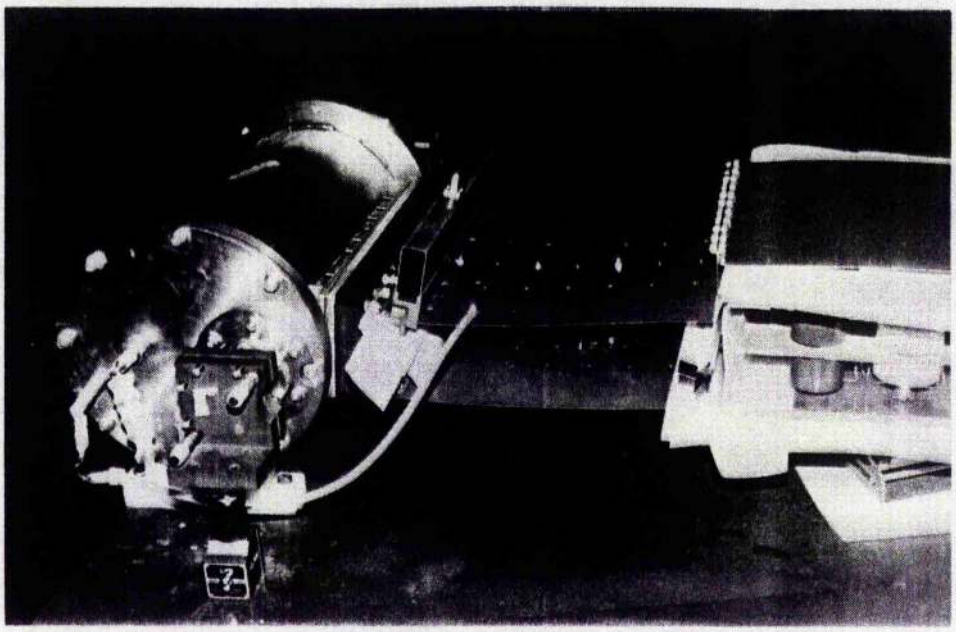

The nonlinear pulse sharpening section from chapter 3 shown in position between the linear pulse forming network and the laser head. The top current return plate includes a current viewing resistor to monitor the discharge current.